

MULTIDISCIPLINARY STUDIES ON RECENT ADVANCES IN SCIENCE AND ENGINEERING – EXPERIMENTAL AND THEORETICAL

EDITED BY

Asst. Prof. Dr. Ege Anıl DİLER

AUTHORS

Prof. Dr. Hatice GUZEL

Assoc. Prof. Dr. Ayla BILGIN

Assoc. Prof. Dr. Imran ORAL

Assist. Prof. Dr. Abdulvahap KORKMAZ

Assist. Prof. Dr. Akın ATAŞ

Assist. Prof. Dr. Ege Anıl DİLER

Assist. Prof. Dr. Mikail ASLAN

Assist. Prof. Dr. Mustafa ÖZDEMİR

Dr. Erdal ÇILGIN

Dr. Fatih BALIKOĞLU

Dr. Tayfur Kerem DEMİRCİOĞLU

Lecturer Sümeyye ERDEM

Teacher Mehmet KARABULUT



İKSAD
Publishing House

MULTIDISCIPLINARY STUDIES ON RECENT ADVANCES IN SCIENCE AND ENGINEERING – EXPERIMENTAL AND THEORETICAL

EDITED BY

Asst. Prof. Dr. Ege Anıl DİLER

AUTHORS

Prof. Dr. Hatice GUZEL

Assoc. Prof. Dr. Ayla BILGIN

Assoc. Prof. Dr. Imran ORAL

Assist. Prof. Dr. Abdulvahap KORKMAZ

Assist. Prof. Dr. Akın ATAŞ

Assist. Prof. Dr. Ege Anıl DİLER

Assist. Prof. Dr. Mikail ASLAN

Assist. Prof. Dr. Mustafa ÖZDEMİR

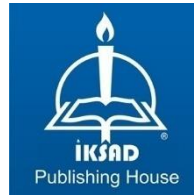
Dr. Erdal ÇILGIN

Dr. Fatih BALIKOĞLU

Dr. Tayfur Kerem DEMİRCİOĞLU

Lecturer Sümeyye ERDEM

Teacher Mehmet KARABULUT



Copyright © 2020 by iksad publishing house
All rights reserved. No part of this publication may be reproduced,
distributed or transmitted in any form or by
any means, including photocopying, recording or other electronic or
mechanical methods, without the prior written permission of the
publisher, except in the case of
brief quotations embodied in critical reviews and certain other
noncommercial uses permitted by copyright law. Institution of
Economic Development and Social
Researches Publications®
(The Licence Number of Publicator: 2014/31220)
TURKEY TR: +90 342 606 06 75
USA: +1 631 685 0 853
E mail: iksadyayinevi@gmail.com
www.iksadyayinevi.com

It is responsibility of the author to abide by the publishing ethics rules.
Iksad Publications – 2020©

ISBN: 978-625-7279-67-3
Cover Design: İbrahim KAYA
December / 2020
Ankara / Turkey
Size = 16 x 24 cm

CONTENTS

PREFACE

Assist. Prof. Dr. Ege Anıl DİLER1

CHAPTER 1

A STUDY ON FLEXURAL BEHAVIOR OF SANDWICH COMPOSITES WITH E-GLASS REINFORCED POLYMER SKINS AND GRID-SCORED PVC FOAM CORE

Dr. Fatih BALIKOĞLU,
Dr. Tayfur Kerem DEMİRCİOĞLU,
Assist. Prof. Dr. Ege Anıl DİLER,
Assist. Prof. Dr. Akin ATAŞ.....3

CHAPTER 2

DETERMINING ELASTIC COEFFICIENTS OF COMPOSITE MATERIALS BY MECHANICAL METHODS

Prof. Dr. Hatice GUZEL, Teacher Mehmet KARABULUT,
Assoc. Prof. Dr. Imran ORAL.....35

CHAPTER 3

ANALYZING THE RELATIONSHIP BETWEEN SURFACE ROUGHNESS VALUES AND CUTTING FORCE DEPENDING ON CUTTING PARAMETERS OF AISI 4140 MATERIAL ON CNC LATHE

Lecturer Sümeyye ERDEM,
Assist. Prof. Dr. Mustafa ÖZDEMİR.....79

CHAPTER 4

RECENT TREND AND DEVELOPMENT OF CAST STEEL

Assist. Prof. Dr Mikail ASLAN.....103

CHAPTER 5

RECENT DEVELOPMENTS OF WELDING OF AEROSPACE MATERIALS

Assist. Prof. Dr Mikail ASLAN.....131

CHAPTER 6

ENVIRONMENTAL IMPACT ASSESSMENT REGULATIONS IN TURKEY: EVALUATION OF METAL RECYCLING PROJECT DECISIONS

Assoc. Prof. Dr. Ayla BILGIN.....145

CHAPTER 7

DETERMINATION OF BIOGAS POTENTIAL OF WASTES FROM DIFFERENT ANIMAL SPECIES IN TUNCELI PROVINCE

Dr. Erdal ÇILĞİN.....159

CHAPTER 8

EVALUATION OF SOME INDUSTRIAL WASTES AND VOLCANIC PUMICE AS BUILDING MATERIALS IN THE CEMENT SECTOR

Assist. Prof. Dr. Abdulvahap KORKMAZ.....179

PREFACE

Developments in the fields of science and engineering have been one of the most crucial factors that have influenced human life and impacted its quality for thousands of years, and the development of new materials and innovations has led to the beginning of new ages in human history. Today, studies on the development and production of new materials, the advancement of existing materials and the recycling of materials are continuing at full pace with great motivation. In this respect, while composite materials come to the fore due to their many advantages, metallic materials and steels are still favored in many applications. On the other hand, the recycling of materials, the evaluation of waste and the more efficient use of resources have become very important, as declining resources and increasing pollution, with increasing demand and consumption, have become one of the biggest problems facing us.

The aim of this book is to put together academic studies in various fields of science and engineering, to present the findings and results of these studies to academicians, researchers and students, and to make reference to the next studies. Therefore, in the expectation that this book would be of interest to all scholars.

Finally, I would like to thank everyone who contributed to the preparation of this book, and I would like to express my special thanks to the authors who contributed to the book chapter.

Assist. Prof. Dr. Ege Anıl DİLER

CHAPTER 1

A STUDY ON FLEXURAL BEHAVIOR OF SANDWICH COMPOSITES WITH E-GLASS REINFORCED POLYMER SKINS AND GRID-SCORED PVC FOAM CORE

Dr. Fatih BALIKOĞLU¹
Dr. Tayfur Kerem DEMİRCİOĞLU²
Asst. Prof. Dr. Ege Anıl DİLER³
Asst. Prof. Dr. Akın ATAŞ⁴

¹ Balıkesir University, Faculty of Engineering, Department of Mechanical Engineering, Balıkesir, Turkey, fatih@balikesir.edu.tr, tkerem@balikesir.edu.tr

² Balıkesir University, Faculty of Engineering, Department of Mechanical Engineering, Balıkesir, Turkey, fatih@balikesir.edu.tr, tkerem@balikesir.edu.tr

³ Ege University, Faculty of Engineering, Department of Mechanical Engineering, Izmir, Turkey, ege.edu.tr

⁴The University of Manchester, Department of Mechanical, Aerospace and Civil Engineering, Manchester, UK, akin.atas@manchester.ac.uk

INTRODUCTION

Sandwich composites are often preferred in engineering applications because of their superior properties such as bending stiffness and light weight characteristics (Carlsson and Kardomateas, 2011). The advantages of sandwich composite structures, such as ease of production and resistance to sea conditions, make these materials an ideal alternative for ship construction (Mouritz and Thomson, 1999; Vinson, 2005; Zenkert, 2009).

Balsa and poly-vinyl chloride (PVC) foam cores are generally used as core material in marine applications. E-glass, carbon or Kevlar® fiber reinforced polymer composites are used as the face sheet materials (Mouritz et al., 2001; Graham-Jones and Summerscales, 2015; Calabrese et al., 2016; Pemberton et al., 2018). Vacuum-assisted resin transfer molding (VARTM) method is widely used for the manufacture of modern boat and yacht hulls and deck parts. The VARTM method ensures that sandwich composites have good dimensional stability and high fiber volume (Dai and Hahn, 2003; Dai et al., 2003).

For infusion methods such as VARTM, SCRIMP, RIFT etc. perforations, grooves and cuts (slits) are machined in closed-cell foam materials to increase the resin permeability and provide sufficient flow and absorption (Reuterlöf, 2002; Reuterlöf, 2003). In other words, perforated and grooved core cuts are used to allow resin flow through the face sheet-core interface of sandwich panels and to wet the face sheet fabrics in a homogeneous manner. The rigid-resin-filled cuts act

as a nail that increases the contact force between the face sheet-core contact surfaces and improves the structural integrity of the sandwich panels. However, such core cuts leads to an increase in the amount of resin and an increase in the weight of sandwich panels (Jhan et al., 2011; Jhan et al., 2012; Truxel et al., 2006; Yokozeki and Iwamoto, 2016).

The effects of core machining configurations on the mechanical performances of sandwich composites have been reported extensively in literature (Abdi et al., 2014; Abdi et al., 2016; Balıkoğlu et al., 2018a; Balıkoğlu et al., 2018b; Balıkoğlu et al., 2020; Fang et al., 2010; Halimi et al., 2013; Juliyana and Krishnan, 2018; May-Pat et al., 2011; Mitra 2010; Mitra and Raja, 2012; Mostafa et al., 2013a; Mostafa et al., 2013b; Mostafa, 2015; Mostafa, 2019). The semicircular grooves milled on the PVC foam surface increased the in-plane shear and compressive strength of sandwich beams (Mitra, 2010; Mitra and Raja, 2012). The effects of the diameter, orientation and pitch values of the grooves on the in-plane shear behavior of sandwich panels were investigated in numerical studies. Based on the non-linear finite element results, it was reported that the surface grooves provided an improvement in the initial stiffness and the in-plane shear strength of the sandwich panel (Mostafa et al., 2013a; Mostafa et al., 2013b, Mostafa, 2015) . As well as semicircular surface grooves, the split semi-torus grooves also increased the shear load carrying capacity of the sandwich beams (Juliyana and Krishnan 2018). The pin reinforced core structures were obtained by filling the holes drilled in the thickness direction in the foam material with resin.

It was determined that resin filled holes provided an improvement in flexural and compression performance of sandwich composites (Abdi et al., 2014; Abdi et al., 2016; Balıkoğlu et al., 2018; Halimi et al., 2013; May-Pat et al., 2011). The grid-scored foams are used in the production of curved parts such as hulls and wind turbine blades. The contour-cuts provide both resin flow and foam deformation on curvilinear surfaces. The resin-rich and the fiber-reinforced cuts increased the bending and compressive strength of sandwich panels (Chen et al., 2018; Fathi et al., 2013; Laustsen et al., 2014; Qi et al., 2016; Wang et al., 2014; Wu et al., 2014).

The aim of this chapter is to describe the advantages & disadvantages of using foam-core sandwich materials, investigate the structural advantages of using grid-scored foam core in sandwich structures in terms of bending strength and stiffness, and compare and validate the analytical formulations with experimental flexural results.

1. SANDWICH COMPOSITES

Sandwich composites are a special type of structural composites in which relatively thicker and lighter core materials are placed between two stiffer and thin face sheets (skin) (Figure 1) (ASTM, 1999). In sandwich concept, stiff and strong face sheets are exposed to in-plane stresses, while the core structure contributes to the balance of the face sheets against general and local buckling by bearing on the shear loads. Also, the core must be rigid against shear and compression loads and must be able to maintain a constant distance between face sheets. Otherwise, especially under the bending loads, the upper and

lower face sheets move independently, the sandwich effect is reduced and the structure may be damaged. The interface between the face sheets and the core materials must provide the transfer of loads in order to continue the cooperation in sandwich components (Carlsson and Kardomateas, 2011; Vinson, 1999; Zenkert, 1995).

Today, there are many materials available for the production of sandwich composites. Commonly used materials for face sheets (skin) can be classified as metallic materials (steel, stainless steel and aluminum alloys) or non-metallic materials (wood plywood, fiber-reinforced plastics), while the cores used in load-bearing sandwich structures are corrugated cardboard or metal structures, honeycomb. (Aluminum, polypropylene, Nomex, Kevlar), balsa wood and polymer foams. Adhesives that hold the face sheets and core structure together and enable them to work together are; epoxy, polyurethane, silicone, acrylic, phenolic etc. chemicals (Karlsson and TomasÅström, 1997; Kaw, 2005).

Foam-core sandwich composites have emerged as a major class of lightweight structural materials (Xiong et al., 2019) (see in Figure 2). The reasons why foam-core sandwich structures are popular materials for use in aerospace, maritime and civil structures can be described as follows;

- High specific bending strength and specific stiffness (Zenkert, 1995),
- High impact resistance and resistant to underwater shock loads (Sutherland, 2018a; Sutherland, 2018b; Sutherland, 2018c),

- Saves weight; contributes to increase in cargo capacity, fuel savings, higher acceleration and stability of the maritime structures (Crupi et al., 2013),
- Corrosion resistant to environmental effects (Kootsookos and Burchill, 2004; Kootsookos and Mouritz, 2004),
- Design and manufacturing flexibility (Karlsson and TomasÅström, 1997),
- Low maintenance costs (Russell, 2005),
- Allows the production of complex and smooth hydrodynamic/aerodynamic surfaces (Mazumdar, 2001),
- Critical properties for military applications: low thermal, acoustic, magnetic and electromagnetic signatures (Mouritz et al., 2001).

One major disadvantage of foam-core sandwich is their higher production costs compared to conventional materials (steel, aluminum and wood); because the production of these materials requires labor intensive. Another disadvantages of these materials are the complexity of the recycling processes resulting from their heterogeneous structure (Singh et al., 2010; Summerscales et al., 2016) and the low thermal resistance such as ignition and flame propagation due to the organic nature of polymers (Egglestone and Turley, 1994; Mouritz and Mathys, 1999).

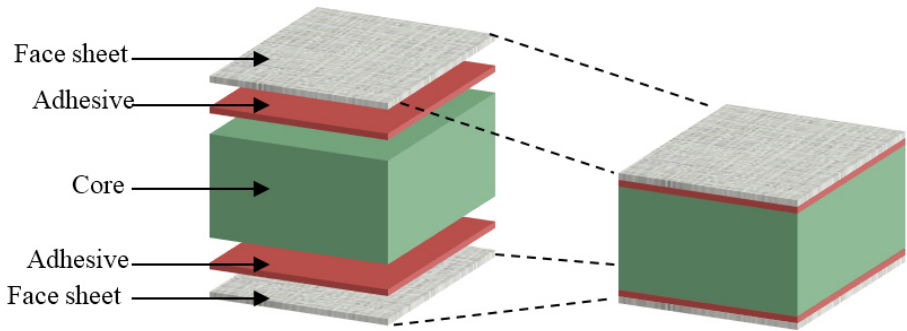


Figure 1: Elements of a Sandwich Structure

Foam-based sandwich structures have been developed to improve the core-face reinforcement. In order to improve their adhesion strength, core machining processes are applied to foam materials (Yokozeki and Iwamoto, 2016). Core cutting also improves the formativeness of foam core and the production quality of foam-core sandwich panels (Halimi et al., 2013; Jhan et al., 2011; Massüger and Gätzi, 2010; Truxel et al., 2006). Core cuts are generally applied to polymer foams in grooved, perforated, and grid-scored (cell, web) patterns. Among these configurations, the grid-scored model allows the production of sandwich composites in curved forms (Figure 3). Therefore, the grid-scored foams are preferred in the production of boat decks and hulls, wind turbine blades, etc. The foams used in the shell structure of the turbine blades are seen in Figure 4 (Laustsen et al., 2014; Pemberton et al., 2018). Another example of such foams is in the hull and deck constructions of military mine-hunter and corvette boats (Branner, 1995; Lindblom, 2003) (see in Figure 5).

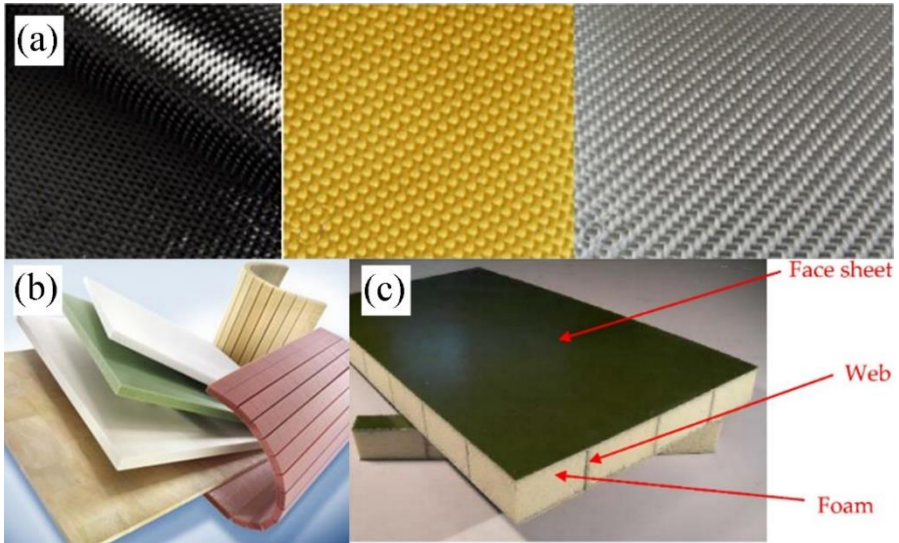


Figure 2: (a) Types of Fibers for Skin (Face-Sheet) (Asmatulu et al., 2018), (b) Types of Core (Web) (Angst and Gätzi, 2009) and (c) Foam Cored Sandwich Structure (Xia et al., 2018)

The grid-scored foam also enables resin flow to the infusion methods through the cuts. The grids were filled with resin after infusion; these rigid-resin-filled cuts significantly increase both the flexural rigidity as well as the shear stiffness of the sandwich beams (Fathi et al., 2013). The grid-scored foams are commercial available in different types of saw-cut, knife-cut and flexible-cut patterns with varying foam densities.

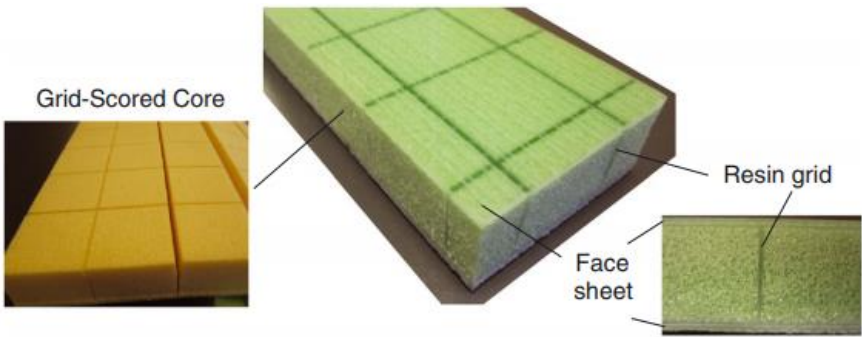


Figure 3: Grid-Scored Foam (Laustsen et al., 2014)

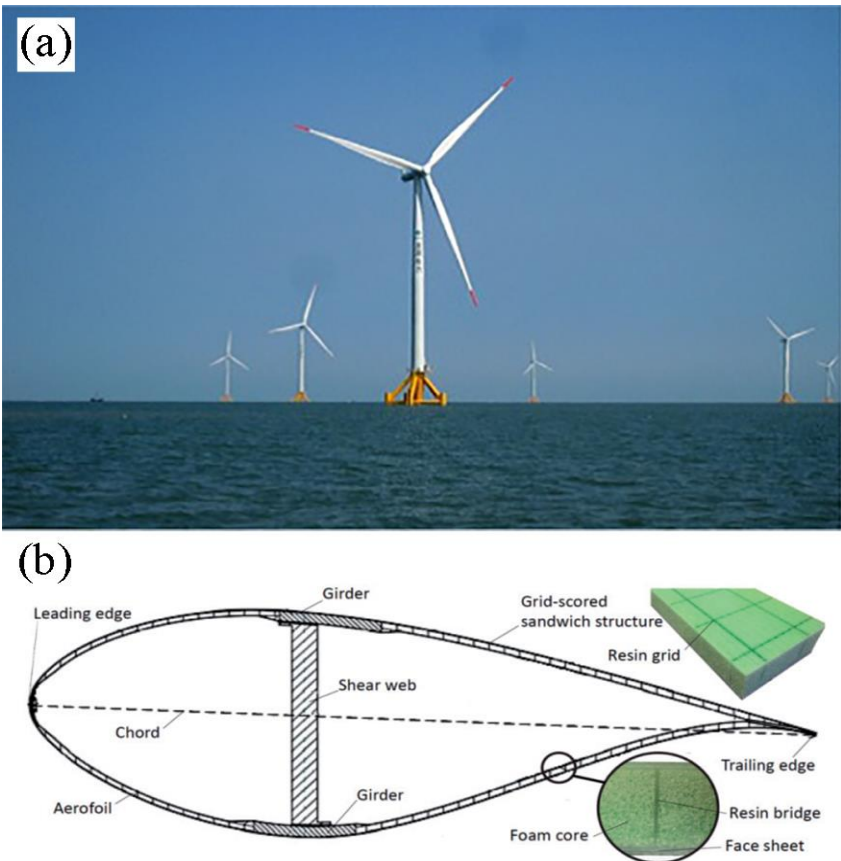


Figure 4: Wind Turbine Application (Laustsen et al., 2014; Pemberton et al., 2018)



Figure 5: Marine Applications (a) Visby corvette (Lindblom, 2003), (b) Standard Flex 300 (Branner, 1995)

2. FLEXURAL BEHAVIOR OF SANDWICH COMPOSITES WITH GRID-SCORED PVC FOAM CORE

2.1. Materials and Manufacturing

Sandwich beams composed of E-glass fabric /vinyl ester face sheets and 25 mm thick Airex C70.75 PVC foam (plain and grid-scored PVC with a density of 80 kg/m³). PVC foam properties were obtained from data sheets and given in Table 1. The grid-scored foam core comprised of 30×30 mm² blocks with a 1.2 mm thickness slit in between and a scrim cloth on the bottom side. [0/90]_{2s}, was selected as skins, with E-glass fabrics (non-crimp stitched) of 850 g/m² areal weight (Metyx Composites Corporation, Istanbul/Turkey). Sandwich composite panels were manufactured by using resin infusion method (VARTM) with a vinyl ester resin system (Polives 702- Bisphenol-A epoxy) (Figure 6).

Table 1: Mechanical Characteristics of the PVC Foam (Datasheet for Airex C70 PVC Foam, 2011)

Properties	Standard	Unit	Value
Density	ISO 845	kg/m ³	80 72 - 92
Compressive strength perpendicular to the plane	ISO 844	N/mm ²	1.45 1.10
Compressive modulus perpendicular to the plane	DIN 53421	N/mm ²	104 80
Tensile strength in the plane	ISO 527 1-2	N/mm ²	2.0 1.6
Tensile modulus in the plane	ISO 527 1-2	N/mm ²	66 50
Shear strength	ISO 1922	N/mm ²	1.2 1.0
Shear modulus	ASTM C393	N/mm ²	30 24
Shear elongation at break	ISO 1922	%	18 10

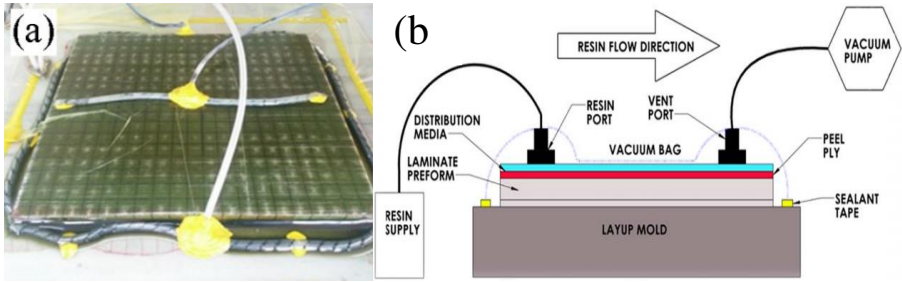


Figure 6: (a) Production of Grid-Scored Foamed Sandwich Composites with VARTM Method and (b) Schematic Illustration of VARTM (Swam et al., 2017)

2.2. Test Set-up

Three-point bending (3PB) and four-point bending (4PB) tests were conducted according to the ASTM C393/C393M-16 standard (ASTM 2016) and schematic representation of flexural loading is given in Fig. 7, where t_c , t_s , b and d refer to the thickness of skin, thickness of the core, beam width and beam depth, respectively. The other test parameters P , a , and L represent the applied load, shear span and support span length of the tested beams. The loading pins and supports had a diameter of 25 mm to avoid premature failure of the beams. The bending tests of the samples were performed using a Zwick Roell Z-250 testing machine with a 250 kN load cell at a constant crosshead speed of 6 mm/min (see in Fig. 8). Five replicates for each sandwich beams were prepared and tested in warp direction. All sandwich beams were tested up to failure to determine the bending strength and failure modes. The dimensions of the sandwich beams are listed in Table 2. In the text, plain foam core sandwich composite is

abbreviated as PFS, and grid-scored foam core sample is abbreviated as GFS.

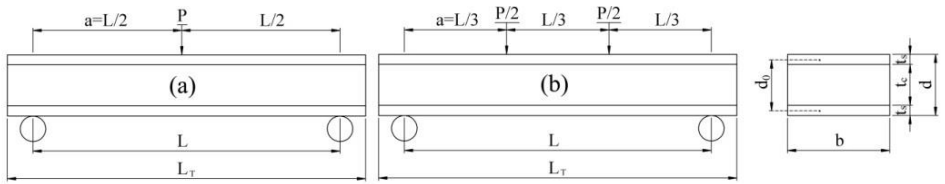


Figure 7: Schematic Representation of Flexural Loading of Composite Sandwich Beams: (a) 3PB Test Set-up, (b) 4PB Test Set-up

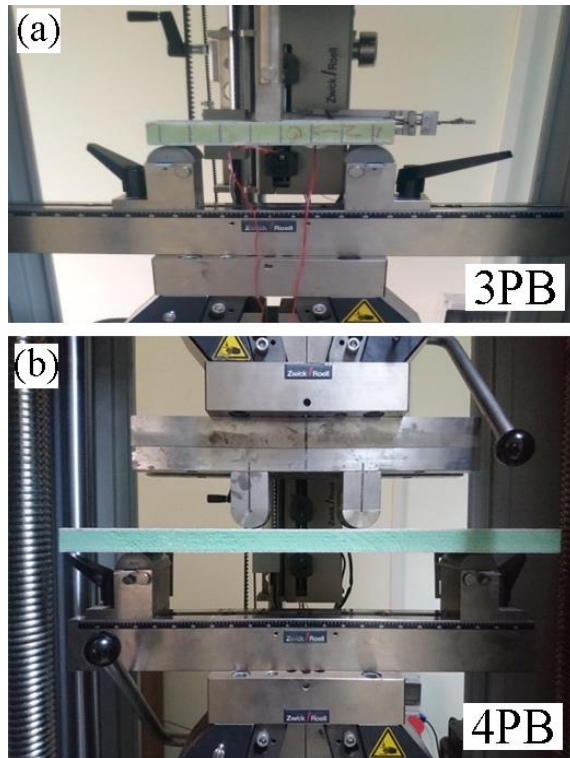


Figure 8: (a) Three-Point (3PB) and (b) Four-Bending (4PB) Tests

Table 2: Details of the Dimensions of Test Specimens

Shear span to depth ratio (a/d)		Total length of the sandwich specimen (L _T), (mm)	Width	Shear span (a), (mm)	Support span (L), (mm)
PFS	GFS				3PB
2	2	180	90	60	120
3	3	240	90	90	180
5	5	360	90	150	300
7.5	7.5	510	90	225	450
					4PB
5	5	510	90	150	450

2.3. Experimental Results and Discussion

Load-crosshead displacement graphs of the sandwich beams with different support spans tested under 3PB and 4PB tests are shown in Figures 9. The test results of all the sandwich beams are given in Table 3, including the failure loads (kN) and failure modes. As seen in Figure 9, the load-displacement curves of the grid-scored foam sandwich composites were stiffer in all span lengths; the rigid-resin cuts increased both the flexural and the shear stiffness of the beams. The results showed that the rigid resin within the core cuts resisted the shear-induced damage and improved the failure load of the beams up to 70% (see in Table 3). Under the similar failure mechanism, the failure loads of the PFS specimens were 65.73% (3PB, 180 mm), 70.1% (3PB, 300 mm), 56.1% (3PB, 450 mm) 28.1% (4PB, 450 mm) higher than those of the PFS specimens. In contrast to the strength improvement, the deflection at failure was decreased in all GFS

specimens in comparison to the PFS beams. This can be due to the limited plastic deformation capability of the resin-filled cuts under shear stresses (Fathi et al., 2013). GFS specimens sustained core shear failure under both 3PB and 4PB when $2 \leq a/d \leq 5$. With increased a/d ratio (7.5), compressive face sheet failure observed in GFS specimens. For $a/d=2$, the resin-filled cuts in the grid-scored foam increased the adhesion between the face sheet and the foam core as well as improving the local stiffness and strength by providing additional support to the upper skin, which prevented the premature failure.

Table 3: Failure Loads and Failure Modes in Glass-Reinforced Polymer Sandwich Composites with Grid-Scored PVC Foam Core

Specimens	Test	Shear-span-to-depth ratio(a/d)	Failure load (kN)	Failure Modes
PFS	3PB	2	5.134	Skin compression
		3	4.377	Core shear+debonding
		5	3.912	Core shear+debonding
		7.5	4.165	Skin compression
	4PB	5	5.620	Core shear+debonding
	GFS	3PB	2	7.904
3			7.254	Core shear+skin compression
5			6.653	Core shear+debonding
7.5			6.501	Skin compression
4PB		5	7.257	Core shear+debonding

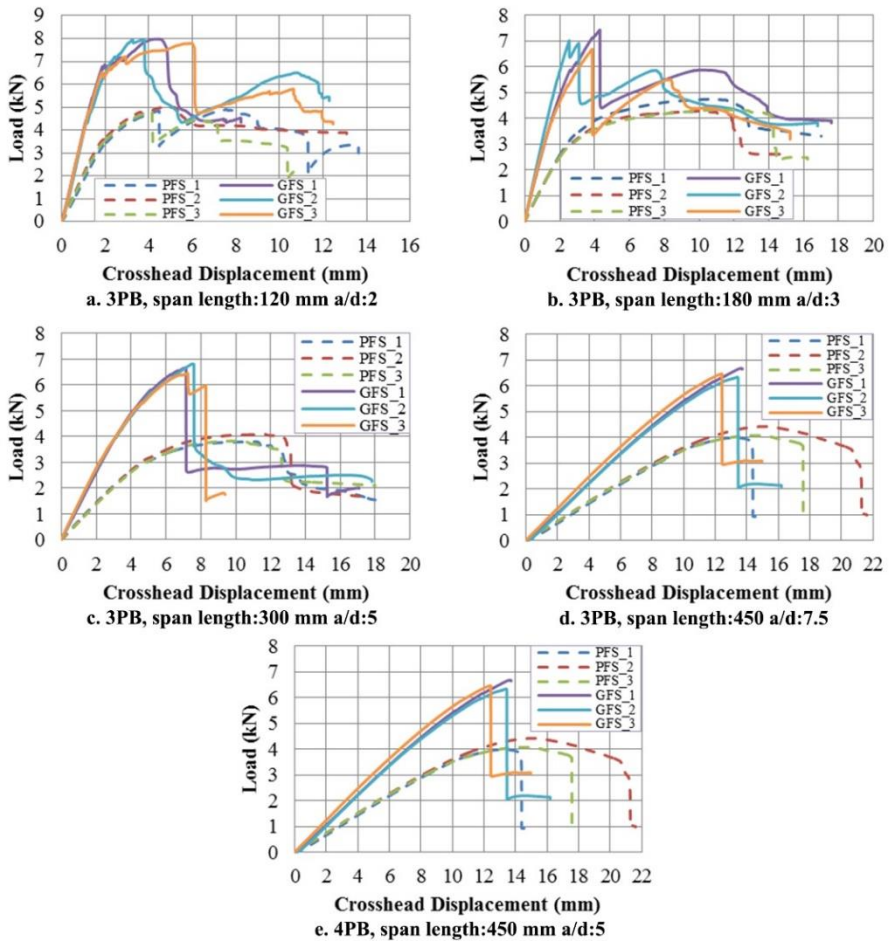


Figure 9: The Relations between Flexural Load and Crosshead Displacement of Glass-Reinforced Polymer Sandwich Composites with Grid-Scored PVC Foam Core (a) 3PB, Span Length: 120 mm , a/d:2, (b) 3PB, Span Length: 180 mm , a/d:3, (c) 3PB, Span Length: 300 mm , a/d:5, (d) 3PB, Span Length: 450 mm , a/d:7.5, (e) 4PB, Span Length: 450 mm , a/d:5

3. ANALYTICAL APPROACH

3.1. Estimation of Equivalent Bending and Shear Stiffness for Grid-Scored Foam Core

Larsen first developed a simple analytical rule of mixtures approach for the accurate prediction of the elastic and shear modulus of grid-scored foam materials (Larsen, 2007; Thomsen and Larsen, 2008). In this proposed method, the unit cell, which is considered to be a perfect bond between the resin grid and the foam components, and which is extracted from the grid-scored foam core structure, is discussed. By looking at a top view of this unit-cell, the Young's modulus in the x direction can be obtained by assuming sections of the cell to be springs in parallel and in series as illustrated in Figure 10.

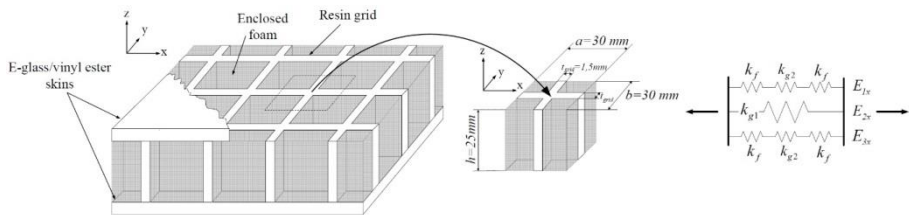


Figure 10: The Unit-Cell Extracted from the Grid-Scored Foam Core and the Spring Analogy of the Elastic Stiffness's of Each Component of the Unit-Cell (Thomsen and Larsen, 2008)

The elastic modulus of the grid scored foam (E_{gsc}) was calculated using Eq. (1) (Thomsen and Larsen, 2008) given below:

$$E_{gsc} = E_x = E_y = \frac{t_{grid}}{b} E_r + \left(1 - \frac{t_{grid}}{b}\right) \frac{E_r E_f}{\left(1 - \frac{t_{grid}}{a}\right) E_r + \frac{t_{grid}}{a} E_f} \quad (1)$$

where t_{grid} is the thickness of the grid and also constant in the whole foam core, a and b are dimensions of the unit-cell and are equals to each other. E_r and E_f are the elastic modulus of the resin and the foam core, respectively. The elastic modulus of the grid-scored foam in the x and y direction are equal. The equivalent bending stiffness ($EI_{eq,gsc}$) of grid-scored foamed sandwich beam can be obtained by Eq. (2):

$$EI_{eq,gsc} = E_s \frac{bt_s d^2}{2} + E_s \frac{bt_s^3}{6} + E_{gsc} \frac{bt_c^3}{12} \quad (2)$$

where E_s and E_c are the elastic modulus of the skin and the foam material, respectively. b is the width of the sandwich beam, $d=t_c+t_s$ is the distance between the center of the face sheets, t_s is the thickness of the face sheet, t_c is the thickness of foam material. In order to determine the shear modulus of the entire unit-cell, it is again required to use the spring analogy of the shear stiffness's of each components of the unit-cell. For this purpose, the adopted unit-cell for the case of the through-thickness shear modulus G_{xz} , is shown in Figure 11.

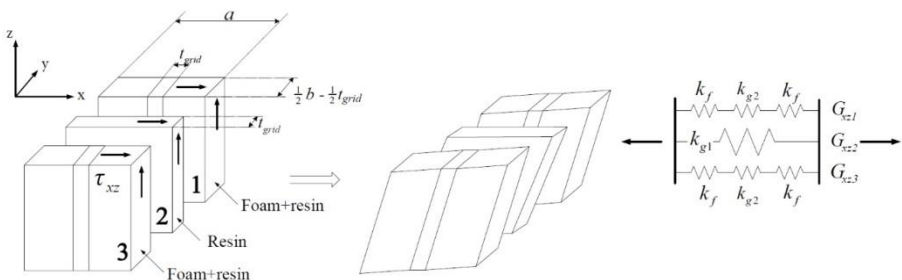


Figure 11: The Illustration of the out-of-Plane Shear Deformations Each Component of the Unit-Cell and the Spring Analogy of the Shear Stiffness's of Each Components of the Unit-Cell (Thomsen and Larsen, 2008)

The shear modulus of grid-scored foam core (G_{gsc}) can be obtained by Eq. (3) (Thomsen and Larsen, 2008):

$$G_{gsc} = G_{xz} = \frac{t_{grid}}{b} G_r + \left(1 - \frac{t_{grid}}{b}\right) \frac{G_r G_f}{\left(1 - \frac{t_{grid}}{a}\right) G_r + \frac{t_{grid}}{a} G_f} \quad (3)$$

in which G_r and G_f are the shear modulus of the resin and the foam, respectively.

The equivalent shear stiffness of the grid-scored foamed sandwich beam ($AG_{eq, gsc}$) can be calculated as Eq. (4):

$$AG_{eq, gsc} = bdG_{gsc} \quad (4)$$

Table 4: The Elastic and Shear Modulus of the Grid Scored Foam Cores

Core material	E_x (MPa)	E_y (MPa)	E_z (MPa)	$G_{xz}=G_{yz}$ (MPa)
Plain PVC foam	50-66	50-60	80-104	24-30
Grid-scored PVC foam	216	216	352	83.5

The elastic and shear modulus of the grid scored plain and grid-scored PVC foam cores are show in Table 4. The modulus of elasticity (E_{gsc}) in the x and y directions of the grid-scored foam core structure was calculated as 216 MPa. This value is equal to 3.27 times the tensile module of the plain PVC foam in the plane. The shear modulus of

grid-scored foam core (G_{gsc}) was calculated as 83.5 MPa, this value is 2.78 times the shear modulus of plain PVC foam.

3.2. Estimation of Mid-Span Deflection of Sandwich Beams

For sandwich beams under bending tests as illustrated in Figure 7, based on the shear deformation theoretical approach, the mid-span displacement is the total of the bending ($\delta_{bending}$) and shear (δ_{shear}) deformation of the beam:

$$\delta_{total,3PB} = \delta_{bending} + \delta_{shear} = \frac{PL^3}{48EI_{eq}} + \frac{PL}{4AG_{eq}} \quad \text{for three-point bending tests} \quad (5)$$

$$\delta_{total,4PB} = \delta_{bending} + \delta_{shear} = \frac{23PL^3}{1296EI_{eq}} + \frac{PL}{6AG_{eq}} \quad \text{for four-point bending tests} \quad (6)$$

where P is the applied load, L is the span of the tested sandwich specimen. The detailed equivalent bending ($EI_{eq,gsc}$) and shear ($AG_{eq,gsc}$) stiffness calculations are given in Section 3.1.

Table 5: Comparison of Experimental and Theoretical Displacement of Glass-Reinforced Polymer Sandwich Composites with Grid-Scored PVC Foam Core

Specimens	Load (kN)	$\delta_{b.th.}$	$\delta_{s.th.}$	$\delta_{tot.th.}$	$\delta_{exp.}$	$\delta_{tot.th.}/\delta_{exp.}$	
		(mm)	(mm)	(mm)	(mm)		
PFS	3PB-180 mm	1 kN	0.071	0.620	0.691	0.72	0.960
		2 kN	0.142	1.240	1.382	1.41	0.980
	3PB-300 mm	1 kN	0.328	1.033	1.361	1.25	1.089
		2 kN	0.657	2.066	2.723	2.44	1.116
	3PB-450 mm	1 kN	1.108	1.550	2.658	2.35	1.131
		2 kN	2.217	3.099	5.316	4.66	1.141
	4PB-450 mm	1 kN	0.944	1.033	1.977	1.74	1.136
		2 kN	1.888	2.066	3.954	3.42	1.156
GFS	3PB-180 mm	1 kN	0.070	0.270	0.339	0.47	0.722
		2 kN	0.139	0.539	0.679	0.85	0.798
	3PB-300 mm	1 kN	0.323	0.449	0.772	0.90	0.858
		2 kN	0.646	0.899	1.544	1.67	0.925
	3PB-450 mm	1 kN	1.089	0.674	1.763	1.86	0.948
		2 kN	2.179	1.348	3.527	3.69	0.956
	4PB-450 mm	1 kN	0.928	0.449	1.377	1.76	0.783
		2 kN	1.856	0.899	2.755	3.23	0.853

Note: $\delta_{b.th.}$: theoretical bending deflection; $\delta_{s.th.}$: theoretical shear deflection; $\delta_{tot.th.}$: total theoretical deflection; $\delta_{exp.}$: total experimental deflection.

Table 5 summarizes the analytical ($\delta_{th.}$) and experimental displacement ($\delta_{exp.}$) values obtained from the linear elastic zone at two particular loads (1 kN and 2 kN). Based on experimental results, as anticipated, the mid-span displacement values of the sandwich beams increased with increasing the shear span to depth ratio (a/d). For GFS

specimen, the greatest variation and the maximum deviation between the analytical and experimental results of mid-span displacements were 0.131 mm and 27.9%, respectively. The proposed reason for this discrepancy is that the theoretical shear modulus of the grid-scored structure is higher than expected. With the shear experiments, the shear modulus of the grid-scored foam material can be obtained and this experimental data may reduce the amount of deviation in the theoretical total displacement values.

CONCLUSION

In this study, the following results were obtained:

- The flexural behavior of plain and grid-scored foam core sandwich beams with different shear span to depth ratios was investigated using 3PB and 4PB bending tests.
- The experimental results indicated that failure loads and failure modes are significantly affected by the shear span to depth ratio. As expected compared to the sandwich beams with a larger a/d ratio, the sandwich beams with a lower a/d ratio damaged at a higher load.
- Using a grid-scored foam core increased the bending strength and stiffness, but the deflection at failure and ductility was significantly decreased.
- The increase in the elastic and shear modulus of the grid-scored foam core compared to plain foam was due to the introduction of the rigid-resin-filled cuts.

- Theoretical results of the sandwich beams, generally underestimated the mid-span displacement values of GFS beams. The possible reason for this difference is that the theoretical shear modulus of the grid-scored foam is higher than expected.
- The shear modulus of the grid-scored foam material can be obtained with the shear experiments and this experimental data could also decrease the amount of deviation in the theoretical total displacement values.

REFERENCES

- Abdi, B., Azwan, S., Abdullah, M., Ayob, A., & Yahya, Y. (2016). Comparison of foam core sandwich panel and through-thickness polymer pin-reinforced foam core sandwich panel subject to indentation and flatwise compression loadings. *Polymer Composites*, 37(2), 612-619.
- Abdi, B., Azwan, S., Abdullah, M., Ayob, A., Yahya, Y., & Xin, L. (2014). Flatwise compression and flexural behavior of foam core and polymer pin-reinforced foam core composite sandwich panels. *International Journal of Mechanical Sciences*, 88, 138-144.
- Angst, P., & Gätzi, R. (2009). One core does not fit all, <https://www.materialstoday.com/composite-applications/features/one-core-does-not-fit-all/>
- Asmatulu, E., Alonayni, A., & Alamir, M. (2018). Safety Concerns in Composite Manufacturing and Machining. *Proceedings of SPIE, Behavior and Mechanics of Multifunctional Materials and Composites XII, Colorado/USA*.
- ASTM. (1999). ASTM C274-99, ASTM standard terminology of structural sandwich constructions. ASTM International.
- ASTM. (2016). ASTM C393 / C393M-16, Standard Test Method for Core Shear Properties of Sandwich Constructions by Beam Flexure ASTM International.
- Balıkoğlu, F., Arslan, N., Demircioğlu, T., İnal, O., İren, M., & Ataş, A. (2020). Improving four-point bending performance of marine composite sandwich beams by core modification. *Journal of Composite Materials*, 54(8), 1049-1066.
- Balıkoğlu, F., Demircioğlu, T., Yıldız, M., Arslan, N., & Ataş, A. (2018a). Mechanical performance of marine sandwich composites subjected to flatwise compression and flexural loading: Effect of resin pins. *Journal of Sandwich Structures & Materials*, 1099636218792671.
- Balıkoğlu, F., Demircioğlu, T. K., İnal, O., & Arslan, N. (2018b). FEM Analysis of Flexural Behavior of Grooved Perforated and Web Foamed Marine Sandwich

- Composite Beams Effects of Core Machining Configuration. 21st International Conference on Composite Structures, Bologna/Italy.
- Branner, K. (1995). Capacity and lifetime of foam core sandwich structures. Institutitet for skibs-og havteknik, Danmarks tekniske universitet.
- Calabrese, L., Di Bella, G., & Fiore, V. (2016). Manufacture of marine composite sandwich structures in: *Marine Applications of Advanced Fibre-Reinforced Composites* (pp. 57-78). Elsevier.
- Carlsson, L. A., & Kardomateas, G. A. (2011). Structural and failure mechanics of sandwich composites (Vol. 121). Springer Science & Business Media.
- Chen, J., Fang, H., Liu, W., Qi, Y., & Zhu, L. (2018). Experimental and numerical analysis of nonlinear flexural behaviour of lattice-web reinforced foam core composite sandwich panels. *Advances in Civil Engineering*, 2018.
- Crupi, V., Epasto, G., & Guglielmino, E. (2013). Comparison of aluminium sandwiches for lightweight ship structures: honeycomb vs. foam. *Marine Structures*, 30, 74-96.
- Dai, J., & Hahn, H. T. (2003). Flexural behavior of sandwich beams fabricated by vacuum-assisted resin transfer molding. *Composite Structures*, 61(3), 247-253.
- Dai, J., Pellaton, D., & Hahn, H. (2003). A comparative study of vacuum-assisted resin transfer molding (VARTM) for sandwich panels. *Polymer Composites*, 24(6), 672-685.
- Datasheet for Airex C70 PVC Foam. (2011).
- Egglestone, G., & Turley, D. (1994). Flammability of GRP for use in ship superstructures. *Fire and Materials*, 18(4), 255-260.
- Fang, H., Liu, W., Lu, W., & Wan, L. (2010). Flexural properties of grooved perforation sandwich composites. *Journal of Wuhan University of Technology-Mater. Sci. Ed.*, 25(4), 583-587.
- Fathi, A., Wolff-Fabris, F., Altstädt, V., & Gätzi, R. (2013). An investigation on the flexural properties of balsa and polymer foam core sandwich structures: Influence of core type and contour finishing options. *Journal of Sandwich Structures & Materials*, 15(5), 487-508.

- Graham-Jones, J., & Summerscales, J. (2015). *Marine applications of advanced fibre-reinforced composites*. Woodhead Publishing.
- Halimi, F., Golzar, M., Asadi, P., & Beheshty, M. (2013). Core modifications of sandwich panels fabricated by vacuum-assisted resin transfer molding. *Journal of Composite Materials*, 47(15), 1853-1863.
- Jhan, Y.-T., Lee, Y.-J., & Chung, C.-H. (2011). Resin flowing analysis in sandwich laminates under VARTM process. *Journal of Reinforced Plastics and Composites*, 30(6), 533-545.
- Jhan, Y.-T., Lee, Y.-J., & Chung, C.-H. (2012). Experimental and numerical investigation of the VARTM process with a sandwich structure. *Journal of Composite Materials*, 46(12), 1417-1430.
- Juliyana, M., & Krishnan, R. S. (2018). Experimental and simulation of split semi-torus key in PVC foam core to improve the debonding resistance of composite sandwich panel. *Materials Research Express*, 5(2), 025307.
- Karlsson, K. F., & TomasÅström, B. (1997). Manufacturing and applications of structural sandwich components. *Composites Part A: Applied Science and Manufacturing*, 28(2), 97-111.
- Kaw, A. K. (2005). *Mechanics of composite materials*. CRC press.
- Kootsookos, A., & Burchill, P. (2004). The effect of the degree of cure on the corrosion resistance of vinyl ester/glass fibre composites. *Composites Part A: Applied Science and Manufacturing*, 35(4), 501-508.
- Kootsookos, A., & Mouritz, A. (2004). Seawater durability of glass-and carbon-polymer composites. *Composites Science and Technology*, 64(10-11), 1503-1511.
- Larsen, J. (2007). *A Study of the Strength and Stiffness of Sandwich Structures Made with GridScored Core*, Aalborg University].
- Laustsen, S., Lund, E., Kühlmeier, L., & Thomsen, O. T. (2014). Failure behaviour of grid-scored foam cored composite sandwich panels for wind turbine blades subjected to realistic multiaxial loading conditions. *Journal of Sandwich Structures & Materials*, 16(5), 481-510.

- Laustsen, S., Lund, E., Kühlmeier, L., and Thomsen, O.T. (2014). Development of a high-fidelity experimental substructure test rig for grid-scored sandwich panels in wind turbine blades. *Strain* 50, 111–131.
- Lindblom, F. (2003). Use of composites in the Visby-class stealth corvette. *Proceedings of the Conference on Marine Composites*.
- Massüger, L., & Gätzi, R. (2010). Effects of groove configurations on fatigue resistance of infused sandwich panels. *Proceedings of the 10th International Conference on Flow Processes in Composite Materials (FPCM-10)*.
- May-Pat, A., Aviles, F., & Aguilar, J. (2011). Mechanical properties of sandwich panels with perforated foam cores. *Journal of Sandwich Structures & Materials*, 13(4), 427-444.
- Mazumdar, S. (2001). *Composites manufacturing: materials, product, and process engineering*. CRC press.
- Mitra, N. (2010). A methodology for improving shear performance of marine grade sandwich composites: sandwich composite panel with shear key. *Composite Structures*, 92(5), 1065-1072.
- Mitra, N., & Raja, B. (2012). Improving delamination resistance capacity of sandwich composite columns with initial face/core debond. *Composites Part B: Engineering*, 43(3), 1604-1612.
- Mostafa, A. (2015). Numerical analysis on the effect of shear keys pitch on the shear performance of foamed sandwich panels. *Engineering Structures*, 101, 216-232.
- Mostafa, A. (2019). Experimental and numerical investigation on enhancing the structural integrity of composite sandwich structure. *Advances in Structural Engineering*, 1369433219836177.
- Mostafa, A., Shankar, K., & Morozov, E. (2013a). Effect of shear keys diameter on the shear performance of composite sandwich panel with PVC and PU foam core: FE study. *Composite Structures*, 102, 90-100.
- Mostafa, A., Shankar, K., & Morozov, E. (2013b). Influence of shear keys orientation on the shear performance of composite sandwich panel with PVC foam core: numerical study. *Materials & Design*, 51, 1008-1017.

- Mouritz, A., Gellert, E., Burchill, P., & Challis, K. (2001). Review of advanced composite structures for naval ships and submarines. *Composite Structures*, 53(1), 21-42.
- Mouritz, A., & Thomson, R. (1999). Compression, flexure and shear properties of a sandwich composite containing defects. *Composite Structures*, 44(4), 263-278.
- Mouritz, A. P., & Mathys, Z. (1999). Post-fire mechanical properties of marine polymer composites. *Composite Structures*, 47(1-4), 643-653.
- Pemberton, R., Summerscales, J., & Graham-Jones, J. (2018). *Marine Composites: Design and Performance*. Woodhead Publishing.
- Qi, Y., Fang, H., & Liu, W. (2016). Experimental study of the bending properties and deformation analysis of web-reinforced composite sandwich floor slabs with four simply supported edges. *PloS one*, 11(2), e0149103.
- Reuterloev, S. (2003). Grooved Core Materials aid resin infusion- influence on mechanical properties. *SAMPE Journal*, 39(6), 57-64.
- Reuterlöv, S. (2002). Cost effective infusion of sandwich composites for marine applications. *Reinforced Plastics*, 46(12), 30-34.
- Russell, C. (2005). Composites: long-term viability and benefits. *Reinforced Plastics*, 49(9), 36-42.
- Singh, M., Summerscales, J., & Wittamore, K. (2010). Disposal of composite boats and other marine composites in: *Management, Recycling and Reuse of Waste Composites*. Elsevier, pp 495-519.
- Summerscales, J., Singh, M., & Wittamore, K. (2016). Disposal of composite boats and other marine composites in: *Marine Applications of Advanced Fibre-Reinforced Composites*. Elsevier, pp 185-213
- Sutherland, L. (2017). A review of impact testing on marine composite materials: Part I–Marine impacts on marine composites. *Composite Structures*, 188, 197-208.
- Sutherland, L. (2018a). A review of impact testing on marine composite materials: Part II–Impact event and material parameters. *Composite Structures*, 188, 503-511.

- Sutherland, L. (2018b). A review of impact testing on marine composite materials: Part III-Damage tolerance and durability. *Composite Structures*, 188, 512-518.
- Swan, S., Yuksel, T., Kim, D., & Gurocak, H. (2017). Automation of the vacuum assisted resin transfer molding process for recreational composite yachts. *Polymer Composites*, 38(11), 2411-2424.
- Thomsen, O. T., & Larsen, J. (2008). Simplified Rule of Mixtures Approach for the Accurate Estimation of the Elastic Properties of Grid-Scored Polymer Foam Core Sandwich Plates. *International Conference on Sandwich Structures*.
- Truxel, A., Aviles, F., Carlsson, L., Grenestedt, J., & Millay, K. (2006). Influence of face/core interface on debond toughness of foam and balsa cored sandwich. *Journal of Sandwich Structures & Materials*, 8(3), 237-258.
- Vinson, J. R. (1999). *The behavior of sandwich structures of isotropic and composite materials*. CRC Press.
- Vinson, J. R. (2005). Sandwich structures: past, present, and future, in: *Sandwich Structures 7: Advancing with Sandwich Structures and Materials*. Springer, pp 3-12.
- Wang, L., Liu, W., Wan, L., Fang, H., & Hui, D. (2014). Mechanical performance of foam-filled lattice composite panels in four-point bending: Experimental investigation and analytical modeling. *Composites Part B: Engineering*, 67, 270-279.
- Wu, Z., Liu, W., Wang, L., Fang, H., & Hui, D. (2014). Theoretical and experimental study of foam-filled lattice composite panels under quasi-static compression loading. *Composites Part B: Engineering*, 60, 329-340.
- Xia, Y., Li, X., Peng, Y., Lai, M., & Wang, L. (2018). Impact and post-impact performance of sandwich wall boards with GFRP face sheets and a web-foam core: The effects of impact location. *Materials*, 11(9) 1714.
- Xiong, J., Du, Y., Mousanezhad, D., Eydani Asl, M., Norato, J., & Vaziri, A. (2019). Sandwich structures with prismatic and foam cores: A review. *Advanced Engineering Materials*, 21(1), 1800036.

- Yokozeiki, T., & Iwamoto, K. (2016). Effects of core machining configuration on the debonding toughness of foam core sandwich panels. *Advanced Composite Materials*, 25(1), 45-58.
- Zenkert, D. (1995). An introduction to sandwich structures. <https://www.diva-portal.org/smash/get/diva2:1366182/FULLTEXT01.pdf>.
- Zenkert, D. (2009). Damage tolerance of naval sandwich panels, in: *Major Accomplishments in Composite Materials and Sandwich Structures* (pp. 279-303). Springer.

CHAPTER 2

DETERMINING ELASTIC COEFFICIENTS OF COMPOSITE MATERIALS BY MECHANICAL METHODS

Prof. Dr. Hatice GUZEL¹, Teacher Mehmet KARABULUT²,
Assoc. Prof. Dr. Imran ORAL³

¹ Karamanoglu Mehmetbey University, Education Faculty, Science Education Department, Karaman, Turkey, haticeguzel@kmu.edu.tr, ORCID ID: 0000-0001-5678-4447.

² Ministry of National Education, Konya, Turkey, mkarabulut42@hotmail.com.

³ Necmettin Erbakan University, Ahmet Kelesoglu Education Faculty, Physics Education Department, Konya, Turkey, oralimran@erbakan.edu.tr, ORCID ID: 0000-0002-5299-5068.

P.S. This chapter of the book is produced from the master of science thesis titled: The Verification of Ultrasonically Determined Material Constants by Mechanical Experiments

INTRODUCTION

Throughout history, people have needed materials to survive and have a better standard of living. Materials are essential components of almost everything we use in our daily life. The materials currently used have failed to technology over time, and it has become necessary to develop materials with superior properties. Naturally formed or artificially produced materials are used in all kinds of sectors, for instance, space, aviation, computer, electronics, automotive, chemical, biomedical, food, etc. Materials can be divided into five main groups; composites, electronic and photonic materials, polymers, ceramics, and metals (Çolak, 2004). Especially after the start of space research, composite materials, which are frequently started to be used in the aviation industry, have become the best alternative in this field. Composite materials are different materials formed by physically combining at least two inorganic or organic components (Kaya and Kılınc, 2008). The composite materials produced by this process can be given properties such as flexibility, strength, and lightness that the components that make up the composite material cannot have alone (Zor, 2018).

Composite materials consist of two basic components called fiber and matrix. While the matrix is used as the main material, fiber provides the durability and load-bearing ability of the materials. The functions of a matrix are to ensure proper placement by connecting the fibers, to protect the fibers against the effects of the environment, to delay the rupture of the material by resisting the spread of the crack in plastic

deformation, and to protect the material against high corrosion and temperature. An ideal matrix material should first be of a low viscosity structure and then easily transform into a solid-state that will enclose the fibers solidly. The fibers used as reinforcement in the matrix are the main strength members of the composite materials. Fibers have high Young's modulus, tensile strength, breaking strength, and hardness. They are also resistant to chemical corrosion as well as their low density. Carbon, glass, ceramic, boron, and aramid fibers are the main reinforcement elements used in composites (Asi, 2008).

The most important element in the production of composite materials is to choose the most suitable fiber and matrix to obtain materials with better properties. To improve properties such as durability, hardness, fatigue, moisture, and thermal resistance, the appropriate fiber direction should be selected during the production phase. These properties vary greatly depending on the fiber direction and angle chosen. For these reasons, matrix and fiber type are very important in composite design (Kaya and Kılınç, 2008).

Fibers are indispensable basic units in the production of modern composites. Glass fiber is the most known and used among fiber-reinforced composites (Mallick, 1993). Carbon, boron, carbide, aramid, and silicon fibers, which are among the fibers developed in recent years, have been used in newly developed composite structures. Thanks to the production of finer fibers, the probability of structural errors in composite production is minimized compared to large and

bulk fibers. Therefore, composites have superior mechanical properties (Asi, 2008).

Glass Fiber

Glass fiber is the most preferred fiber type in the production of composite materials due to its economic nature. It was first produced as A-glass, but later on, E-glass, also known as boron silicate glass, which is more advanced in terms of mechanical properties, has been used. Glass fibers have high impact and tensile strength. Young's modulus is also quite high.

The fibers can corrode each other by rubbing. Its mechanical properties are not affected by high temperatures. The mechanical properties of some glass fibers are given in Table-1.

Table 1. Mechanical Properties of Some Glass Fibers (Kılıç, 2006)

Glass fiber Type	Density (gr/cm³)	Tensile Strength (MPa)	Elongation Ratio (%)	Young's Modulus (GPa)
A-glass	2.45	3100	-	72
C-glass	2.45	3400	4.8	70
S-glass	2.49	4500	5.4	86
E-glass	2.54	3600	4.8	76

Glass fibers are produced in many varieties, from classical glass to a higher purity quartz glass. Glass has a polymer structure and is an amorphous material. In its three-dimensional molecular structure, there is a silicon atom and four oxygen atoms around it. Silicium is light and non-metallic material. In nature, it usually takes place in the form of silica and with two oxygen atoms (SiO₂). To obtain glass,

additives and silica sand are heated up to 1260 ° C in a dry state. As it cools, it turns into a hard structure.

The main properties of glass fibers are given below.

- Their tensile strength is quite high. Their strength per unit weight is higher than steel.
- They can not have the ability to absorb moisture. In composite materials, decomposition may occur between glass fiber and matrix with moisture. However, this can be prevented by the special fiber coating.
- Their thermal resistance is very low. They do not burn but soften at high temperatures.
- They have no electricity conducting properties. It can be used easily when electrical insulation is required
- They have high resistance to chemical materials.

When various additives are added to silica sand in the production of glass fibers, the material has different properties with the effect of the added substances. There are four different types of glass fiber:

- **Alkali (A) Glass:** It is a type of glass with high alkalinity. Therefore, its electrical insulation is bad. It is the most common glass type with the highest chemical resistance.
- **Chemical (C) Glass:** It is very resistant to chemical solutions. For this reason, they are mostly preferred in storage tanks.
- **Electrical (E) Glass:** Due to its low alkali rate, its electrical insulation is very good. Its durability and resistance to water are

very high. E-glass is used in composites produced for most humid environments.

- **Strength (S) Glass:** It is a high strength glass. Its tensile strength is 33% higher than E-glass. Also, high-temperature fatigue resistance is very good. With these features, they are preferred in the space and aviation industry.

Glass fibers are the most used fiber type among polymer composites. Today, more than 2/3 of the reinforcement elements used with thermoset resins are glass fibers. The melting point of silica, which is the main material of glass fiber, is approximately 840 ° C.

The properties of glass fibers can be changed positively by adding different materials. While glass fibers are advantageous with their high tensile strength, chemical resistance, low production cost, and superior insulation properties; They are disadvantageous with their low young modulus, fatigue resistance, high hardness, and easy corrosion during their usage.

Unlike other reinforcement elements, glass fibers have an anisotropic structure. This is because of the 3-dimensional lattice in their structure. Glass fibers can be easily damaged by friction. Coating with a material such as slashing product can protect glass fibers from this damage.

Moisture resistant glass fiber types are used in the production of liquid tanks, racing boots, and boats. More durable and light fiber types are preferred in the production of helicopter and aircraft fuselage and wings, and automobile panels.

Glass fiber is known as the most used reinforcement element among the materials used in the reinforcement of thermoset and thermoplastic composites. Due to its high tensile strength and low elongation ratio, glass fiber increases the bending, tensile, and impact strength of composites and provides high elastic modulus properties to them. Besides, the low water absorption property of glass fibers provides them good dimensional stability and high resistance to climatic conditions.

It is possible to classify glass fiber products depending on their production processes and intended use as follows:

- Multi end roving (trimmable roving)
- Single-end roving (direct winding roving)
- Felt (fluid bonded felt, powder bonded felt)
- Woven fabric
- Chopped strand

Carbon Fibers

Carbon fibers are the most preferred reinforcement structures for composite material production that requires high performance. Carbon fibers are produced as continuous fibers with high Young's modulus, durability, high strength at high temperatures, and no discontinuity feature. Thanks to its superior mechanical properties, it is one of the advanced composites used in the aerospace and aircraft industry.

Carbon fibers can be used in situations that require lightness and durability. These fibers are used in the aviation industry as control

elements such as stabilizers, airfoils, and elevator controls, in the marine and automobile industry as structural support elements, in some structures of racing car hoods, in some parts of spacecraft and missiles, in production of fishing rods, rackets, and bicycle pedals.

Among the advantages of carbon fiber is less deformation under constant load, and less fatigue resistance at normal temperatures. Being very easily breakable, having a low expansion coefficient against high loads and high production costs make these composites disadvantageous (Kaya and Kılınç, 2008).

Advantages of Composite Materials

- By using different materials in different layers and combinations, composite materials with targeted mechanical properties can be produced.
- Composites can withstand chemical corrosion and harsh weather conditions.
- Producing complex structures as a whole reduces the number of parts. This makes the production process shorter.
- It provides the opportunity to produce lighter and stronger materials as an alternative to standard lightweight and strong materials.
- Materials with low specific bulk density and high strength can be produced.
- Materials with low weight and high modulus of elasticity can be produced

- Thanks to their flexibility during the production phase, it is possible to produce materials that are more resistant to corrosion, with long fatigue life and low thermal conductivity compared to conventional materials.

Disadvantages of Composite Materials

- Production costs can be high.
- The properties of composites combined with heat and pressure cannot always give the desired result. Composite produced too thick can have low durability and low shear strength.
- If the production method is not good enough, the material quality may be lower.
- Composites are brittle (fragile) materials so they can be easily damaged. Sometimes repairing this damage can lead to new problems.

Mechanical Properties of Materials

The materials should be resistant to various effects where they are used. The resistance of the structure to the load it encounters depends on the mechanical properties of the materials preferred in production. Therefore, the mechanical properties of the materials used are very important (Yılmaz and Altıntaş, 1997).

Material properties are mostly determined by the internal structure of atoms and molecules. The three-dimensional arrangement of atoms in space and the bonding forces between atoms determine the internal

structure. Electrons are the main reason for the formation of these bonds. It is the valence electrons in the outermost orbit that determine the chemical, physical and mechanical properties of substances. The forces that bind atoms to each other determine the internal structure of the atom. This internal structure creates the durability, heat, and electrical properties of the materials. The stronger the bonds between atoms, the higher the modulus of elasticity, strength, and melting temperature, against this, the lower the expansion (Oral, 2011).

The bond type, bond energy, and atomic arrangement between atoms determine the properties of the material. The material resists external forces applied, thanks to the bonding forces between atoms. This prevents the shape-changing and breaking of the material (Onaran, 2006).

The concept of stress and strain can be used to explain the elasticity properties of materials.

Stress

The external force that is proportional to the force causing deterioration in the material and acting per unit cross-section in the material is called Stress. The mathematical equality of force shown with the symbol σ is given in equation (1) (Serway and Brichner, 2002).

$$\sigma = \frac{F}{A_0} \quad (1)$$

Tensile Strength, σ_{ts} : The maximum tensile stress that the material

will withstand until rupture and fracture is called **tensile strength**.

This value corresponds to the greatest stress in the stress-strain graph obtained in the tensile test. The mathematical expression of tensile strength is as in equation (2).

$$\sigma_{ts} = \frac{F_{max}}{A_0} \quad (2)$$

Ultimate Stress, σ_u : It is expressed as the stress at the moment when the test sample breaks. The mathematical expression of the breaking stress is defined as in equation (3).

$$\sigma_u = \frac{F_k}{A_0} \quad (3)$$

Strain

The strain is the change in size as a result of the materials showing fluid properties when stress is applied to them. In short, the shape change that occurs on the unit surface is called strain. Strain as a physical quantity indicated by the symbol ε is mathematically represented by equation (4) (Serway and Brichner, 2002).

$$\varepsilon = \frac{\Delta L}{L_0} \quad (4)$$

Elasticity Modulus

Under sufficiently small tension; Stress is directly proportional to strain. This ratio constant depends on the type of material and the nature of the deterioration. This ratio is called elasticity modulus or

elasticity constant (Oral,2011). Thus, the elasticity constant is formulated as the ratio of force to strain, as seen in equation (5)

$$\text{Elasticity} = \frac{\text{Stress}}{\text{Strain}} \quad (5)$$

Different modulus of elasticity can be explained as transverse, longitudinal, and bulk modulus depending on the form of deterioration.

Young's Modulus

Young stated that in small sufficiently tensions; the stress varies in direct proportion to the strain and the proportional constant depends on the type of material and the nature of the deterioration (Oral, 2011). This ratio constant is called Young's modulus. Young's modulus is a function of orientation, denoted by "E".

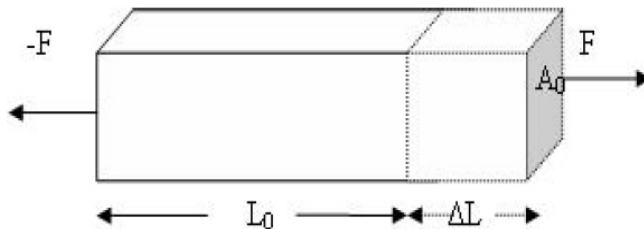


Figure 1. A Long Rod Extended by ΔL under the Influence of the Force F (Oral, 2011)

As in Figure-1, if a force F is applied from the outside perpendicular to the cross-sectional area to a rod with an area A_0 and a length L_0 , the internal forces in the rod resist the change of its shape. Eventually, external and internal forces acting on the rod are balanced. The length

of the bar increases slightly when the forces are in balance. In this case, it can be said that the rod is under the influence of stress. The ratio of the external force (F) to the cross-sectional area of the bar (A_0) is called stress (σ), while the ratio of the length change (ΔL) in the rod to the first length (L_0) of the rod is expressed as the strain (ϵ). By writing these in equation (6), the elastic modulus (E) of this rod is obtained;

$$\text{Elasticity} = \text{Stress/Strain} \rightarrow E = \frac{\frac{F}{A_0}}{\frac{\Delta L}{L_0}} \text{ N/m}^2 \quad (6)$$

The high ratio obtained indicates the strength of the material. The modulus of elasticity gives information about how strong the bonds between atoms and molecules in a crystal structure are (Dinçer, 2004). The greater the modulus of elasticity, the stronger the bonds between atoms. If the modulus of elasticity is high, the material is more resistant to tension or pressure in the direction of the force. In the directions where this ratio is low, the substance easily deteriorates.

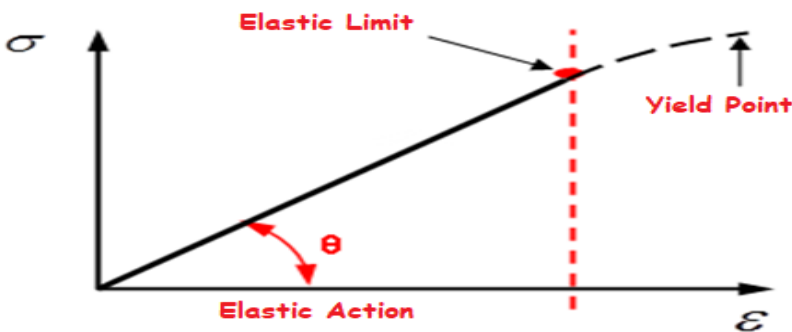


Figure 2. The Change Graph of Stress (Σ) / Strain (E) for Material at the Elastic Limit

The stress and strain relationship on the elastic part of the object to which external force is applied is expressed by the following equation.

$$\sigma = E \cdot \varepsilon \quad (7)$$

Equation (7) is known as Hook's law. As can be understood from Figure-2, the slope in the elastic region gives E, which is the modulus of elasticity. By applying greater tension, the elasticity limit of the material can be exceeded. When the tension exceeds this limit, the object is extremely distorted. Even if the force is not applied, the object can not return to its original form. After the elastic limit, the stress-strain curve is not linear. Thus, the slope is changed. When the stress is increased further, the material breaks.

Shear Modulus

As seen in Figure-3, if one side of the material is fixedly fastened by F_f friction force, and the force F is applied tangent to the surface on the other side, a different form of distortion occurs. The cross-section of the material, which is initially in the form of a rectangular prism, turns into a parallel edge due to the shear stress. The stress that causes this situation is called the shear stress and is represented by the symbol τ . As a result of this deterioration, there is no change in the volume of the material. The shear stress (τ), the ratio of the force F which is tangent to the surface A_0 to the surface A_0 is defined as seen in equation (8) (Oral,2011).

$$\tau = \frac{F}{A_0} \quad (8)$$

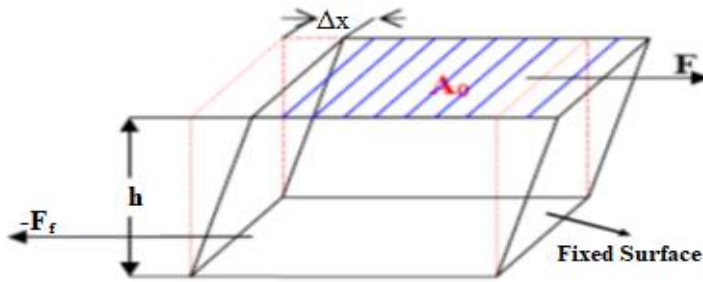


Figure 3. The Shear Deformation in the Block Whose One Surface is Fixed Due to the Force F Tangent to the Other Surface (Oral, 2011)

As for shear strain, it is represented by the symbol, γ , and is found by the equation $\gamma = \Delta x/h$. Δx is the displacement of the sheared surface in the direction of the force, and "h" is the height of the object. In the elastic deterioration of the bodies, the shear stress and the shear strain are directly proportional. This ratio constant is also known as the Modulus of Shear, denoted by G . The ratio of the shear stress (τ) and the shear strain (γ) from here gives G (Oral,2011).

$$G = \frac{\tau}{\gamma} = \frac{F/A_0}{\Delta x/h} \quad (9)$$

Shear Modulus is a measure of the resistance of the body to the motion caused by the shift of the atomic planes of the body on each other.

The shear modulus is related to hydrogen or Van der Waals bonds, which are very weak (Serway and Brichner, 2002).

Bulk Modulus

We suppose that external forces applied to an object act on all surfaces of the object at right angles and this is equally distributed over all surfaces. In such a situation, the volume of the object decreases but its shape does not change. The volume of stress is denoted by ΔP . The ratio of the magnitude of the force F applied perpendicular to the surface of the material to the material surface (A) gives the volume stress. $\Delta P = F / A$ equation is also defined as pressure. The ratio of the change in the volume of the object (ΔV) to its initial volume (V) is called volume strain. Bulk modulus (K) can be expressed mathematically using equation (10):

$$\text{Bulk Modulus} = \frac{\text{Volume Stress}}{\text{Volume Strain}} \rightarrow K = -\frac{F/A}{\Delta V/V} = -\frac{\Delta P}{\Delta V/V} \quad (10)$$

The “-” sign in Equation (10) has been put to ensure that B is a number with a “+” sign. Because an initial increase ($+\Delta P$) causes the volume to decrease ($-\Delta V$). If the pressure becomes smaller ($-\Delta P$), the volume increases ($+\Delta V$) (Serway, 2002)

The inverse of the volume constant is called the compressibility of the substance. While solids and liquids have volume constants, liquids have no shear modulus and Young's modulus. Because shear stress cannot be applied to liquids. Because they are real fluids (Oral,2011).

Poisson's Ratio

Simeon Denis Poisson has made important experiments and developed theories on the lateral contraction of materials. The Poisson ratio, defined by the French scientist Simeon Denis Poisson and named after him, is a mechanical parameter that provides important information about the structure of many materials. Under small stresses in linear elastic materials, the lateral contraction ($\epsilon_{\text{lateral}}$) is proportional to the longitudinal elongation (ϵ_{axial}) and the proportional coefficient is called the Poisson's ratio (Onaran, 2006; Abi, 2007). Poisson's ratio can be both positive and negative. Many materials have a positive Poisson's ratio. However, in some natural and artificial materials defined as auxetic materials, the Poisson's ratio is negative. The Poisson's ratio has values between -1 and 0.5 in isotropic materials. While the Poisson's ratio increases positively inelastic materials such as rubber, it is close to zero in solid material. (Uzun,2010). The Poisson ratio is shown by ν in some sources (Abi, 2007), and in some sources, it is denoted by μ (Perepechko, 1975).

$$\mu = -\frac{\epsilon_{\text{lateral}}}{\epsilon_{\text{axial}}} \quad (11)$$

The value of the Poisson ratio is positive for materials other than auxetic materials. For this reason, (-) minus sign is added in equation (11) so that the Poisson's ratio is (+) positive in other materials except for auxetic materials. Since ϵ_{axial} will be positive and $\epsilon_{\text{lateral}}$ negative when the material is pulled, the Poisson ratio (μ) calculated by equation (11) is found greater than zero ($\mu > 0$).

It is known that lateral contractions against elongation occur when a material is pulled. Poisson determined that the unit elongation in the z and y axes of the materials pulled in one direction will be proportional to the strain occurring in the x-axis. He stated that lateral deformations can occur even when there is no force applied in these axes. The small Poisson's ratio in materials is an indication that those materials have a higher resistance to external impacts (Oral, 2011). Poisson ratio values of some materials are given in Table 2.

Table 2. Poisson Ratio Values for Some Materials (Uzun, 2010)

Material	Poisson's Ratio
Aluminum	0.334
Copper	0.355
Bronze	0.140
Ice	0.330
Concrete (high performance)	0.13-0.16
Glass	0.240
Steel (high-tensile)	0.27-0.30
Steel (high-strength)	0.30
Epoxy Resin	0.38-0.40
Silver	0.37
Rubber	0.48-0.50
Nylon	0.40
Sulfur	0.21-0.34
Polystyrene	0.340
Porcelain	0.208
PVC	0.35
Teflon	0.399
Cork	0
Ceramic	0.290

In the case of pulling in one direction, if the Poisson's ratio is known, deformations perpendicular to the force can be calculated without measuring. Thanks to the known Poisson ratio, the change in the

volume of the material as a result of deterioration can also be calculated (Postacioğlu,1981).

In linear isotropic flexible materials, only two of the elastic constants (E), (G), (μ), and (K) are independent (Oral, 2011). By using Equation (12) and equation (13), others can be found:

$$G = \frac{E}{2(1+\mu)} \quad (12)$$

$$K = \frac{E}{3(1-2\mu)} \quad (13)$$

As it can be seen in Equation (13), the Poisson's ratio should be less than 0.5. When the Poisson ratio is $\mu = 0.5$, the value of K becomes infinite. In this case, even if the pressure on the material is infinite, the volume of the material cannot be changed. Material with this property is called incompressible. For incompressible materials $\mu = 0.5$. It is $\mu < 0.5$ in polymers and they can be slightly compressed (Onaran, 2006). Since $\mu = 0.49$ for rubber, an incompressible body assumption can be made for rubber.

Tensile Test

In the tensile test, the two ends of the test sample prepared by considering the standards are clamped between the jaws in the standard test set. While one end of the test sample is fixed, the other end is pulled at a determined constant speed and the sample is stretched from both ends. Tensile test speeds are selected by following the type of test material. The stretching process is continued in one

direction, at a certain speed, and a certain temperature until the sample breaks. During the test, a constantly increasing tensile force is applied to the standard test specimen and simultaneously the elongation amount of the material is recorded (Savaşkan, 1999).

In the tensile test, firstly, a tensile sample is prepared by considering the standards of the material to be tested. Tensile test samples prepared in standards are given in Figure 6. The test specimen, which is clamped smoothly and centered on the two jaws in the tensile test device, is pulled with a continuously increasing load until it is broken. As a result of the tensile test, the stress (σ)-strain (ϵ) curve, that is, the tensile diagram, is drawn and the strength values such as proportional limit, elasticity limit, yield limit, and tensile strength and ductility values such as elongation, shrinkage, and toughness are determined (Savaşkan, 1999). Besides, Young's modulus of the material can be calculated by using the slope of the drawn stress (σ)-strain (ϵ) curve.

Composites are produced by combining different materials, and this process gives composite materials beneficial properties such as high durability, abrasion resistance, appropriate fatigue strength, and lighter weight. The most preferred types of composite materials today are the combinations of carbon fiber/epoxy, glass fiber/polyester, and aramid fiber/epoxy. Most of the composite materials produced today are used in the automotive, boat building, and aerospace industries. The main reason why composites are preferred and increased in use today is their lightness and strength. It is possible to obtain more useful products by reinforcing various plastic materials with metal, ceramic,

or hard polymer fibers. We frequently encounter these materials, which are easily shaped because they contain plastic and are hard, light, and extremely durable with the effect of reinforcement fibers, in different application areas. Also, compared to metals, composites are more advantageous in terms of material fatigue, resistance to damage, and abrasion on the material.

The tensile test is more preferred in determining the mechanical properties (elasticity coefficients) of materials. The results found with the tensile test are used in direct engineering calculations. Although the tensile test is one of the destructive test techniques that damage the tested material, it is one of the most preferred test techniques in engineering calculations. This research was carried out to measure the mechanical properties (Young's Modules, Tensile Stress, Tensile Stress, and Poisson's Ratio) of orthotropic composite plates made of E-glass fiber/epoxy and carbon fiber/epoxy by tensile test. Within the scope of this research, the tensile strength, Young's modulus, and Poisson's ratios of some E-glass fiber/epoxy and carbon fiber/ epoxy composites manufactured by a private company were calculated by the tensile test. The Young's modulus and Poisson's ratio values calculated by the tensile test of E-glass fiber/epoxy and carbon fiber/epoxy composites were compared with the values calculated by an ultrasonic method and tensile test of the same materials in the literature.

1. MATERIAL AND METHOD

1.1. The Materials Used in the Experiment and Their Mechanical Properties

Within the scope of this study, the fiber orientation has been chosen as the $x(1)$ direction shown in figure 4. Therefore, in the production of both E-glass fiber/epoxy and carbon fiber/epoxy composites, 3mm thick plates were obtained by arranging the fibers in the $x(1)$ direction. From these plates prepared in $x(1)$ orientation, A and B samples were prepared in the dimensions given in Figure 6. The A samples in the $x(1)$ direction and the B samples in the $y(2)$ direction were prepared by the Izoreel Company for both types of composite materials to be used in the tensile test. The fiber orientations are expressed by considering the coordinates given in Figure 4.

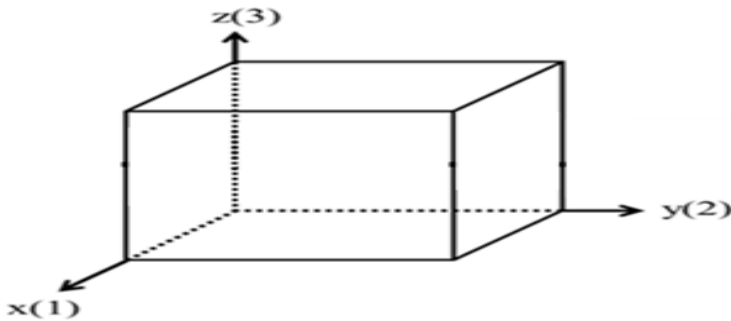


Figure 4. The Coordinate Chart Showing the Arrangement Orientations of the Fibers Epoxy resin system used as matrix material in the production of E-glass fiber/epoxy and carbon fiber/epoxy materials: It consists of a combination of two artificial resins (100 units Bakelite EPR840 and 80 units Bakelite EPH875). E-glass fiber, produced by Şişecam Cam

Elyaf Sanayii A. Ş., and carbon fiber, produced by Akxa Karbon Elyaf Sanayii A. Ş, are used in the production of composite materials. Mechanical properties of epoxy resins and fibers used in the production of composites are given in Table 3.

Table 3. The Mechanical Properties of Epoxy Resins and Fibers Used in the Production of Composites

Properties	Epoxy resin	E-glass fiber	Carbon fiber
Tensile Strength (MPa)	70-80	2400	4200
Modulus of elasticity (GPa)	3,5	73	240
Elongation (%)	-	3-5	4-5

1.2. The Production Process of E-Glass Fiber/Epoxy and Carbon Fiber/Epoxy Composites

First of all, for the matrix system used in composite materials, after mixing 100 units of EPR840 and 80 units of EPH875 resins, this mixture was heated at approximately 70 °C. This resin was applied to the specified number of fibers and stacked on top of each other. After the desired number of layers was formed, the material was placed under a hot press and compressed under a pressure of $P = 3 \text{ kg / cm}^2$. Finally, the produced materials are pressed at 120 ° C for 4 hours and hardened.

1.3. Devices Used in the Experiment

Instron 3520 device was used for the tensile test. The tensile test system consists of the tensile tester Instron 3520 (Figure 5-a), the pulling process of the samples (Figure 5-b), and the desktop computer

with software that controls the tensile test and records the data (Figure 5-c).

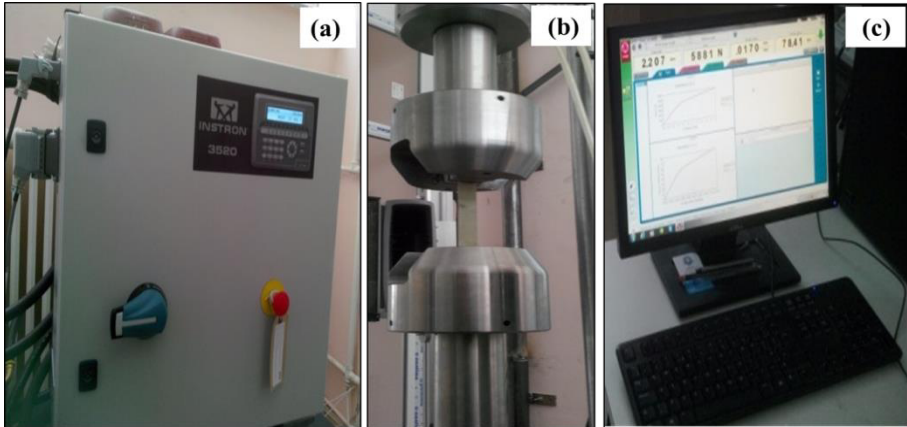


Figure 5. Tensile Test System: A-) Tensile Test Device, B-) The Tensile Operation, C-) Software Loaded Computer

1.4. Tensile Testing

As seen in Figure 6, the A sample (230mmx12mmx3mm) parallel to the fiber direction, that is in the x (1), and the B sample (230mmx25mmx3mm) in the direction of the fiber direction, that is y (2) produced and was prepared for the tensile test. In the tensile test, aluminum parts were added to the ends of both E-glass fiber/epoxy and carbon fiber/epoxy composites according to the relevant standards to strengthen the ends of these materials (50x12 mm for the A sample, 50x25 mm for the B sample). The samples prepared for the tensile test were carried out by the ASTM D3039 standard. With this tensile test, the tensile strength, Young's modulus, and Poisson's ratio were determined.

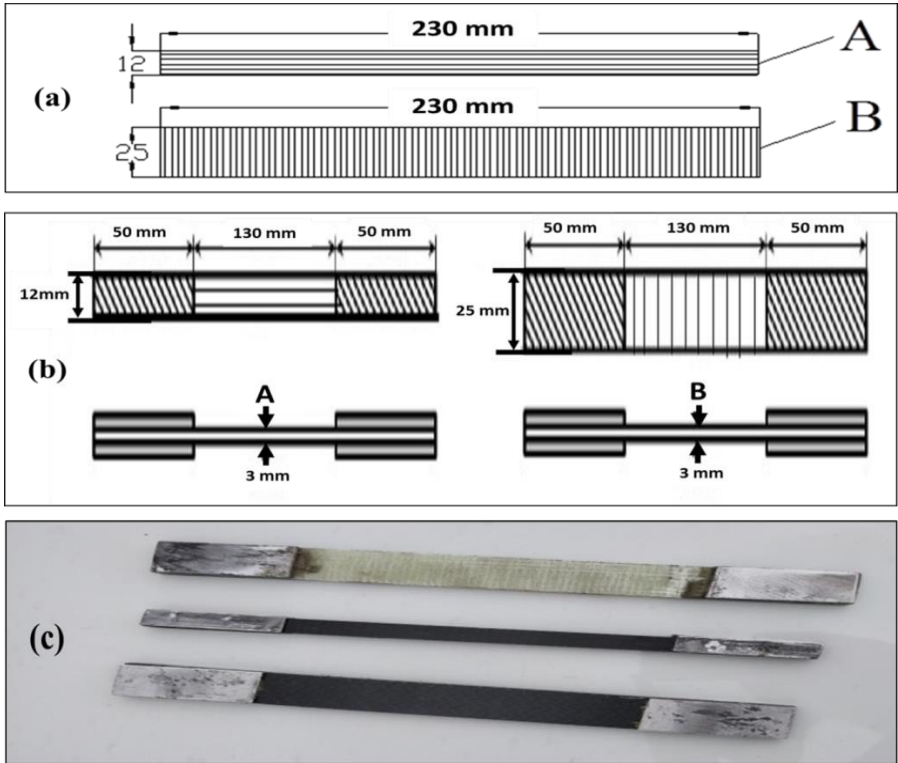


Figure 6. Tensile Test Samples: A-) Dimensions of A and B Samples, B-) Supporting A and B Samples with Aluminum and Their Thickness, C-) Ready-To-Test Samples

For both types of composite materials, 10 pieces of A samples prepared for tensile in x (1) direction and 10 pieces of B samples prepared for tensile in y (2) direction were prepared following with ASTM D3039 standard (Figure 6) and the tensile test was performed with these samples.

1.5. Calculation of Mechanical Properties with Tensile Test

The tensile stress (σ_{ts}) and ultimate tensile stresses (σ_u) of the A samples for both composite types were calculated using equation (2)

and (3). Average values were determined by calculating the breaking and tensile values in 10 samples from both E-glass fiber/epoxy and carbon fiber/epoxy composites. Similar procedures were performed for the B samples and the tensile and breaking stresses were calculated.

The values of the force applied in the tensile test and unit elongation (strain) of E-glass fiber/epoxy and carbon fiber/epoxy samples are given in Table 4.

Table 4. Forces Applied in E-Glass Fiber/Epoxy and Carbon Fiber/Epoxy Tensile Test and Strains

Samples	P (N)	$\epsilon_{lateral}$	ϵ_{axial}
E-glass fiber/epoxy	2531	0,00223	0,00327
	5022	0,00456	0,01312
Carbon fiber/epoxy	5012	0,00170	0,00414
	11000	0,00388	0,00950

The Poisson ratio (μ_{12}) of the A samples was calculated by using the data shown in Table 4, and the equation (11). Stress values are calculated using equation (1). Using these stress values in equation (7), Young's modulus (E_1) values were calculated for A samples. Similar procedures to those of A samples were performed for B samples, and the Poisson ratio, stress, and Young's modulus values of the B samples were calculated.

2. RESULTS

As a result of the tensile test performed on the test samples prepared following the standards, the forces applied, the calculated tensile stresses, and the calculated elastic constants of the materials are given in this section.

After the experiments are done, the force-elongation diagram of a single sample is shown in Figure 7. The stress-strain graph of a single sample is given in Figure 8.

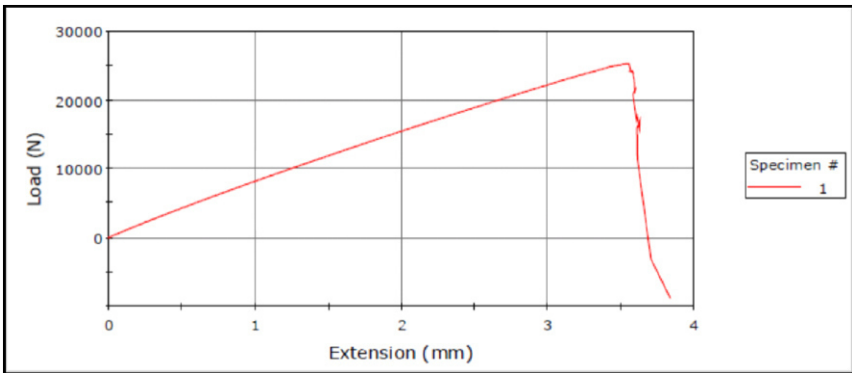


Figure 7. Force-Elongation of a Single Sample

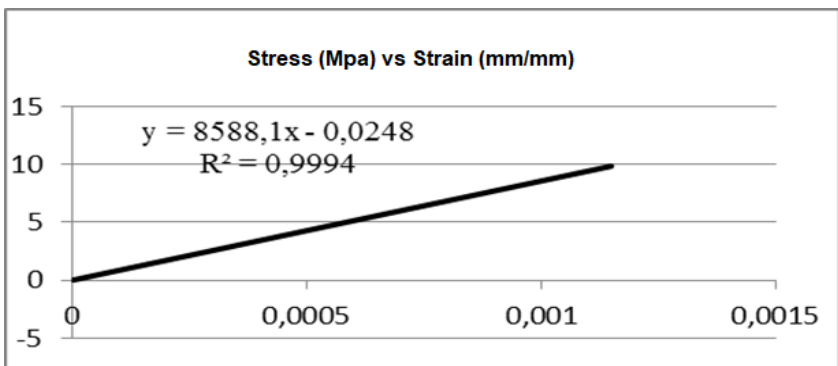


Figure 8. Stress-Strain Plot of a Single Sample

The tensile test results in the direction of x (1) of E-glass fiber/epoxy composites are given in Table 5.

Table 5. The Tensile Test Results in the Direction of X (1) of E-Glass Fiber/Epoxy Composites

Test No	Elongation (mm)	Maximum Tensile Force (N)	Tensile Stress σ_{ts} (MPa)	Ultimate Stress σ_u (MPa)	Elasticity Modulus E_1 (GPa)
1	3,55	25284	702,35	572,95	30,50
2	3,90	26948	748,58	538,54	29,65
3	4,24	27967	776,89	539,27	29,12
4	4,65	30727	853,53	660,40	28,90
5	4,62	30787	791,19	720,19	29,24
6	4,32	26884	746,80	698,11	27,21
7	4,28	29600	822,23	761,65	31,36
8	4,64	31032	862,00	776,36	28,97
9	4,00	27687	769,10	750,89	30,75
10	4,11	28644	795,67	792,02	30,59
Mean	4,27	28753	792,90	695,21	29,59
Std.Dev.	0,34	1868	48,72	99,64	1,10
Var.	0,12	3490267	2373,56	9928,02	1,21

The tensile test is applied to 10 E-glass/epoxy composite samples. The elongations and maximum forces obtained in Table 5 consist of the data taken from the computer program used in the tensile test. Other results have been obtained by calculation. According to these results, the samples elongated approximately 4.27 mm on average. The average maximum tensile force was 28753 N. As a result of the calculations made, the tensile stress was found to be 792.90 MPa and the ultimate stress as 695.21 MPa. From here, the average E1 value in the fiber direction was calculated as 29.59 GPa. Table 6 shows the tensile test results of the carbon/epoxy composite samples in the direction of x (1).

Table 6. The Tensile Test Data for Carbon Fiber/Epoxy Composites in X (1) Direction

Test No	Elongation (mm)	Maximum Tensile Force (N)	Tensile Stress σ_{ts} (MPa)	Ultimate Stress σ_u (MPa)	Elasticity Modulus E_1 (GPa)
1	4,08	57323	1592,30	1592,17	78,75
2	3,44	52987	1471,85	1421,57	81,89
3	3,05	44276	1229,88	1173,57	73,81
4	3,64	50830	1411,94	1400,34	71,92
5	2,95	41570	1154,72	1145,25	75,75
6	3,02	48664	1351,79	1351,79	79,18
7	3,30	48748	1354,11	1352,70	68,93
8	2,31	39569	1099,15	1094,11	80,66
9	3,47	51314	1425,37	1389,74	81,68
10	3,24	46845	1301,24	1290,45	69,68
Mean	3,25	48212	1339,24	1321,17	76,23
Std.Dev.	0,47	5364	148,99	149,68	4,91
Var.	0,22	28773029	22200,16	22406,24	24,14

The tensile test is applied to 10 samples. The elongations and maximum forces obtained in Table 6 consist of the data taken from the computer program. Other findings have been obtained by calculation. According to these results, the samples elongated by 3.25 mm on average. The maximum tensile force was 48212 N. As a result of the calculations, the tensile stress was found as 1339.24 MPa and the ultimate stress as 1321.17 MPa. From here, the average E_1 value in the direction of the fiber was calculated as 76.23 GPa.

When the data in Table 5 and Table 6 are compared, the elastic modulus E_1 of carbon/ epoxy composites is higher than that of E-glass/epoxy composites. Accordingly, it shows that carbon/epoxy composites are more rigid and stronger than E-glass/epoxy composites in the fiber direction. E-glass/epoxy materials, on the other hand, have

higher elongation amounts than carbon/ epoxy materials in the tensile test. This shows that E-glass/epoxy materials have a more elastic but more fragile structure.

The tensile test results of the E-glass fiber/epoxy composite samples in the y(2) direction (perpendicular to the fiber orientation) are given in Table-7.

Table 7. The Tensile Test Data in the Direction of Y (2) for E-Glass Fiber/Epox Composites

Test No	Elongation (mm)	Maximum Tensile Force (N)	Tensile Stress σ_{ts} (MPa)	Ultimate Stress σ_u (MPa)	Elasticity Modulus E_2 (GPa)
1	2,28	5674	75,65	75,47	10,32
2	2,21	5887	78,50	78,38	9,91
3	2,46	6439	85,85	84,76	11,36
4	2,30	6370	84,94	84,25	11,57
5	2,49	6247	83,30	83,08	11,03
6	2,15	6065	80,87	79,47	11,40
7	2,08	6179	82,39	81,94	10,90
8	1,74	5669	75,58	74,98	11,08
9	2,23	6430	85,74	85,15	11,11
10	1,89	5530	73,73	72,28	10,23
Mean	2,18	6049	80,66	79,98	10,82
Std.Dev.	0,23	340	4,53	4,58	0,55
Var.	0,05	115255	20,52	20,97	0,30

The tensile test is applied to 10 samples. The elongations and maximum forces in Table7 consist of the data taken from the computer program. Other findings have been obtained by calculation. According to these results, the samples elongated by 2.18 mm on average. The maximum tensile force was realized as 6049 N on average. As a result of the calculations, the average tensile stress is

found to be 80.66 MPa, and the average ultimate stress is 79.98 MPa. From here, the E_2 value perpendicular to the fiber direction (90^0) has been calculated as 10.82 GPa. According to the data in Table-6 and Table-8, the average E_1 value in the direction of the fiber is found 29.59 GPa, while the E_2 value perpendicular to the fiber direction is found 10.82 GPa. This shows that E-glass/epoxy composite materials are more durable in the fiber direction.

The tensile test results of carbon fiber/epoxy composite samples carried out perpendicular to the fiber direction are given in Table 8.

Table 8. The Tensile Test Data for Carbon Fiber/Epoxy Composites in the Direction of Y (2)

Test No	Elongation (mm)	Maximum Tensile Force (N)	Tensile Stress σ_{ts} (MPa)	Ultimate Stress σ_u (MPa)	Elasticity Modulus E_2 (GPa)
1	0,61	2828	37,70	35,88	8,59
2	0,57	2632	35,09	33,27	8,50
3	0,59	2790	37,21	34,36	8,70
4	0,61	3014	40,19	40,18	9,03
5	0,64	3243	43,24	43,23	9,29
6	0,60	2726	36,35	34,23	8,29
7	0,70	3122	41,63	38,98	8,39
8	0,65	2927	39,03	39,02	8,33
9	0,48	2295	30,60	29,45	8,54
10	0,55	2753	36,70	36,58	9,29
Mean	0,60	2833	37,77	36,52	8,70
Std.Dev.	0,06	267	3,56	3,97	0,37
Var.	0,003	71421	12,70	15,73	0,14

The tensile test is applied to 10 samples. The elongations and maximum forces in Table 8 consist of the data taken from the computer program. Other findings have been obtained by calculation.

According to these results, the samples elongated by 0.60 mm on average. The maximum tensile force was realized as 2833 N. As a result of the calculations, the tensile stress was found to be 37.77 MPa on average and the ultimate stress to be 36.52 MPa on average. From here, the Elastic Modulus, E_2 value perpendicular to the fiber direction was calculated as 8.70 GPa.

When the data in Table 7 and Table 8 are compared, the flexibility modulus, E_2 of carbon/epoxy composites is lower than that of E-glass/epoxy composites. Accordingly, it shows that E-glass/epoxy composites are more rigid and stronger than carbon/epoxy composites. E-glass/epoxy materials have higher elongation amounts than carbon/epoxy materials in the tensile test. This shows that E-glass/epoxy materials are more elastic.

As can be seen in Table 5 and Table 7, Young's modulus of the E-glass/epoxy composite material decreased from 29.59 GPa in the x (1) direction to 10.82 GPa in the y (2) direction. Again, as can be seen from Table 6 and Table 8, Young's modulus of carbon fiber/epoxy composite decreased from 76.23 GPa in the x (1) direction to 8.70 GPa in the y (2) direction. According to these findings, the values of Young's modulus found for both materials in the direction of x (1) are much smaller than the values in the direction of y (2). The calculated Poisson's Ratio (ν_{12}) values are included in Table 9.

Table 9. The Poisson's Ratio Values Determined by the Tensile Test of Materials

Material	Poisson's Ratio (μ_{12})
E-glass fiber/epoxy	0,236
Carbon fiber/epoxy	0,40

According to Table 9, the Poisson ratio of E-glass / epoxy composites is 0.236, while the Poisson ratio value of carbon fiber/epoxy composites is 0.40.

The results obtained from the tensile test from this study compared with the results of the previous studies with similar materials, and are given in Table 10.

Table 10. Comparison Of The Tensile Test And Literature Results In This Study

Materials	Mechanical Properties	Tensile Test	Literature	Comparison %
E-glass fiber/epoxy	E_1 (GPa)	29,59	35,94(1)	82
	E_2 (GPa)	10,82	11,24(1)	96
	μ_{12}	0,236	0,30(1)	87
Carbon fiber/epoxy	E_1 (GPa)	76,23	67(2)	88
	E_2 (GPa)	8,70	7,60(2)	87
	μ_{12}	0,40	0,35(2)	88

Source: ⁽¹⁾ Poyraz,2010. ⁽²⁾ AL-Qrimli, Mahdi, and Alnaimi, 2015.

As can be seen in Table10, the tensile test results obtained in this study, and the results in the literature have high similarity.

CONCLUSIONS AND DISCUSSION

In this study, tensile and ultimate stresses, Young's modulus and Poisson's ratios of E-glass fiber/epoxy and carbon fiber/epoxy composite materials were measured by mechanical tests. The results obtained have been compared with the elasticity coefficients previously determined by mechanical tests on the same materials in the literature.

Fiber-reinforced polymer matrix composite materials are produced and widely used in many sectors. It is preferred as an alternative to other materials due to its superior properties such as durability, lightness, and abrasion resistance. Carbon fiber or glass fiber reinforced plastic composite materials are preferred compared to metals especially in aviation, automobile, marine, transportation, construction, and military sectors because of their higher strength/weight ratios, and not corroding. Therefore, it is necessary to know the mechanical properties of composite materials to design and analyze them.

Composite materials can have different mechanical properties according to their fiber directions. In the direction where Young's modulus is higher, the body is more resistant to tension and pressure, so its solidity and strength are higher. In the direction where Young's modulus is smaller, it is easier for the matter to deteriorate. At the atomic level, when the elastic modulus increases, the bond between atoms becomes stronger, and when this modulus decreases, the bonds

between atoms become weaker. In other words, knowing the elastic properties of materials can also give information about the bonding forces between atoms and molecules of those materials.

While the Young modulus of the epoxy resin that forms the matrix part of the composite materials is 3.5 GPa, the E-glass fiber with a Young modulus of 73 GPa is reinforced to this matrix and the highest Young's modulus value measured by the tensile test of the E-glass fiber/epoxy composite is determined as 29.59 GPa. When the carbon fiber with Young's modulus of 240 GPa is reinforced to the matrix, the average value of Young's modulus of the carbon fiber/epoxy composite formed is found to be 76.23 GPa. As a result, Young's modulus measured by the tensile test of both composite samples came out between the matrix forming the sample and Young's modulus of the fiber, and it was observed that the strength of the weak resin was increased by reinforcing the fiber.

According to the results obtained from the research, Young's modulus (E1) in the x (1) direction, 76.23 GPa for carbon fiber/epoxy and 29.59 GPa for E-glass fiber/epoxy, Young's modulus (E2) measured in the direction of y (2) is designated as 8.70 GPa for carbon fiber/ epoxy and 10.82 GPa for E-glass fiber/epoxy. As can be seen from these results, Young's modulus (E1) measured in the x (1) direction in both composite types were higher than the Young's modulus (E2) measured in the y (2) direction. In other words, while the elasticity module in the fiber direction has a large value, it has a small value in the vertical

direction of the fiber direction. According to this result, it can be said that Young's modulus values change according to the fiber orientation.

According to the values given in Table10, the results obtained for E-glass fiber/epoxy composites in this study are compatible with the results made by Poyraz (2010) for the same materials, while the values obtained for carbon fiber/epoxy composites are also in the same materials Al-Qrimli et al., (2015) is compatible with the results obtained by the tensile test. Accordingly, the proximity rates are between 82% and 96%. As a result, the results obtained in this study largely agree with the results in the literature.

When the relevant literature is examined, it is seen that the mechanical properties of the materials are measured with mechanical tests, similar to this study, while it is seen that the mechanical properties of the materials are measured by non-destructive methods such as ultrasonic methods, as well as these recently destructive methods

Wang, Li, and Zhao, (1994) in their research; studied the flexibility properties of glass fiber and Kevlar woven fabric reinforced epoxy composites by performing uniaxial tensile, bend, and compression tests. As a result of the research, they found that the shear strength of Kevlar fibers was less due to the shear forces. They concluded that glass fiber reinforced composites deteriorated less.

In Murugan, Ramesh, and Padmanabhan's (2014) research; they investigated the tensile, bending, and impact strength of composites with four layers produced by arranging glass fiber and carbon fiber

fabrics. As a result of the research, they found that the composite materials reinforced with carbon fiber have higher tensile, bending strengths but have less resistance to impact strength than the composite materials reinforced with glass fiber.

Valença, Griza, Oliveira, Sussuchi, and Cunha's (2014) investigated the tensile, bending, and impact load behavior of the composites they obtained by using aramid fiber reinforced epoxy and aramid, glass fiber hybrid obtained by hand lay-up technique. They concluded that hybrid composite materials gave more positive results in experiments against aramid materials.

Song (2015) investigated the properties of composites produced using different sequences of carbon/glass fiber and carbon/aramid fibers in tensile testing. It has been revealed that the different fiber arrangement of composites affects the material properties.

It has been observed that the mechanical properties and quality controls of materials such as polymer composites can be made by ultrasonic methods without damaging the material, and these studies have become increasingly important. For example, Wrobel and Pawlak (2006) produced composites using different proportions of glass fiber and epoxy composition in their research and examined these composites with ultrasonic pulse-echo technique.

In their research, they looked at the ultrasonic wave velocity changes in the samples according to the glass fiber amounts. From the results found with the pulse-echo technique, it was observed that there are

differences in ultrasonic velocity propagation in composites depending on the glass fiber ratios.

In another study conducted by Wrobel and Pawlak (2007), glass fiber/epoxy and glass fiber/polyester composites were produced by mixing different proportions of glass fiber/epoxy and polyester matrix. Ultrasonic sound wave velocity changes in the produced composites were investigated for both composites. According to the data in this study, it was determined that while the amount of glass fiber used in composite synthesis increased, the ultrasonic velocity values in both composites increased.

Oral (2011) found that modification of pure polystyrenes with succinic anhydride, maleic anhydride, and phthalic anhydride increased longitudinal and transverse sound wave velocities and elastic modulus values. Also, it was revealed that the values of elastic modulus of pure polystyrene and polystyrene composites measured using the tensile test and ultrasonic method are very close to each other.

In another study, İşler (2015) measured the elastic constants of E-glass fiber/epoxy and carbon fiber/epoxy materials by ultrasonic method. He found that the elasticity coefficients he calculated and the ultrasound velocities he measured were dependent on the fiber orientation.

As a result, determining the mechanical properties of materials by the ultrasonic method, which is a cheaper and easier and non-destructive

method, can be used instead of tensile testing, which is a destructive and more laborious method and also damages the material. In the coming years, mechanical properties of similar materials can be measured by both mechanical and ultrasonic methods and their results can be compared.

REFERENCES

- Abi, Erdiñç (2007). *Yapı seramiklerinde ultrases geçim hızıyla malzeme parametreleri ilişkisinin incelenmesi*, Yayınlanmamış Yüksek Lisans Tezi. Afyon Kocatepe Üniversitesi, Fen Bilimleri Enstitüsü, Afyon.
- AL-Qrimli, Haidar, Mahdi, Fadhil A., and Alnaimi, Firas B. I. (2015). Carbon/epoxy woven composite experimental and numerical simulation to predict tensile performance. *Advances in Materials Science and Applications, June 2015, Vol. 4 Iss. 2*, 33-41.
- Asi, Dilek (2008). *Cam elyaf takviyeli kompozit malzemelerin aşınma performansının incelenmesi*. Yüksek Lisans Tezi. Afyon Kocatepe Üniversitesi, Fen Bilimleri Enstitüsü, Afyon.
- Çolak, Fatih (2004). *Kimyasal metotla nikel kaplanmış tungsten karbür tozları kullanılarak seramik-metal kompozit malzeme üretimi ve özelliklerinin incelenmesi*. Yayınlanmamış Yüksek Lisans Tezi, Afyon Kocatepe Üniversitesi, Metal Eğitim Anabilim Dalı, Afyon.
- Dinçer, Nihan (2004). *Hegzagonal kristallerin esneklik özellikleri üzerine araştırma*. Yayınlanmamış Yüksek Lisans Tezi, Dokuz Eylül Üniversitesi, Fen Bilimleri Enstitüsü, İzmir.
- Kaya, Kerim D. ve Kılınç, Servet S. (2008). *Kompozit malzemelerin kayma testi için aparat tasarımı, imalatı ve kayma gerilmesi analizi*. Bitirme Projesi, Dokuz Eylül Üniversitesi, Mühendislik Fakültesi Makina Mühendisliği Bölümü, İzmir.
- Kılıç, Erdoğan (2006). *Kompozit malzemedeki yapılan yaprak yayların analizi*. Yayınlanmamış Yüksek Lisans Tezi, Dokuz Eylül Üniversitesi, Fen Bilimleri Enstitüsü, İzmir.
- İşler Hüseyin (2015). *Elyaf takviyeli kompozit malzemelerin esneklik katsayılarının ultrasonik ölçümü*. Yayınlanmamış Yüksek Lisans Tezi, Necmettin Erbakan Üniversitesi, Eğitim Bilimleri Enstitüsü, Konya.

- Murugan, R., Ramesh, R., and Padmanabhan, K. (2014). Investigation on static and dynamic mechanical properties of epoxy-based woven fabric glass/carbon hybrid composite laminates. *Procedia Engineering*, 97, 459-468.
- Onaran, Kaşif (2006). *Mazeme bilimi*. Ankara. Bilim Teknik Yayınevi.
- Oral, İmran (2011). *Çeşitli polifonksiyonel gruplu modifiye polistirenler ile epoksi reçinelerin sentezi ve bunlardaki ultrases hızlarının ölçülmesi*. Doktora Tezi, Selçuk Üniversitesi, Fen Bilimleri Enstitüsü, Konya.
- Postacıoğlu, Bekir (1981). *Cisimlerin yapısı ve özellikleri, cilt1, iç yapı ve mekanik özellikleri*. İstanbul, İ.T.Ü. İnşaat Fakültesi. İ.T.Ü. Matbaası.
- Poyraz, Mehmet (2010). *Kompozit malzemelerin yay elemanı olarak kullanılması*. Yayımlanmamış Yüksek Lisans Tezi, Süleyman Demirel Üniversitesi, Fen Bilimleri Enstitüsü, Isparta.
- Savaşkan, Temel (1999). *Malzeme bilgisi ve muayenesi*. Trabzon. Derya Kitabevi.
- Serway, A.R. and Brichner, R. (2002). *Fen ve mühendislik için fizik 1*. Ankara.
- Song, Jun H. (2015). Pairing effect and tensile properties of laminated high-performance hybrid composites prepared using carbon/glass and carbon/aramid fibers. *Composites Part B: Engineering*, 79, 61-66.
- Uzun, M. (2010). Negatif poisson oranına sahip (auxetic) malzemeler ve uygulama alanları. *Tekstil ve Mühendis*, 17(77),13-18.
- Valença, Silvio L., Griza, Sandro, Oliveira, Vandalucia G., Sussuchi, Eliana M., and Cunha, Frederico G. (2014). Evaluation of the mechanical behavior of epoxy composite reinforced with kevlar plain fabric and glass/kevlar hybrid fabric. *Composites Part B: Engineering*, 70, 1-8.
- Wang, Y., Li, J., and Zhao, D. (1994). Mechanical properties of fiberglass and kevlar woven fabric reinforced composites. *Composites Engineering*. 5: 1159-1175.
- Wrobel, G.I, and Pawlak, S. (2006). Ultrasonic evaluation of the fiber content in glass/epoxy composites. *Journal Of Achievements In Materials And Manufacturing Engineering*. Volume 18, Issues 1-2.

- Wrobel, G., and Pawlak, S.(2007). The effect of fiber content on the ultrasonic wave velocity in glass/polyester composites. *Journal of Achievements in Materials and Manufacturing Engineering, Vol.20, Issues 1-2.*
- Yılmaz, M. ve Altıntaş, S. (1997). Al-sicp kompozitinin ısıı çevrim koşulu altında davranışının teorik ve deneysel incelenmesi. 9. *Uluslararası Metalürji ve Malzeme Kongresi. İstanbul.* 721-726.
- Zor, M.(2018). *Kompozit Malzeme mekaniđi-ders notları.* http://kisi.deu.edu.tr/mehmet.zor/composite%20materials/2-Genel_bilgiler.pdf. Erişim Tarihi: 30.01.2019.

CHAPTER 3

ANALYZING THE RELATIONSHIP BETWEEN SURFACE ROUGHNESS VALUES AND CUTTING FORCE DEPENDING ON CUTTING PARAMETERS OF AISI 4140 MATERIAL ON CNC LATHE

Lecturer Sümeyye ERDEM¹
Assist. Prof Dr. Mustafa ÖZDEMİR²

¹ Karamanoğlu Mehmetbey University, Vocational School of Technical Sciences,
Department of Machine and Metal Technology, Karaman, Turkey, Email:
sumeyyeerdem@kmu.edu.tr

² Yozgat Bozok University, Vocational School of Technical Sciences, Department of
Machine and Metal Technology, Yozgat, 66100, Turkey, Email:
mustafa.ozdemir@bozok.edu.tr

INTRODUCTION

In today's industry, many materials with different properties are used to meet human needs. More economical and efficient productions can be realized by using chip removal operations on materials suitable for processing, appropriate cutting tools, and cutting parameters (Kam, 2016; Şeremet and Kam, 2019). In cutting processes performed with unsuitable cutting tools and cutting parameters, the surface quality of the product, and deterioration in cutting tool geometries occur [Kesti, 2009; Şahinoğlu and Rafighi 2020).

There are several studies in the literature that use different cutting tools and cutting parameters. Özses found in his study that the V had a positive effect on the roughness value, but shortened the tool life (Özses, 2002). In another study using AISI 4140 steel, it was found that the V has a direct impact on the life of the cutting tool and the life of the cutting tool decreases due to the increased V (Şahin and Motorcu, 2004). Yallese et al. Comparison of the roughness values of X200Cr12 steel with ceramic cutting tools and CBN tools. It was found that ceramic tools give better results with regard to the roughness value (Yallese et al., 2005). Altinkaya, In the study to investigate the influence of austenitic steel AISI 416 on the roughness value it was found that the V has a negative effect on the roughness value and the f has a positive effect on the roughness value (Altinkaya, 2006). In another study, in which the effect of cutting tools and cutting parameters on the roughness value was examined, it was found that the roughness value decreased due to the increased V

and the f (Demirayak, 2006). In parallel to this study, another study on AISI 4140 found that the most effective parameters for the roughness value are the f and the V (Hessainia et al., 2013). Aslan et al. found that an increase in the V and a decrease in the a values have a positive effect on the roughness value (Aslan et al., 2006). Aslantaş et al. investigated the effect of cutting parameters on the roughness value of AISI 52100 steel and found that increasing the V had a positive effect on the roughness value (Aslantas et al., 2012). Elbah et al. In their study on AISI 4140 steel, it was found that among the cutting parameters, the f and the a are the factors influencing the roughness value (Elbah et al., 2013). In a similar study it was found that the f is the parameter that most influences the roughness value (Shiddique et al., 2017). İynen et al. experimentally investigates the effect of AISI4140 steel on the cutting forces as a function of the cutting parameters. According to the ANOVA analysis, it was found that while the f was effective on the radial and tangential force, the a was effective on the feed force (İynen et al., 2020). Pınar and Firat found in their study processing AISI 4140 steel with a multidirectional cutting tool that the parameters that most influenced the roughness value were the radius of the tool tip and the type of chip breaker (Pınar and Kafkas, 2016). On the other hand, Yardımeden found in his study that the V had a positive effect on the roughness value, while the parameters a and f had a negative effect on the roughness value (Yardımeden, 2018). Gürbüz et al. The shape of the cutting tool was found to have a significant impact on surface integrity. Under all cutting conditions, it was found that the surface integrity deteriorates

with increasing a and f , while surface integrity improves with increasing V (Gürbüz et al., 2020).

In the study, the effect of different cutting parameters on the roughness value and cutting force of AISI 4140 steel was investigated. Three different cutting speeds (120-160-200 m / min), feed rate (0.1-0.13-0.16 mm / rev) and cutting depth (1.0-1.5-2.0 mm) were used as cutting parameters. The effects of cutting parameters on roughness value and cutting forces were analyzed using the data obtained as a result of the experiment.

1. MATERIAL AND METOD

In the study, AISI 4140 steel in dimensions of $\text{Ø}80 \times 160$ mm, which is frequently used in the automotive, defense, and aircraft industries and has high strength and toughness value. ISO 3685 standards have complied with the preparation of test samples. In the machining process, the Kennametal DCMT11T304MP KCP250 cutting tool and Kennametal SVJBL 2525M16 tool holder were used. In the experiments performed on CNC lathe, the effect of parameters on cutting force and roughness value was examined. The values of the chemical components of AISI 4140 steel are given in Table 1.

Table 1: Chemical Components of AISI 4140 Steel (Weight by %)

Element	C	Si	Mn	P	S	Cr	Mo	Al
%	0.39	0.27	0.74	0.008	0.01	1.06	0.2	0,03

To get efficient and accurate results from the study results, the connections of the equipment in the experimental setup should be made precisely and securely. In the study, AISI 4140 steel samples were connected between the mirror center and the cutting tool connection was made precisely after the process. Figure 1 shows the test setup and surface roughness device.

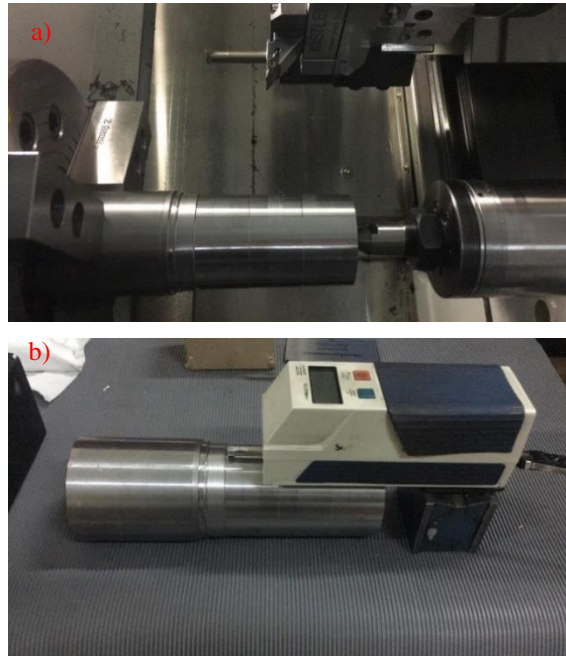


Figure 1. Test Setup, a) Measurement of Cutting Force, b) Measurement of Surface Roughness

The cutting force measurements were determined with the KISTLER TYPE 9129AA dynamometer and the same brand TYPE 5070 amplifier (Figure 1a). Three different cutting force values were measured, namely radial force (F_x), tangential force (F_y), and feed force (F_z) in the cutting force calculation of turned AISI 4140 steel. Mitutoyo brand SJ-400 surface roughness device was used to measure

the roughness value of AISI 4140 steel. Roughness value measurements were made separately from 3 different points of the processed surfaces and after the measurement, the average roughness values (Ra and Rz) were determined. Roughness measurements were carried out following LC ISO-16610-21 standards.

2. TAGUCHI L9 EXPERIMENTAL DESIGN

The Taguchi method has been used as an experimental design and analysis method in research. Dr. The Taguchi method, a method developed by Genichi Taguchi, expresses results using a statistical measure of performance called the S / N ratio. In the method in which the test results are evaluated by converting them into the S / N ratio, the actual value obtained by the system relates to the signal factor, and the factors that influence the result, although they are not included in the test arrangement, are the noise factor. All variables that lead to the experimental results deviating from the desired best values are defined as sources of noise (Taguchi and Konishi, 1987; Taguchi et al., 1989; Özdemir et al., 2020). In the method, the S / N ratios can be calculated according to the nominal best method, the smallest being the best and the largest being the best method. Equation 1 is used in this study because the minimum values for roughness and cutting force are desired.

$$\frac{S}{N} = -10 \cdot \log \left(\frac{1}{n} \cdot \sum_{i=1}^n Y_i^2 \right) \quad (1)$$

Cutting parameters constitute one of the important criteria effective in creating ideal cutting conditions. The experiments were repeated three

times to obtain the optimum cutting parameters. In the research, 9 experiments were carried out using three different V (120, 160, and 200 m / min), f (0.10, 0.13, and 0.16 mm / rev), and a (1, 1.5, and 2 mm) parameters in processing AISI 4140 steel. Each parameter was repeated 3 times and a total of 27 experiments were conducted. Cutting parameters and levels used in turning AISI 4140 steel are given in Table 2.

Table 2: Cutting Parameters and Levels Used in the Experiments

Parameters	Symbol	Unit	Level 1	Level 2	Level 3
Cutting Speed	V	m/min	120	160	200
Feed Rate	f	mm/dev	0.1	0.13	0.16
Cutting depth	a	mm	1	1.5	2

A 95% confidence interval ANOVA was used to determine the effect of control factors on roughness and cutting force. The data obtained as a result of the experimental design and statistical analysis with the Minitab 16 program were expressed in graphs.

3. EXPERIMENTAL RESULTS AND ANALYSIS

The effects of different V , f , and a parameters on cutting force (F_x , F_y , F_z) and roughness (R_a and R_z) of AISI 4140 steel were analyzed. The experimental setup was designed according to the Taguchi L9 Orthogonal array and the results obtained are shown in Table 3.

Table 3. Taguchi L9 Orthogonal Index and Experiment Results

V	f	a	F_x	F_y	F_z	R_a	R_z
120	0.1	1	73.51	481.3	388.2	1.55	10.1
120	0.13	1.5	78.77	553.2	413.4	2.12	10.9
120	0.16	2	86.16	815.4	562.1	2.34	11.4
160	0.1	1.5	58.55	418.1	322.2	1.62	11.3
160	0.13	2	60.19	649.4	465.1	1.84	12.4
160	0.16	1	94.49	640.3	415.1	2.36	15.8
200	0.1	2	53.62	520.7	387.2	2.21	11.9
200	0.13	1	75.62	518.3	341.9	2.78	14.2
200	0.16	1.5	76.41	599	376.6	3.13	14.8

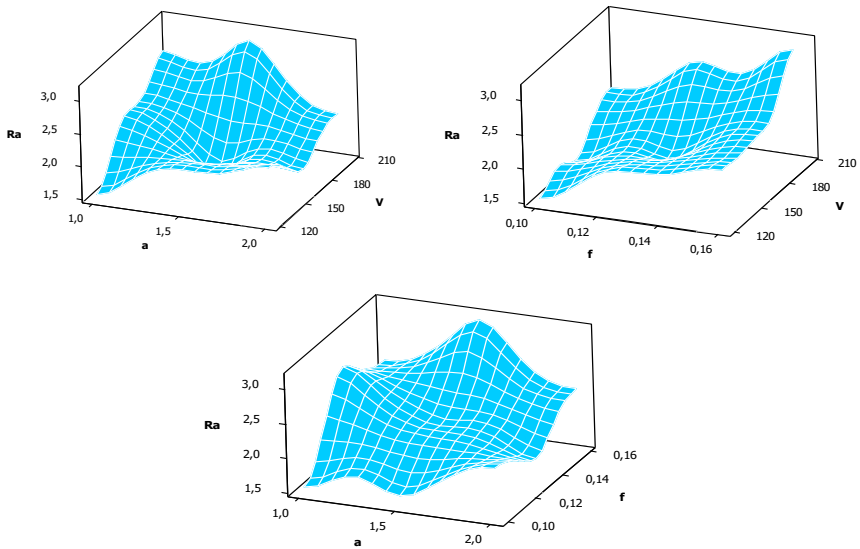
ANOVA was used to specify the effect of parameters on cutting force and roughness. The p-value (probability/significance) obtained from the ANOVA test indicates whether the control parameters are effective for the experimental parameters. The confidence interval in determining the level of effect of parameters in the study was defined as 95% ($p < 0.05$) (Erbaş, 2020; Çınarler et al., 2020). The contribution levels (PC%) of each factor influencing the experimental parameters are shown. ANOVA results for roughness (Ra and Rz) are shown in Table 4.

Table 4. Surface Roughness Values ANOVA Results

a- Surface Roughness (Ra)						
Cutting Parameters	DF	SS	F	P	PC (%)	R ²
Cutting Speed	2	15.5873	24.58	0.039	47.50	%92.3
Feed Rate	2	16.4057	25.87	0.037	49.99	
Cutting Depth	2	0.1876	0.30	0.772	0.57	
Error	2	0.6342			1.93	
Total	8	32.8148			100	
b- Surface Roughness (Rz)						
Cutting Speed	2	6.8104	35.05	0.028	48.93	%94.4
Feed Rate	2	5.7197	29.43	0.033	41.09	
Cutting Depth	2	1.1951	6.15	0.140	8.59	
Error	2	0.1943			1.40	
Total	8	13.9196			100	

When Table 4 is examined, the parameters with the highest level of influence on Ra (average roughness) roughness value are the f with 49.9% contribution and the V with 47.5% contribution rate, respectively; On the Rz (maximum roughness) value, it was determined that there was 48.93% V and 41.09% f . It is seen as a result of ANOVA that the a is also effective on the roughness value of AISI 4140 steel, but it was determined that it is lower compared to the V and f parameters. By using the Taguchi method S / N ratios, the

cutting parameters that provide optimum Ra and Rz values were determined. 3D surface graphics were used to determine the effects of cutting parameters on experimental parameters and optimum cutting parameters. The effects of V , f , and a parameters on the roughness value of AISI 4140 steel are shown in Figure 2.



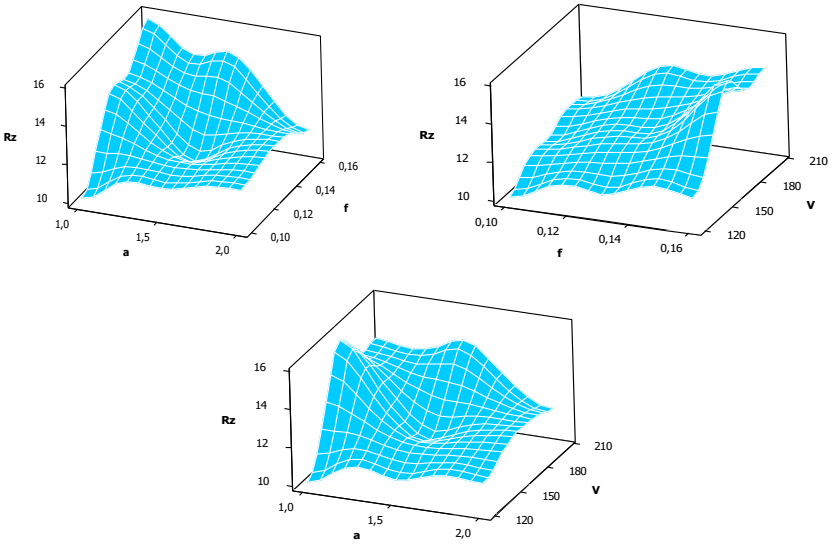


Figure 2: Change of Roughness Value of AISI 4140 Steel According to Cutting Parameters

When Figure 2 is examined, as the a increases, the chip cross-sectional area will increase, so the temperature and pressure to which the cutting tool is exposed during machining will increase. Since the plastic deformation in the cutter will increase, the surface quality will start to deteriorate in parallel. For this reason, it is seen that R_a and R_z values increase. R_a and R_z 's roughness increases depending on the increase in f . Therefore, a directly proportional relationship has been observed between roughness value and f . To improve roughness value, lowering f and increasing V is another common method (Boothroyd, 1981; Özdemir, 2019; Şahinoğlu and Ulas, 2020). A graph of the main influence of cutting parameters on R_a and R_z is shown in Figure 3. The cutting parameters that should be used to obtain an optimal R_a value are defined as 2nd level of V (V_2), 1st

level of f (f_1) and 3rd level of a ($V_2-f_1-a_3$). The R_z values were obtained at a V of 120 m / min, f of 0.1 mm / rev and a of 2 mm ($V_1-f_1-a_3$).

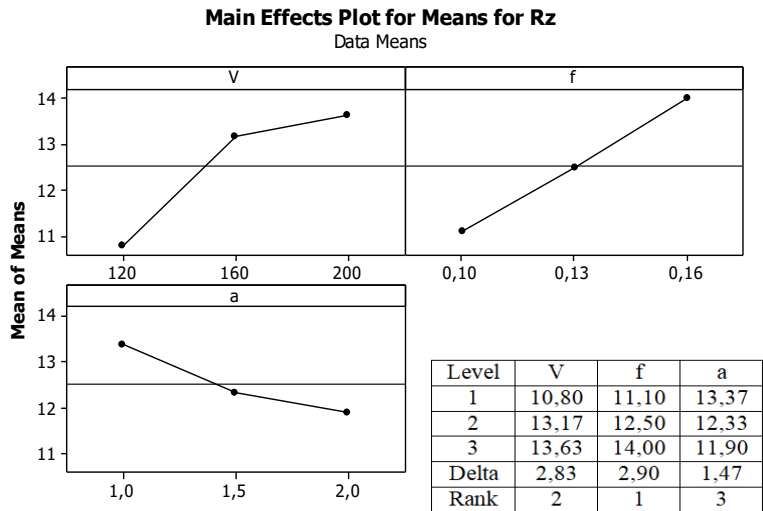
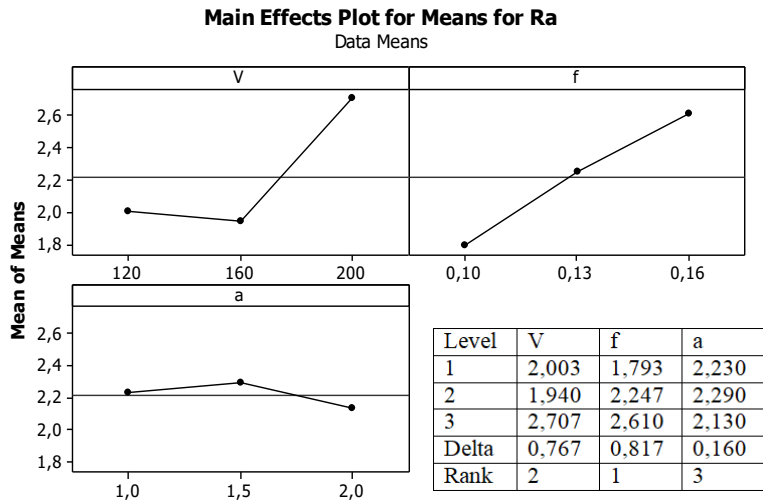


Figure 3: Main Effect Graph for Ra and Rz

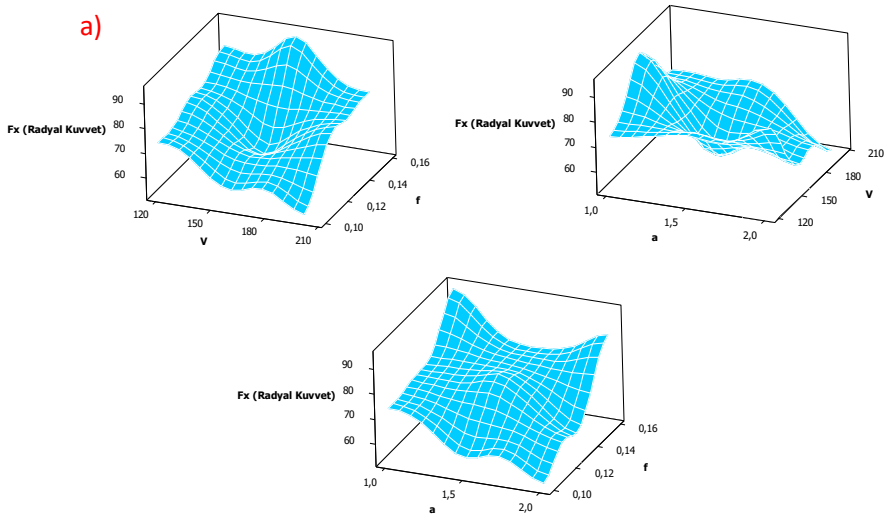
ANOVA was performed to determine the degree of influence of cutting parameters on cutting forces (F_x , F_y , F_z). The ANOVA results are shown in Table 5. When reviewing Table 5, it was determined that although f is the most effective parameter for F_x and F_y forces at 58.29% and 66.65%, respectively, there is a a of 44 for F_z , 54%. The a , which is the second effective factor for the forces F_x and F_y , was found to be 24.40% and 28.96%, respectively, and 27.52% of the V at F_z . Finally, it was determined that the lowest effective speeds were the V for cutting parameters F_x and F_y and the f at F_z .

Table 5. ANOVA Results for Cutting Forces

Fx (Radial Force)						
Cutting Parameter	DF	SS	F	P	PC (%)	R ²
Cutting Speed	2	3.3162	8.96	0.100	15.57	%93.0
Feed Rate	2	12.4147	33.55	0.029	58.29	
Cutting depth	2	5.1965	14.04	0.066	24.40	
Error	2	0.3701			1.74	
Total	8	21.2975			100	
Fy (Tangential Force)						
Cutting Speed	2	1.1872	26.18	0.037	5.179	%99.2
Feed Rate	2	15.0485	331.89	0.003	66.65	
Cutting depth	2	6.6382	146.41	0.007	28.96	
Error	2	0.0453			0.2	

Total	8	22.9192			100	
Fz (Feed Force)						
Cutting Speed	2	4.516	37.77	0.026	27.52	%97.1
Feed Rate	2	4.4637	37.34	0.026	27.21	
Cutting depth	2	7.308	61.13	0.0016	44.54	
Error	2	0.1196			0.73	
Total	8	16.4073			100	

The effects of cutting parameters (V , f , and a) on cutting force (F_x , F_y , and F_z) on AISI 4140 steel are shown in Figure 4.



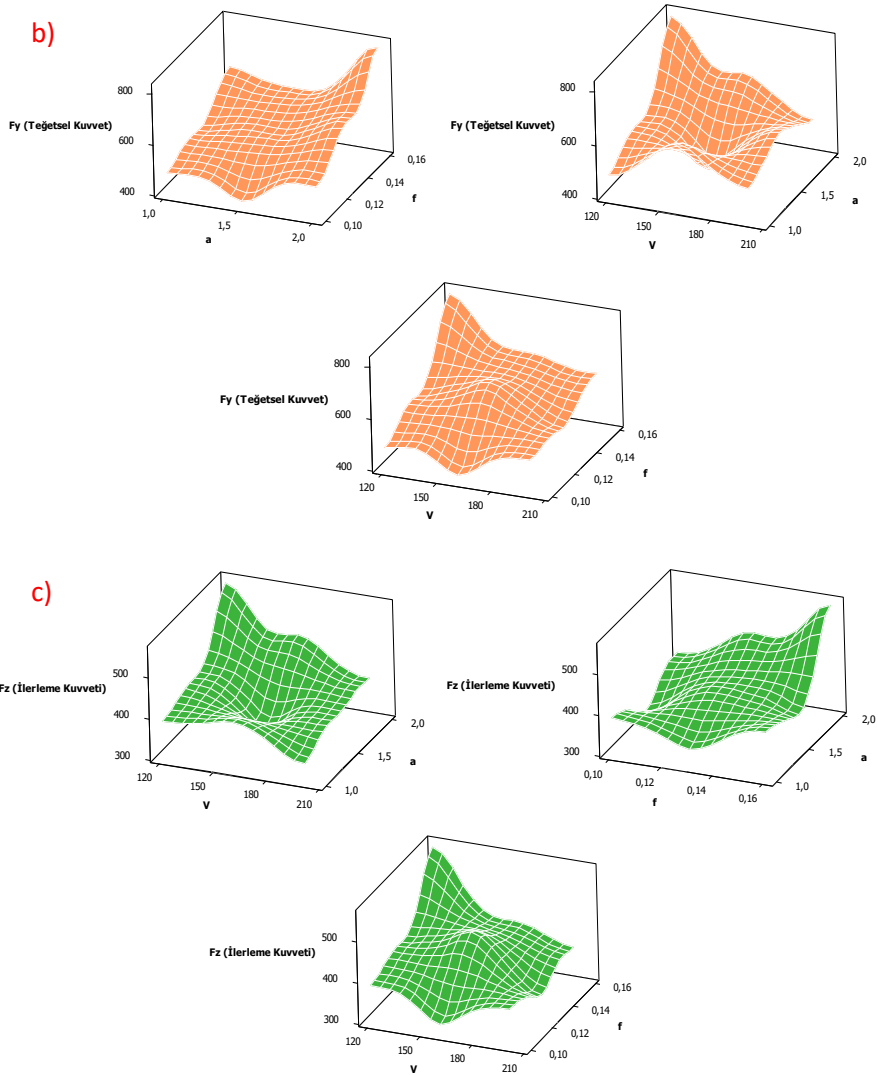
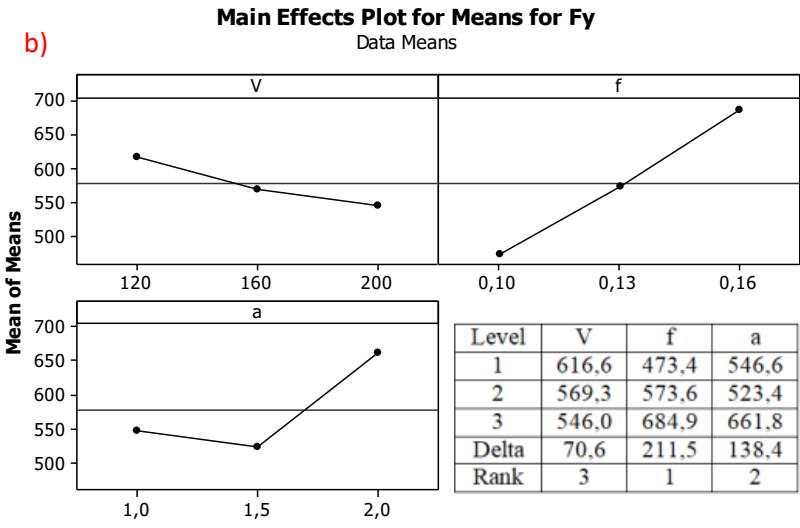
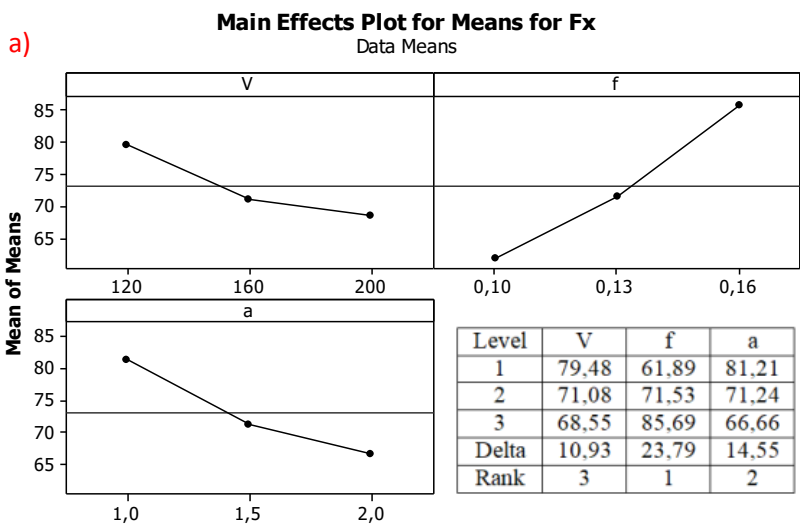


Figure 4: Cutting Force Change Graphs According to Cutting Parameters

When Figure 4a is examined, it is seen that F_x value decreases with increasing a and V . The reason for this is that the specific cutting resistance of the material will decrease as the V increases, that is, less force will be needed to remove chips since the heat generated in the cutting area will increase. It is seen from the combinations of V - f and f - a that F_x cutting force value increases depending on the increase in f . To obtain the optimum F_x value, the cutting parameter combination required to be used was determined as V (200 m / min), f (0.1 mm / rev), and a (2 mm) (Figure 5a). When Figure 4b is examined, it is seen that there is a statistically significant relationship between the cutting parameters on the F_y value of all cutting parameters (Table 5). It is seen from the combinations of V - f , V - a , and f - a that the F_y cutting force value increases due to the increase in the a and the fluctuating movement in the V . To obtain the minimum F_y value, the cutting parameter combination required to be used was determined as V (200 m / min), f (0.1 mm / rev), and a (1.5 mm) (Figure 5b). When Figure 4c is examined, it is seen that there is a statistically significant relationship on the F_z value of all cutting parameters. It has been determined that the F_z cutting force decreases with the increase in the f and V but increases with the increase of the cutting value. It was determined that the combinations of V - f , V - a , and f - a were effective on the F_z cutting force value. The cutting parameter combination required to obtain the minimum F_z value was determined as 200 m / min of V , 0.1 mm / rev of f , and 1.5 mm of the a (Figure 5c).



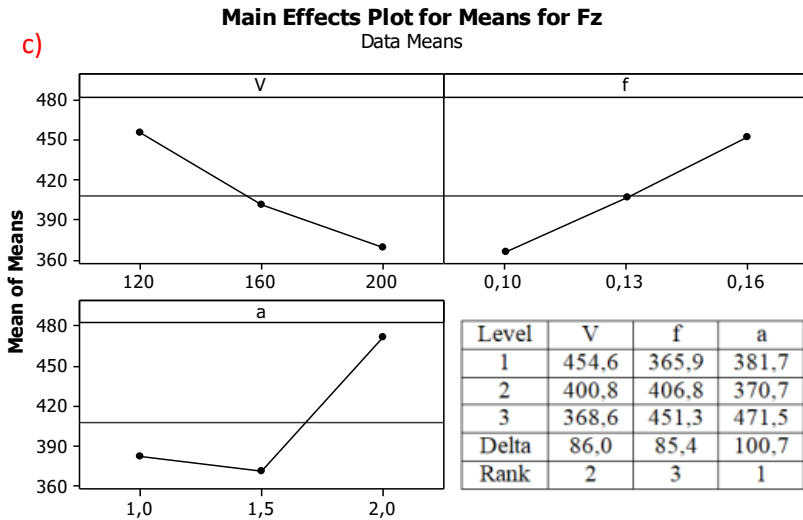


Figure 5. Main Effect plot for Fx, Fy and Fz Forces

Using the Taguchi optimization method, the optimum results of roughness value and cutting force values were obtained in the experimental study and the percentage distributions of the parameters that had an effect on the result were determined by ANOVA analysis. The last step of the optimization process is to perform validation experiments and to test the validity of the optimization process. Optimization process was completed by using parameters outside the experimental setup. Optimization result table is shown in Table 6. In this context, verification tests on ignoring the difference between the results obtained from the Taguchi approach was determined to be at a level which may be.

Table 6. Comparison of the prediction (P) and experimental results (E)

Parameters			Ra (µm)		Rz (µm)		Fx (N)		Fy (N)		Fz (N)	
V	f	a	P	E	P	E	P	E	P	E	P	E
120	0.1	2	1.49	1.58	8.73	8.4	61.9	64.2	597.2	583.3	475.9	481.1
160	0.1	2	1.43	1.55	11.1	10.4	53.5	56.4	549.8	555.6	422.1	429.7
200	0.1	5	2.35	2.62	12	11.1	55.6	58.5	388.2	375.7	289.2	297.6
200	0.1	2	2.19	2.32	11.56	12.25	51	54.2	526.6	515.9	389.9	381.6

4. CONCLUSION

It was found that the Ra and Rz values increased with increasing V , f and a values. The most effective parameters for the Ra and Rz roughness values were determined as f , V and a , respectively. According to ANOVA, it was found that the percentage effects of the parameters on Ra were 49.99% f , 47.5% V and 0.571% a . With an Rz value it was found that 48.93% V , 41.09% f and 8.59% a .

Optimal Ra cutting parameters were obtained at a V of 160 m / min, f of 0.1 mm / rev and a of 2 mm. In Rz, optimal values were obtained at a V of 120 m / min, f of 0.1 mm / rev and a of 2 mm. After the verification tests, the approximate ratio between the experimental and predicted values in Ra and Rz values was found to be 95.33% and 94.3%, respectively. The validity level of the models developed for

estimating the Ra and Rz roughness values was determined to be 92.3% and 94.4%, respectively.

The most effective parameters for the Fx and Fy forces were determined as an effect level from large to small as *f*, *a* and *V*, respectively. As a result of the ANOVA analysis, the contribution rate of the cutting parameters to the Fx and Fy forces became 58.29% and 66.65%, the *a* of 24.40% and 28.96%, and finally the *V* of 15.57 % and 5.179% determined. The effect levels of the cutting parameters on Fz were determined as *a*, *V* or *f*. According to the ANOVA analysis, it was found that the *a* 44.54%, the *V* 27.52% and the *f* 27.21% were effective on the Fz force. After the experiment using the optimal cutting parameters (V3-f1-a3) of the Fx value, the approximation ratio was found to be 94.1%, the Fy and Fz values (V3-f1-a2) to be 96.78% and 97.18% determined, respectively. The validity level of the models developed for the estimation of the cutting force values Fx, Fy and Fz was calculated approximately at the level of 96%.

REFERENCES

- Altinkaya, E. (2006). AISI 316 Östenitik çeliğın işlenmesinde kesme değerlerinin ve takım kaplamasının yüzey pürüzlülüğüne ve takım aşınmasına etkilerinin incelenmesi. Yüksek Lisans Tezi, Gazi Üniversitesi Fen Bilimleri Enstitüsü, Ankara.
- Aslan, E., Camuşcu, N., Birgören, B. (2006). Design optimization of cutting parameters when turning hardened AISI 4140 Steel (63 HRC) with Al₂O₃+ TiCN mixed ceramic tool, *Materials and Design*, 28(5), 1618-1622.
- Aslantaş, K., Uçun, İ. ve Çiçek, A. (2012). Tool life and wear mechanism of coated and uncoated Al₂O₃/ TiCN mixed ceramic tools in turning hardened alloy steel, *Wear*, 275, 442-451.
- Boothroyd, G. (1981). *Fundamentals of Metal Machining and Machine Tools*, International Student ed. 5th Printing, McGraw-Hill, ISBN 0-07-085057- 7, New York.
- Çınarlar, G., Emiroğlu, B. G., & Yurttakal, A. H. (2020). Prediction of Glioma Grades Using Deep Learning with Wavelet Radiomic Features. *Applied Sciences*, 10(18), 6296.
- Demirayak, İ. (2006). Kesme parametreleri ve kaplama tabakasının talaş kaldırma işlemine etkileri. Yüksek Lisans Tezi, Uludağ Üniversitesi Fen Bilimleri Enstitüsü, Bursa.
- Elbah, M., Yallese, M.A., Aouici, H., Mabrouki, T., Rigal, J.F. (2013). Comparative assessment of wiper and conventional ceramic tools on surface roughness in hard turning AISI 4140 steel, *Measurement*, 46(9), 3041-3056.
- Erbaş, N. 2020. Restructuring Efforts in the Turkish Agriculture, Availability of Resources and Developments in Rural: An Overall Analysis from 2001 to 2016. *Iğdır University Journal of the Institute of Science and Technology*, 10(1): 636- 647, Iğdır, Turkey.
- Gürbüz, H., Seker, U., Kafkas, F. (2020). Effects of cutting tool forms on the surface integrity in turning of AISI 316L Stainless Steel. *Journal of The Faculty Of Engineering and Architecture Of Gazi University*, 35(1), 225-240.

- Hessainia, Z. Belbah, A., Yallese, M.A., Mabrouki T., Rigal, J.F. (2013). On the prediction of surface roughness in the hard turning based on cutting parameters and tool vibrations, *Measurement*, 46(5), 1671-1681.
- İynen, O., Şahinoğlu, A., Özdemir, M., Yılmaz, V. (2020). Optimization of the Effect of Cutting Parameters on the Cutting Force in the Gradual Turning Process by Taguchi Method. *Journal of the Institute of Science and Technology*, 10(3), 1909-1918.
- Kam, M. (2016). Kriyojenik işlem görmüş millerin dinamik davranışlarının deneysel analizi. Doktora Tezi, Düzce Üniversitesi Fen Bilimleri Enstitüsü, Düzce.
- Kesti, E. (2009). Ç-4140 çeliğinin mikro yapı ve mekanik özelliklerine su verme ortamının etkilerinin araştırılması, Yüksek Lisans Tezi, Selçuk Üniversitesi Fen Bilimleri Enstitüsü, Konya.
- Özdemir, M. (2019). Optimization with Taguchi Method of Influences on Surface Roughness of Cutting Parameters in CNC Turning Processing. *Mechanics*, 25(5), 397-405.
- Özdemir, M., Kaya, M. T., Akyıldız, H.K. (2020). Analysis of surface roughness and cutting forces in hard turning of 42CrMo4 steel using Taguchi and RSM method. *Mechanics*, 26(3), 231-241.
- Özses, B. (2002). Bilgisayar sayısal denetimli takım tezgâhlarında değişik işleme koşullarının yüzey pürüzlülüğüne etkisi, Yüksek Lisans Tezi, Gazi Üniversitesi Fen Bilimleri Enstitüsü, Ankara.
- Pınar, A.M., Fırat, K. (2016). AISI 4140 çeliğin çok yönlü takımla tormalanmasında yüzey pürüzlülük performansının optimizasyonu, *Politeknik Dergisi*, 19(4), 491-498.
- Shiddique, M.S., Akhtar, M.N., Ziaulhaque, M. (2017). Turning parameter optimization for surface roughness of AISI 4140 alloy steel by taguchi method, *Ijsart Journal*, 3(5), 36-44.
- Şahinoğlu, A., Rafighi, M. (2020). Investigation of Vibration, Sound Intensity, Machine Current and Roughness Values of AISI 4140 During Machining on the Lathe. *Arabian Journal for Science and Engineering*, 45(2), 765-778.

- Şahinoğlu, A., Ulas, E. (2020). An investigation of cutting parameters effect on sound level, surface roughness, and power consumption during machining of hardened AISI 4140. *Mechanics & Industry*, 21(5), 523.
- Şahin, Y., Motorcu, A.R. (2004). AISI 4140 çeliğinin farklı kaplamalı karbür ve sermet kesici takımlarla işlenebilirliği, On Birinci Uluslararası Makine Tasarım ve imalat Kongresi, 1-13.
- Şeremet, M., Kam, M. (2019). AISI 4140 ıslah çeliğinin tornalama işleminde parametrelerin yüzey pürüzlülüğü ve takım aşınmasına etkisi üzerine bir değerlendirme. *Uluslararası Marmara Fen ve Sosyal Bilimler Kongresi* 2(1), 2030-2037.
- Taguchi, G., Elsayed, E., Hsiang, T. (1989). *Quality Engineering in Production Systems*, McGraw-Hill, Books, pp. 235-241. New York.
- Taguchi, G., Konishi, S. (1987). *Orthogonal Arrays and Linear Graphs*, American Supplier Institute.
- Yallese, M.A., Rigal, J.F., Chaoui, K., Boulanouar, L. (2005). The effects of cutting conditions on mixed ceramic and cubic boron nitride tool wear and on surface roughness during machining of X200Cr12 steel (60 HRC), *Proceedings of the Institution of Mechanical Engineers, Part B: Journal of Engineering Manufacture*, 219(1), 35-55.
- Yardımeden, A. (2018). Farklı kesme parametreleriyle AISI 1040 çeliğin tornalanmasında oluşan titreşimlerin ve yüzey pürüzlülüğün incelenmesi, *DÜMF Mühendislik Dergisi*, 9(1), 269-278.

CHAPTER 4
RECENT TREND AND DEVELOPMENT OF
CAST STEEL

Assist. Prof. Dr Mikail ASLAN¹

¹Metallurgical Material Science Engineering, Gaziantep University, Gaziantep, Turkey. Email:aslanm@gantep.edu.tr

INTRODUCTION

Steel is a versatile engineering material and is widely used today. Steel materials attract attention with their easy welding, easy production and high workability rate. Steel materials are versatile materials, their strength values, corrosion resistance and abrasion resistance are quite high. Due to these properties, steel materials are suitable for use in most industries.

Steel castings, on the other hand, are produced by pouring the melted steel into a specific mold by shaping the steel. Spilled liquid steel cools in the mold cavity. Later, the steel is cleaned. Sometimes, heat treatment may also be required (tempering etc.).

The most significant difference between steel castings and normal (wrought) steels is the production technique. Forged cast steels are ingot, tubular, rod-shaped, etc. They can be produced and processed in different ways. The most interesting aspect of steel castings is that steel castings are produced ready for use and are not subjected to shaping afterwards.

There are about 1,200 steel foundries in Turkey. In these steel foundries, different styles of casting are produced to meet the needs of the casting market. Each casting plant addresses a different part of the market. These markets are as follows.

- In the automotive industry (crankshafts, differential boxes, steering gearbox, etc.)
- Agricultural machinery (transmission boxes, front wheel forks, etc.)
- In machinery industry (hydraulic presses, forging presses heads and cylinders, gears, axles, machine tools, etc.)
- Oil and gas tanks
- Railways
- Power Plants
- General engineering equipment
- Nuclear power plants
- Defense equipment
- Motor Vehicles
- Shipbuilding
- Mining equipment
- Quarrying and dredging
- Construction equipment
- City infrastructure industry

1. TYPES AND CHEMICAL COMPOSITIONS OF CAST STEEL

Cast steel (steel casting) is an iron-carbon alloy. The carbon in its composition is mostly affected by the properties of cast steel. There are big differences in the properties of cast steel according to the amount of carbon. Types of cast steel are as follows

1.1. Non-alloy cast steels

Non-alloy cast steels are steels cast from plain carbon material. In the composition of plain carbon steels, aluminum, copper, etc., which remain in the composition as a result of processes such as silicon, manganese, phosphorus, sulfur purification, other than carbon elements can be found. The chemical composition of cast steels can be seen in Table 1.

Table 1. Chemical composition of cast steels [1].

Name of the Element	% Amount
Carbon (C)	0,25-1,7 (2,0)
Manganese (Mn)	0,50-1,00
Silicon (Si)	0,20-0,80
Phosphorus (P)	Max 0.05
Sulfur (S)	Max 0.06

1.2. Alloy cast steels

Alloy cast steels are steels cast from alloy steel. Alloy steels are steels in their composition that exceed the specified ratios in plain carbon steels (non-alloy steels) and have one or more of the other alloying elements for specific purposes. Alloy steels are as follows according to the sum of the alloying element in its composition. The most important alloying elements can be listed as follows:

Aluminum; the addition of aluminum up to 1% in alloy steels gives the hardness to the alloy. Abrasion resistance is gained on the outer parts with the azotting process.

Chrome; small amounts of chrome balance the formation of hard carbides and improve the heat treatment precision of steels. Grain formation increases with the addition of chromium to alloys. The addition of large amounts of chromium improves heat and corrosion resistance.

Cobalt; while it causes slowing of the heat-treatment conversion of steel, it improves the ability of tool steels to work at high temperatures without softening. Cobalt is an essential alloying element for super air steels.

Copper; the addition of up to 0.5% copper to the alloy improves the corrosion resistance of alloy steels.

Lead; Adding up to 0.2% lead to the alloy increases the workability of the steel and decreases its strength.

Manganese; manganese is always present in steel. After manganese melting, it combines with the remaining sulfur to form iron sulfur and reduces the brittleness of the steel.

Molybdenum; in steel alloys, it increases creep resistance at high temperatures, balances carbide, improves the red hardness of cutting tools. Reduces temper fragility in Nickel-Chrome steels.

Nickel; it improves resistance by improving grain boundary. On the downside, it affects the balance of carbides in the structure.

Tungsten; while it helps alloy steels to form very hard carbide, it causes delay in the conversion of heat treatments. This allows steels to maintain their hardness at high temperatures.

Silicon; with up to 0.3 % silicon phosphorus, it increases the fluency of the alloy without reducing its mechanical properties. Adding up to 1% silicon to the alloy improves the heat resistance of steels.

1.3. Low alloy cast steels

Low-alloy steels contain specified amounts of carbon chromium, nickel or molybdenum to enhance hardness and toughness. Low-alloy steels are most widely used in oil and gas parts as well as in the pump and valve sectors, but are also appropriate for combat vehicles and equipment for earth movement and construction. Nickel (Ni), Chromium (Cr), and Molybdenum (Mo) are common elements used in carbon steels. Nickel is used for corrosion resistance and for strength, stability and durability. Chromium is used to prevent wear and corrosion, and to help steel improve strength and durability. To withstand temperatures, molybdenum is added to improve the steel's strength and hardness.

1.4. High alloy cast steels

High alloy steels are a type of steel that contains alloy elements such as chrome, nickel, molybdenum in high rates in order to develop properties such as strength, corrosion resistance, and thermal resistance. The two main groups of these steels are tool steels and stainless steels. Tool steels are used in heavy working conditions such as cutting, punching and shaping various materials. Stainless steel, another important high alloy steel group, is preferred especially in applications where corrosion is important.

2. Recent Development and New Trends for Casting of Steel

J. Hufenbach et al. [2] added selenium to the structure of the $\text{Fe}_{85}\text{Cr}_4\text{Mo}_8\text{V}_2\text{C}_1$ cast iron and observed the change in its microstructure and mechanical properties. In this study, the structural changes on the $\text{Fe}_{85}\text{Cr}_4\text{Mo}_8\text{V}_2\text{C}_1$ cast iron with the addition of selenium (0.03%, 0.1 and 0.3% by weight) are examined and the results are as follows.

It found cubic (CeO_2), trigonal (Ce_2O_3) crystalline and two kinds of Ce-rich carbon oxide, as well as rectangular structure (CeC_2) and Ce carbides, with a content of 0.3 wt% Ce (see Figure 1). The addition of cerium to the structure led to the removal of coarse carbides from the structure, and carbides caused compact, round-shaped changes from fine lamellae (see Figure 1a). In addition, carbide nets have shown continuous necking and interruption with increasing Ce content, which has been monitored until the effect of rare soils on solidification behavior by activating primary austenite. In this study, it is clear that microstructural changes caused by the addition of cerium have a serious effect on the strength and deformation movement of alloys under compression and tensile load. The addition of 0.3 percent cerium provided a very significant improvement in yield and ultimate fracture strength under compression and tensile load compared to the FeCrMoVC alloy.

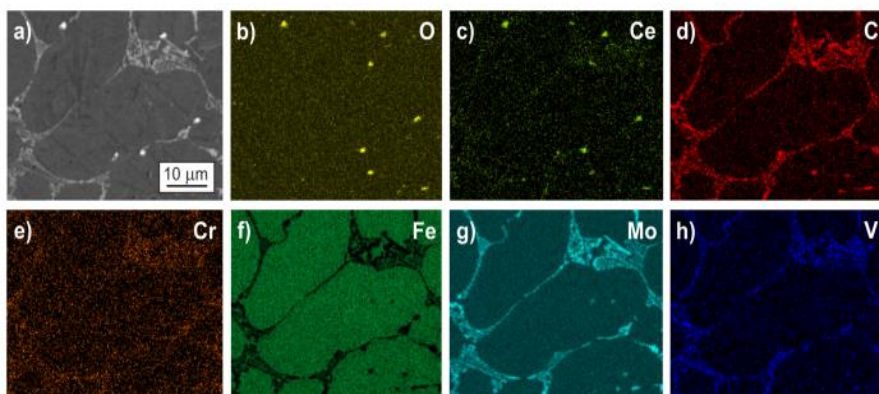


Figure 1. (a) SEM image of the alloy Ce 0.3% showing the carbide network within the matrix. Linked WDX simulation showing the distribution of (b) O as well as EDX mappings showing the distribution of (c) Ce, (d) C, (e) Cr, (f) Fe, (g) Mo and (h) V.

The addition of higher amounts of cerium (0.1% or 0.3% by weight) gave better results under pressure load than FeCrMoVC. Besides the changes in the phase fractions, this effect mainly caused changes in the carbide arrangement. The complex carbide network along the austenite grain boundaries observed in the FeCrMoVC alloy was gradually interrupted by the addition of Seryum, and the crack spreading along the road was prevented. It has been observed that by adding small Cerium particles combined with a special casting process to the $Fe_{85}Cr_4Mo_8V_2C_1$ base alloy, it is possible to obtain high-strength and simultaneously ductile cast steels that are promising for advanced tool steel design. A study on the Cracking Mechanism of Ferritic Austenitic Cast Steels was conducted by G. Stradowski [3]. In high alloy, ferritic-austenitic (duplex) stainless steels, especially when hot, the tendency to crack is high, and the presence of intergranular fractures indicates that the crack initiation is at high temperature and can be initiated by brake shrinkage associated with its

geometry. The occurrence of the brittle transcrystalline crack ipresented in Figures 2 and 3 indicates that another crack spread is due to fragile deposits of the secondary phases, especially the sigma phase, which can produce stress up to 2.0 GPa. For the material analyzed, a more or less continuous film form at the ferrite-austenite boundary is undesirable because it can cause delamination of the ferritic-austenitic structure, as mentioned. The change in the morphology of sigma phase precipitation is almost impossible for slow cooling castings. Its solution seems to be the acceleration of cooling in this phase secretion range by opening the mold. Qiming Wang et al. [4] achieved various results in their studies on the large inclusion mechanism in 80t 20Cr-8Ni stainless steel casting for nuclear energy. According to this study, it has been observed that the formation and evolution of inclusions during the oxygen decarburization furnace (AOD) refined Ca treatment ingot casting process reveals the mechanism of the formation of large inclusions in 80t 20Cr-8Ni stainless steel casting.

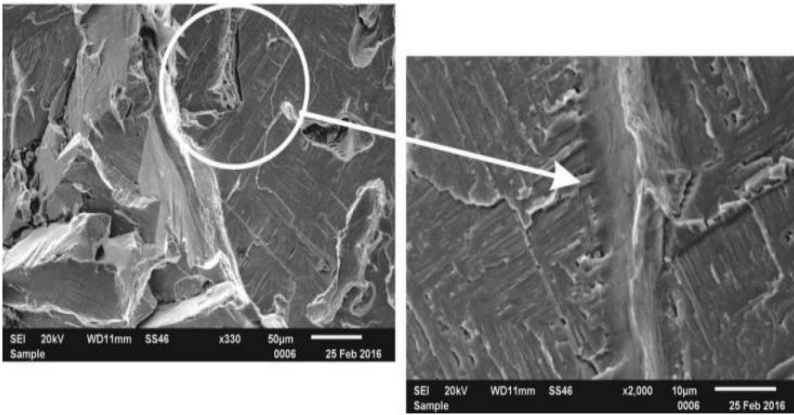


Figure 2. Area of columnar grains. The transcrystalline brittle cracking with numerous faults on the borders subgrains [3].

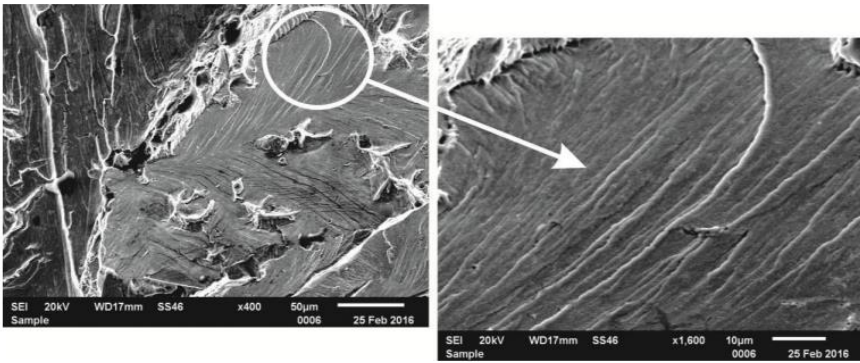


Figure 3. Area of equiaxed grains. The transcrystalline brittle cracking with many "rivers lines" [3].

According to the inclusion properties, thermodynamic calculations, inclusion growth and aggregation calculation, the following results are obtained:

The inclusion collection area on the nugget surface caused penetrating test failure. Al_2O_3 clusters and single Al_2O_3 particles were typical large inclusions for nugget. The size of Al_2O_3 clusters was used as $> 50 \mu m$ and single Al_2O_3 particles $> 10 \mu m$.

Typical additions were spinel or dual-phase CaO– MgO – Al₂O₃ after addition of aluminum into AOD. Common inclusions were liquid or dual-phase CaO–MgO–Al₂O₃ following treatment with Ca. However, with temperature declining during casting, Al₂O₃'s mass fraction in additions continued to increase due to lowering oxygen and aluminum solubility. One typical ingot oxide was Al₂O₃.

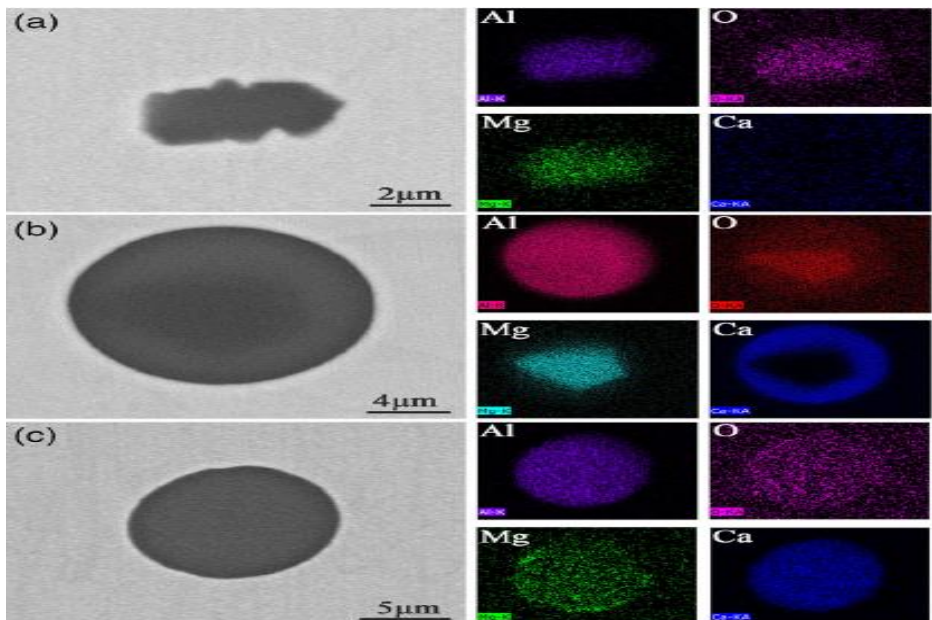


Figure 4. Elemental mapping of a)spinel, b)dual-phase oxides, c) liquid oxides [4].

During casting, Al₂O₃ particles can become larger up to $\geq 7.5 \mu\text{m}$. During the casting, Al₂O₃ particles can become larger up to $\geq 7.5 \mu\text{m}$. As the particle size of the single Al₂O₃ enhanced, Al₂O₃ clusters occurred due to stokes and turbulent collisions. Meanwhile, inclusions and slow cooling rate were observed at the required level. Finally, the single Al₂O₃ particles on the surface of the nugget were clustered, causing penetrating jugs to fail.

In-Sung Cho et. al. [5] made a study on the development of a thermophysical calculator using the CALPHAD approach of stainless steel casting alloys. In this study, a calculator that can calculate the thermophysical properties of stainless steel consisting of eight iron-based components was developed. The structure of stainless steels generally includes FCC solid solution, Me_7C_3 type carbides and BCC solid solution. Balance and out of balance solidification calculations are used to measure the solidification behavior of stainless steels, and from the results of this calculation, liquidity and solid, density and thermal conductivity values can be easily seen. S. B. Pratomo et al. [6] observed how the addition of Nickel to low alloy Cr-Mo cast steel changes the microstructure (see Figure 5). It was observed that increasing the nickel content from 0.3 % to 1 % increased tensile strength and hardness, but impact toughness did not change significantly. The addition of nickel provided increased strength with the solid solution reinforcement mechanism. Iron was replaced in the ferrite matrix by the substitution solid solution mechanism that resulted in a compressive stress field within the crystal lattice and caused the strengthening of the bainitic ferrite phase dissolved in nickel. Compressive stress has been observed to absorb impact energy, which increases toughness resistance. The addition of nickel particles to low-alloy Cr-Mo cast steel allowed fine grain size and greater grain boundary. As a result, Ni additions to low-alloy Cr-Mo cast steel prevent crack propagation, increasing strength and durability. Susil K. Putatunda [7] studied the effect of cooling temperature on microstructure and fracture toughness of cast steel.

This research includes the effect of high carbon, high silicon and high manganese on cast steel in terms of microstructure and fracture toughness.

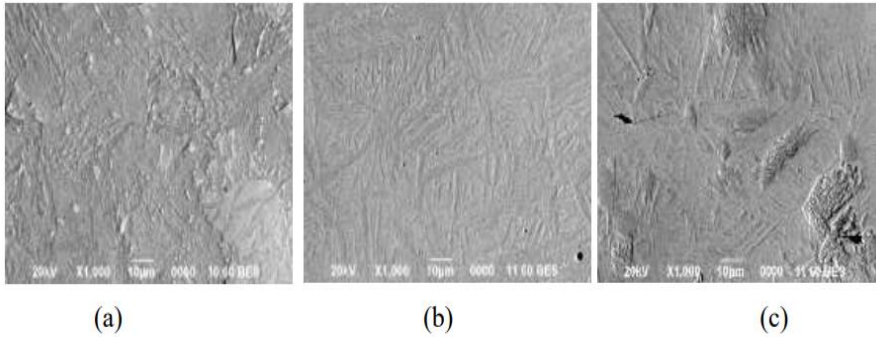


Figure 5. BSE-SEM images of sample with: (a) 0.3 % Ni, (b) 0.5 % Ni, (c) a 1.0 % Ni [6].

As a result of the studies, globalized cast steel with 85 % austenitic structure was produced. In the structure of this, steel includes 2% manganese 3.00% silicon and 1.00% carbon. This steel is manufactured using austenitic ductile iron (ADI) technology.

With the increase of the austenite content, a decrease in the volume fraction and the austempering temperature have been observed to increase up to 343.8 °C. The reason for this is thought to be that the reaction in the second stage of the ADI process occurs at a higher temperature. Due to the increased temperature of impregnation, serious improvements were observed in the properties of the material (yield and tensile strength). However, increasing the temperature of austempering causes the ductility to decrease. The highest fracture toughness of the material was observed between 316 °C and 393 °C temperatures. Ganwarich Pluphrach et al. [8] investigated the ferrite

grain size and mechanical properties of Mn₂₂V₆ micro-alloy low carbon cast steels and in these studies, they achieved: The Hall-Petch connecting can be used to examine the dependence of yield stress on ferrite grain size of cast steels. However, the expanded Hall-Petch relationship can be used to develop testing of heat treatment programs. Since the austenitizing temperature increases, the effects of austenitizing time and cooling rate on the ferrite grain size decrease. Also, an increase in cooling rate or a decrease in austenitization time and temperature can be shown as in the equation when continuous cooling conversion is reduced. In addition, there is a good correlation between the experimental and estimated ferrite grain size and yield stress of the material examined in this research study.

$$d_{\alpha} = 18152 \exp\left(\frac{-10174}{T}\right) (CR)^{-0.19} t^{0.37}$$

Roney Eduardo Lino et al. [9] researched how the chemical composition affects the structure of steel casting and the results from this study are briefly as follows.

Targetable calcium content and calcium range in the castability window were evaluated by computer thermodynamic evaluations. Based on this, it has been reached that the amount of calcium in the alloy is very important. It has been observed that the calcium element enables the replacement of inclusions and the sustainability of the continuous casting process. Increasing aluminum and sulfur elements in the structure under applied conditions decreases castability. On the

other hand, it has been observed that silicon can significantly improve castability. A multiple linear regression equation was created with the suitable correlation factor R_2 and this equation ensures a faster calculation than thermodynamic calculations. The equation calculates the requested calcium content in the function of aluminum, silicon, carbon and sulfur contents. Triple diagrams made from SEM semi-quantitative analysis indicated the formation of the following types of containment: spinel, corundum and CaS / aluminates. Spinel and corundum phases state a heterogeneous containment process after calcium therapy. By Huiji Fan et al. [10], the influence of tempering temperature on the microstructure and mechanical properties of G₁₈NiMoCr₃₋₆ cast steel was studied and they reach these outcomes: The normalized microstructure of G₁₈NiMoCr₃₋₆ cast steel is granular bainite, consisting of bainitic ferrite and some insulated grain or strip (M/A) islands. The carbides and (M/A) islands are gradually separated from each other because the tempering temperature increases. The temperature of the tempering must increase from 500 to 600 C for the carbides to be fully combined and spheroidized and to separate the islands (M/A) completely. When the temperature of tempering increases to 200 to 400 C (M/A), the islands are separated from each other and precipitation occurs in carbides, however, little by little diminishing has occurred in yield strength, tensile strength and hardness. After the temperature of tempering exceeded 400 C, a significant decrease occurred in these values. There was some reduction in elongation values, but later enhanced. After 400 C, it is the place where the elongation is the least impact energy.

When the temperature of tempering is 200 to 400 C, little by little diminished, also brittleness happened. After tempering temperature exceeds 400 C, it creates a significant reduction in toughness and impact energy.

E. Olejnik et al. [11] investigated the ward and wear resistance of TiC-Fe-Cr local reinforcement produced in cast steel. It allows the use of cast alloys and hard ceramics to pour composite materials such as TiC-Fe-Cr where they are produced. It is possible for TiC-Fe-Cr type composite cast steel materials to perform approximately five times better than chromium white cast irons, which are most resistant to abrasion. The increase of cast functional machines and similar machines enables a serious increase in service rate. R. O. Sousa et al. [12] studied on the inverse methodology of estimating the heat transfer coefficient in duplex stainless steel castings. The determination of the heat transfer coefficient (HTC) functions is crucial for a particular casting geometry, alloy chemical composition, and composition of the mold sand mixture.

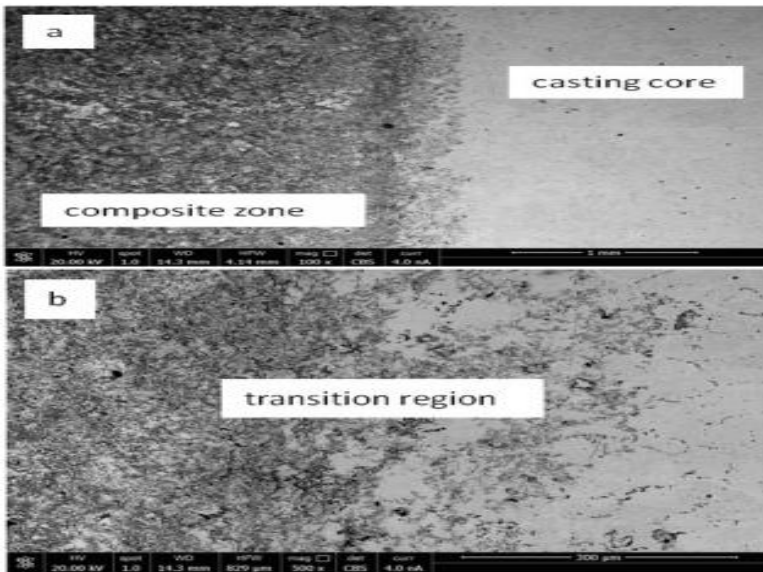


Figure 6. BSE images of the transition zone between the TiC-Fe-Cr composite regions and the casting core [11].

It has been observed that the commonly used HTC functions are not sufficient to replicate the experimental thermal data obtained for the casting of complex shapes with a C shape. The reverse analysis process can be used to identify HTC for a specified installation and as an adjustment for a numerical modeling. In addition, it has been observed that temperature distribution residual stress values may shed light on future studies. Jinxing Gao et al. [13] investigated on the impact of slag-steel reaction on the structure and viscosity of CaO-SiO₂-based mold flux during high-Al casting. The structure and viscosity properties of 3D-networks modified before and after the slag-steel reaction.

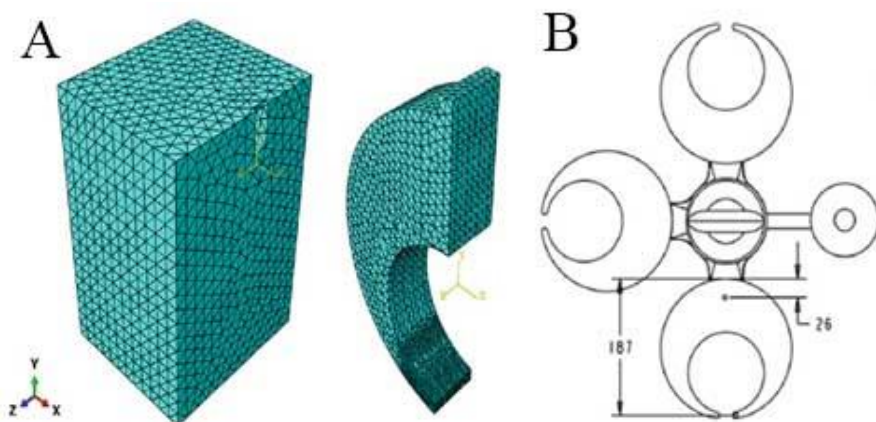


Figure 7. A) Finite element mesh for furan mold and C-ring. For computational cost saving, half of model was considered. B) Position of thermocouples on C-ring specimen (dimensions in mm) [12].

The original CaO-SiO₂-based flux has a silicate structure, and the Si-O-Si linkages primarily bind the 3D-network structure. Si atoms are gradually replaced by Al atoms, acting as network formers and transformed into the aluminosilicate structure principally connected by Si-O-Si, Al-O-Al, and Al-O-Si linkages after the slag-steel response. Al has three types of coordinating environments (species IVAl, V Al, and VIAl), but only the species IVAl can participate in 3D-network formation primarily in the form of AlO₄ and AlO₃F. The relative content of the species IVAl is influenced by the mold fluxes' chemical composition (specially associated with SiO₂). The degree of polymerization first reduces, and then rises throughout the phase of slag-steel reaction. The improvement in the degree of polymerization and chemical bond property will affect the structure and the rheological characteristics will deteriorate. To design the CaO-SiO₂-based mold flux for high-Al steel, it is therefore important to

change the mold flux composition and to improve the structural stability of mold flux to regulate the viscosity.

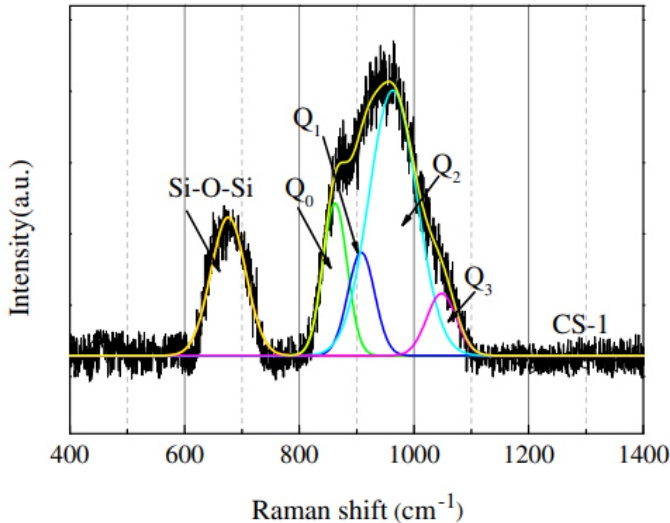


Figure 8. Typical Raman spectra deconvolution obtained for the mold flux [13].

P. Xue et al. [14] reached the following in their study on the improved mechanical properties of medium carbon steel casting by friction stir procedure (FSP) and subsequent annealing. The medium carbon steel workpiece was also run at 400 rpm, with additional rapid cooling at a rotational speed of 50 mm/min, and a friction mixing experiment was observed, with a depth of 1.6 mm. Analysis was made on the ferrite and martensite structure of FSP steel. Compared to the obtained process zone and base material, its hardness and strength are well developed. The hardness values of FSP steel are increased significantly and enhanced from 240 hv to 650 hv. The yield strength of FSP steel is enhanced from 590 MPa to 2070 MPa.

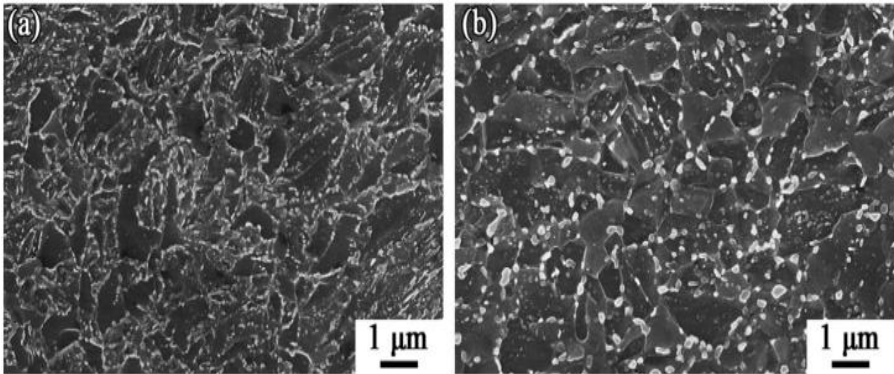


Figure 9. SEM microstructure of annealed FSP steel: (a) FSP-500 and (b) FSP-600 [14].

These results have been found quite satisfactory. After annealing, carbide particles precipitated from the martensite part. A very good strength and ductility compatibility have been achieved in FSP steel. The yield strength of FSP-500 work pieces is diminished to 1270 MPa. On the FSP-600 workpiece, yield strength is diminished up to 925 MPa. However, a sufficient ductility has been achieved after annealing. Jaromin et al. [15] investigated the effect of freckle type and shape on the solidification process of steel casting. This study did not examine the cooling calculations of a new optimization for cooling application during the steel casting manufacturing process. Construction variants 1 and 3 led to the creation of artificial end-feeding zones that separate the feeding areas of neighboring feeders, resulting in a reduced porosity trend. Chills caused a serious acceleration in the production cycle because of the shortening of the solidification time. Compared to other casting technologies, the solidification time is shortened by 2 hours, which is a great advantage. Optimization of this technology has yielded a yield of 15 percent,

which corresponds to 1595 kg. In addition, a 60 percent reduction in the weight of the feeders was observed. As a result of these developments, 1000 kWh of energy was saved.

Jie Xu et al. [16] investigated the fracture toughness of G20Mn5QT cast steel according to the acoustic emission technique. The achieved results are the same as those of other studies. On the other hand, AE technique will be of great help in detecting fractures in advance. The macroscopic and microscopic examination of the fracture, which is given in Figure 10-11, should be performed to determine the fracture toughness of the G20Mn5QT cast steel. Fracture values of G20Mn5QT cast steel were observed to be pit-microporous aggregate fracture in ductile fracture. According to the inspection of the size, quantity, depth and smoothness of the inner walls of the pits, G20Mn5QT cast steel has very good plasticity. This study researched the founding relationships of G20Mn5QT cast steel. The techniques developed in this study may inspire future research. The study of Jan Jezierski et al. [17] based on optimizing the grid system in steel castings. In some cases, it is necessary to reduce the metal speed, and to do this, the metallostatic pressure must be reduced. A pouring basin or intermediate pot should be used to prevent unwanted metal mixing. The gating system made is a nice method to measure the speed of the metal entering the mold cavity.

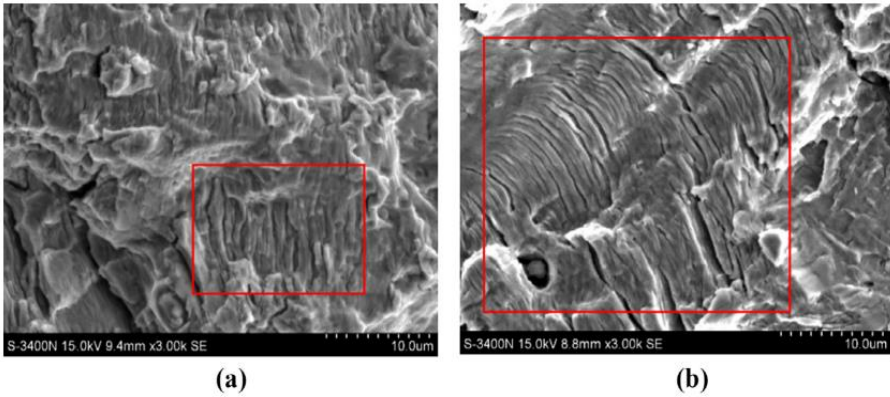


Figure 10. SEM images of the first fatigue zone and the second fatigue zone: (a) The first fatigue zone (b) The second fatigue zone for G20Mn5QT [16].

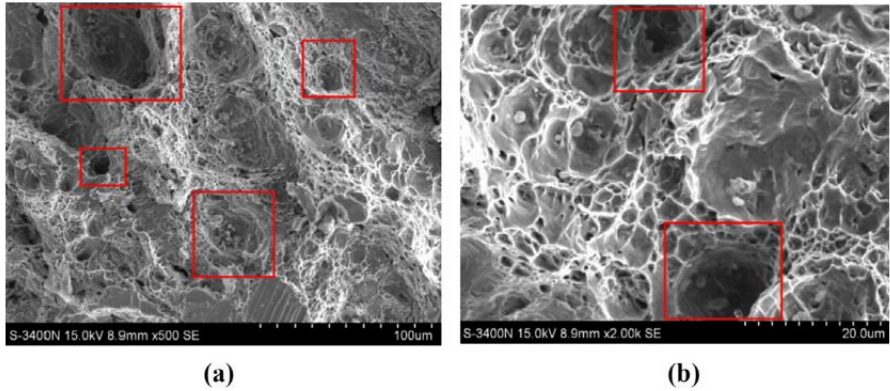


Figure 11. SEM images of the fracture toughness zone and the tensile fracture zone: (a) The fracture toughness zone (b) The tensile fracture zone for G20Mn5QT [16].

On the other hand, the gating system has enabled the system to have a more accurate and smooth metal flow (see Figure 12). Harpoon gates, spin trap and bubble trap are a combined system and are the most convenient method. This method is an optimized technique for castings produced in one piece. Since the molds are handmade, it is possible to cast complex shapes. In addition, researches and developments are continuing to ensure quality control and ease of application of the steel castings produced. On the other hand,.

application of the presented solutions can reduce metal efficiency. The increase in mechanical properties, the decrease in the number of errors and the decrease in efficiency are normal. The door system can improve the production and solidification process better.

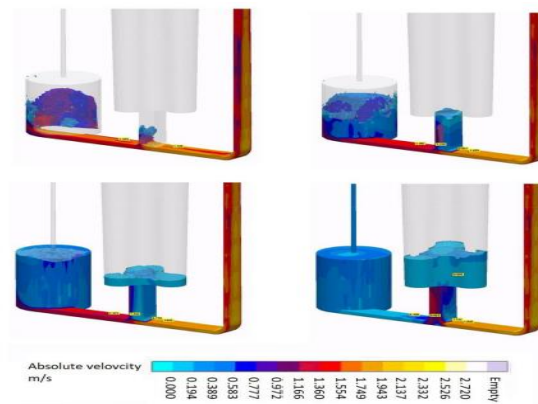


Figure 12. Spin trap gating system; filling time 10 sec. [17].

CONCLUSION

Cast steel has been used for a long time in various industrial sectors. The structure of cast steel can be easily changed by applying some processes. It is possible to produce steels that can be used in different fields according to the needs of the industry. For example, when tungsten is added to the structure of the steel, increase the strength of the steel. Therefore, the production of cast steel has been an interesting subject from past to present. Therefore, various techniques have been applied in the production of cast steel. These techniques aimed to improve product quality and many studies have been done on this subject.

REFERENCES

- [1] Adams, R. V. (1969). *U.S. Patent No. 3,478,808*. Washington, DC: U.S. Patent and Trademark Office.
- [2] Hufenbach, J., Helth, A., Lee, M. H., Wendrock, H., Giebeler, L., Choe, C. Y. & Eckert, J. (2016). Effect of cerium addition on microstructure and mechanical properties of high-strength Fe85Cr4Mo8V2C1 cast steel. *Materials Science and Engineering: A*, 674, 366-374.
- Eckert, J. (2016). Effect of cerium addition on microstructure and mechanical properties of high-strength Fe85Cr4Mo8V2C1 cast steel. *Materials Science and Engineering: A*, 674, 366-374.
- [3] Stradomski, G. (2016). The cracking mechanism of ferritic-austenitic cast steel. *Archives of Foundry Engineering*, 16.
- [4] Wang, Q., Cheng, G., Li, J., Dou, W., & Hu, X. (2019). Formation Mechanism of Large Inclusions in 80t 20Cr–8Ni Stainless Steel Casting for Nuclear Power. *steel research international*, 90(12), 1900349.
- [5] Cho, I. S., Savelyev, K. D., & Golod, V. M. (2017). Development of thermophysical calculator for stainless steel casting alloys by using CALPHAD approach. *China Foundry*, 14(5), 353-358.
- [6] Pratomo, S. B., Oktadinata, H., & Widodo, T. W. (2019, June). Effect of nickel additions on microstructure evolution and mechanical properties of low-alloy Cr-Mo cast steel. In *IOP Conference Series: Materials Science and Engineering* (Vol. 541, No. 1, p. 012050). IOP Publishing.
- [7] Putatunda, S. K. (2003). Influence of austempering temperature on microstructure and fracture toughness of a high-carbon, high-silicon and high-manganese cast steel. *Materials & design*, 24(6), 435-443.
- [8] Pluphrach, G., & Yamsai, S. (2018). Estimation of Ferrite Grain Size and Mechanical Properties of a 22MnVNb6 Microalloyed Low Carbon Cast Steel. *Periodica Polytechnica Mechanical Engineering*, 62(1), 83-89.

- [9] Lino, R. E., Marins, Â. M. F., Marchi, L. A., Mendes, J. A., Penna, L. V., Neto, J. G. C., & Caldeira, J. H. P. (2017). Influence of the chemical composition on steel casting performance. *Journal of Materials Research and Technology*, 6(1), 50-56.
- [10] Fan, H., Li, Y., Jin, X., Chen, B., Tang, C., & Zhu, P. (2018, July). Effect of tempering process on microstructure and mechanical properties of G18NiMoCr3-6 cast steel. In *IOP Conference Series: Materials Science and Engineering* (Vol. 394, No. 3, p. 032128). IOP Publishing.
- [11] Olejnik, E., Szymański, Ł., Kurtyka, P., Tokarski, T., Grabowska, B., & Czapla, P. (2016). Hardness and wear resistance of TiC-Fe-Cr locally reinforcement produced in cast steel. *Archives of foundry engineering*, 16.
- [12] Sousa, R. O., Felde, I., Ferreira, P. J., Deus, A. M., & Ribeiro, L. M. M. (2019). Inverse Methodology for Estimating the Heat Transfer Coefficient in a Duplex Stainless-Steel Casting. In *Materials Design and Applications II* (pp. 59-69). Springer, Cham.
- [13] Gao, J., Wen, G., Huang, T., Bai, B., Tang, P., & Liu, Q. (2016). Effect of slag-steel reaction on the structure and viscosity of CaO-SiO₂-based mold flux during high-Al steel casting. *Journal of Non-Crystalline Solids*, 452, 119-124.
- [14] Xue, P., Li, W. D., Wang, D., Wang, W. G., Xiao, B. L., & Ma, Z. Y. (2016). Enhanced mechanical properties of medium carbon steel casting via friction stir processing and subsequent annealing. *Materials Science and Engineering: A*, 670, 153-158.
- [15] Jaromin, M., Dojka, R., Jezierski, J. R., & Dojka, M. (2019). Influence of type and shape of the chill on solidification process of steel casting. *Archives of Foundry Engineering*.
- [16] Xu, J., Sun, T., Xu, Y., & Han, Q. (2020). Fracture toughness research of G20Mn5QT cast steel based on the acoustic emission technique. *Construction and Building Materials*, 230, 116904.
- [17] Jezierski, J., Dojka, R., & Janerka, K. (2018). Optimizing the gating system for steel castings. *Metals*, 8(4), 266.

- [18] Fu, H., Xiao, Q., Kuang, J., Jiang, Z., & Xing, J. D. (2007). Effect of rare earth and titanium additions on the microstructures and properties of low carbon Fe–B cast steel. *Materials Science and Engineering: A*, 466(1-2), 160-165.
- [19] Gao, W. L., Leng, Y., Fu, D. F., & Teng, J. (2016). Effects of niobium and heat treatment on microstructure and mechanical properties of low carbon cast steels. *Materials & Design*, 105, 114-123.

CHAPTER 5
**RECENT DEVELOPMENTS OF WELDING OF AEROSPACE
MATERIALS**

Assist. Prof. Dr Mikail ASLAN¹

¹Metallurgical Material Science Engineering, Gaziantep University, Gaziantep, Turkey. Email:aslanm@gantep.edu.tr orcid id:0000-0003-0578-5049

INTRODUCTION

Aerospace industry is one of the most important sciences that greatly developed in the recent years. So, as the space structures have to be huge, they also have to be light in the same time. For these reasons, very good mechanical properties, low density, corrosion resistance materials were used in aerospace manufacturing, such as titanium and stainless-steel alloys [1]. The graphic analysis in Figure 1 shows the percentage of materials used in aerospace field.

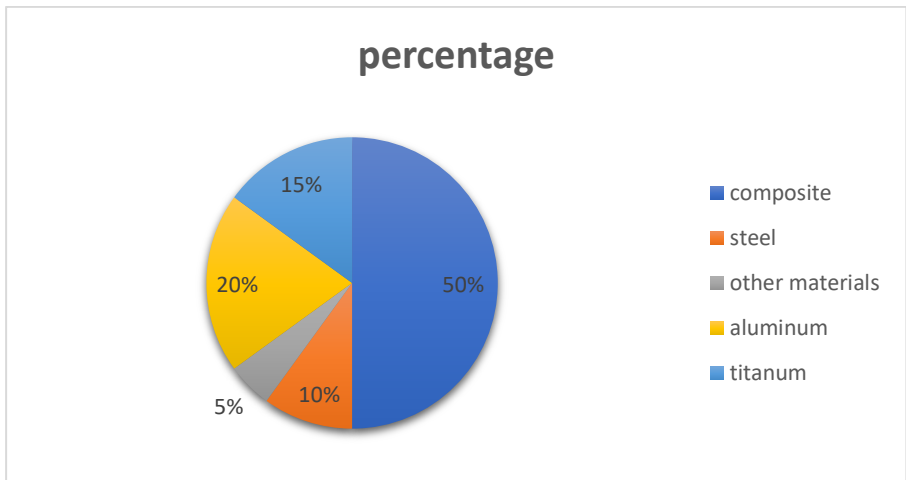


Figure 1. Graphical analysis the percentage of used materials in aerospace industry [1].

Due to the easy manufacturing of these materials it was frequently used in aerospace field. And to make high mass production of industrialization these types of materials, there were a need to joint it using a very high-quality welding methods. But because of the phase transportation of these materials during welding at high temperature, undesirable changes and reduction in mechanical properties of joints were occurred. A lot of researches have been done to skip these

problems in welding of aerospace materials. Recently, laser welding and gas tungsten arc welding (TIG) methods have been a good choices to weld both of titanium and stainless-steel alloys for aerospace constructions [2-3]. Because of its big depth to width weld ratio and less welding distortion when comparing with other welding process [4-5]. But because of the low thermal conductivity and the changing of temperature distribution its mechanical properties have changed to negative situation.

For these reasons new laser welding techniques was developed to overcome these problems, such as laser welding associated by new energetic multilayer [6]. This process increases the strength of joints to a big ratio, also the changing of laser speed and power output value has a noticeable change on the depth of underfill defects whose occurred when using laser welding with normal speed, such as shown in Figure 2.

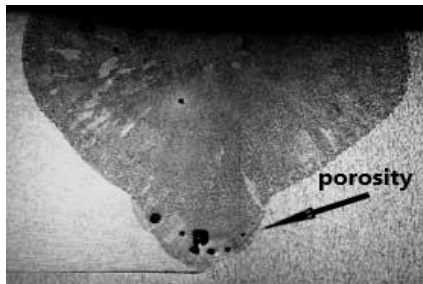


Figure 2 laser welded joint by normal laser speed. Adapted from [7] © 2019 TWI Ltd.

While for TIG welding process a new development named by active flux TIG welding obtained to control the Marangoni convection. All these developments and its effects on weld quality are discussed in these papers.

Recent development in laser welding for aerospace materials

In the last twenty years, great importance has been given to weld aerospace materials by laser welding method in order to make a good mass production method. The development of laser welding technique still plays a very important role for making a good joined parts for aerospace machines and one of this technics was related to the use of nanometric energetic layers made from nano aluminum and metal oxide films that has been used as reacted multilayer films (RMFs) between the welded parts, to improve the laser welding process. These layers provides the laser welding process to give high strength joined parts and better weld quality for aerospace materials when comparing with parts welded by normal laser welding process and to examine the effect of these new welding method on the weld quality of aerospace materials, Ti6Al4V titanium alloys were examined with 1 mm thickness and chemical composition, as shown in Table 1 and 40 micro meter thickness of Ni/Al RMFs layers were placed between two the titanium alloys parts. By applying a 700 W laser power on these parts the RMFs layers burned and led to a self-propagation exothermic reaction that destroy the structure of the reactive multilayer films [8]. This destruction is due the external welding heat source for Ti6Al4V titanium alloys.

Table 1. The Chemical Composition of Ti6Al4V Used in Welding Process

Components	Percentage (by wt)
V	4.22
Al	5.48
Ti	90
Fe	0.112
Si	0.0222
C	0.369
Ni	<0.0010
Nb	0.0386
Sn	0.0625
Zr	0.0028
Mo	0.005
Cr	0.0099
Cu	<0.02

That has been led to welded joints with higher strength. When applying a different laser power on the welded part by this method, the obtained welded part from these reactive layers increase the strength of welded joints about 2-3 times compared with joints welded by the normal laser welding process (without interlayer), as shown in Figure 3.

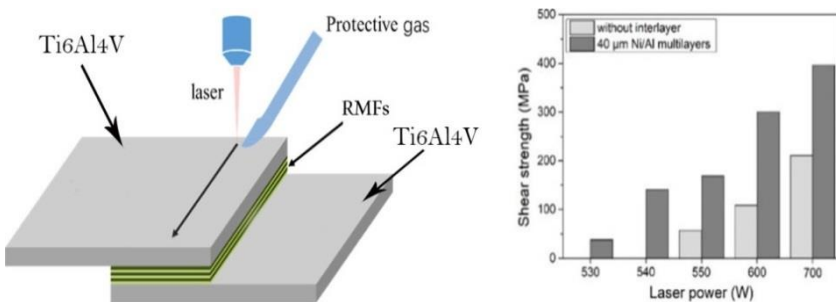


Figure 3. Laser power and relationship with shear strength. Adapted from [6]

On the other hand, regarding to the microstructure of joints welded by using this new laser welding method, the disappearance of partial dimple has been occurred in addition to the decrease in the area of flat section. Also, the formation of high number of net-like shape structure appear in the welding area of parts due to the reaction between the energetic RMFs layers and Ti6Al4V titanium alloys. The new method increased the strength of welded joints to approximately 40% better than joints welded in same situation but with normal laser welding process. The laser welding supported by RMFS energetic layers between Ti6Al4V titanium alloy increases the strength of joints approximately 400 MPa and it is 3 times better than joints welded by normal laser welding method. Also, it reduced the power of used laser to about 14%, without decreasing the strength of Ti6Al4V titanium alloys welded joints [6]. Thus, this process is a very useful technique and widely used method for applying welding works between aerospace materials for high welding quality.

Another development in laser welding of aerospace materials is related to the laser speed and applied power. It provides another effecting ways to join aerospace materials such as Ti6Al4V titanium alloys and to produce higher strength welded joint and better weld quality than materials welded with normal laser speed and normal power. When 5mm thickness of Ti6Al4V titanium alloys sheet are welded by using 4 Kw of laser power applied by Nd:YAG laser system and with using various speed values of applied laser, many changes have occurred in the mechanical properties of welded joints. At normal speed about 1.25 cm per second, the formation of under fill

defects and porosity was seen in welded zone of joints. This was due to the vaporization and expelling of the molten materials in the welding area of joints [9]. In addition, the formation of wide fusion zone for comparing with the depth of welded joints is shown in Figure 4a.

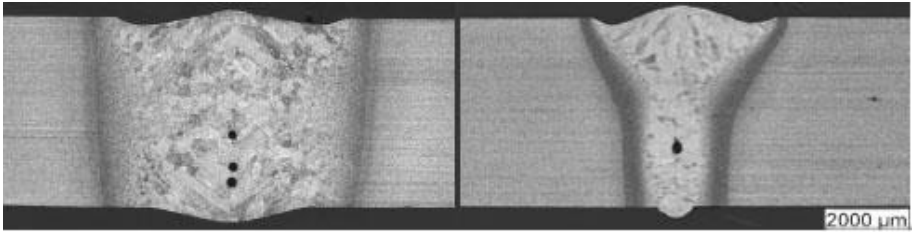


Figure 4. cross section of laser welded joint by different speeds. (a) Laser speed of 1.25 cm/s (b) laser speed of 3 cm/s. Adapted from [9]

These caused a significant decreasing in all of weld quality, tensile strength and thickness of Ti6Al4V titanium alloys welded joints. Depending on the AWS D17.1 rules [10], the design of fusion welding joints of aerospace materials has to be with a maximum underfill depth about 0.06 of the welded material thicknesses so when the speed of Nd:YAG laser system increased the weld speed of 3 cm per second, the ratio of permeation increased and the wide of fusion zone in the joints decreased, as shown in Figure 4b, and a high decrease was found in the depth of underfill defects due to the reduction in the weld pool flow and decreasing of solidification time of fusion zone because of the high cooling speed that happened after high speed laser welding process [11]. Also, by scanning the microstructure of sheets joined by using high speed laser welding process, a high reduction in grain size was observed when comparing with joints welded by normal laser speed. This also led to improve the

mechanical properties of Ti6Al4V titanium alloys welded joints, such as hardness and yield strength. In general, increasing the speed of laser has a significant effect on all of mechanical properties, width to depth ratio and underfill defects.

Recent development in TIG welding for aerospace materials

TIG welding process is another technique chosen for welding of aerospace materials such as stainless steel or titanium alloys due to its high ability for weld dissembler materials but because of the narrow propagation in normal TIG welding process, it could not weld thick structures in one pass of welding, and this makes it less productive method. Therefore, to skip this problem, many researches have been investigated to improve the TIG welding process and to control the Marangoni convection for increasing the weld quality and productivity. Recently, as a new TIG welding process named by active flux TIG welding has been introduced to make a shallow and wide joint between aerospace materials with a good mechanical property for joints [12]. In this method, a tungsten electrode with a double shielding torch inner and outer is used. The inner torch was from helium, while the outer was from mixture of helium and oxygen (heliox), which is illustrated in Figure 5.

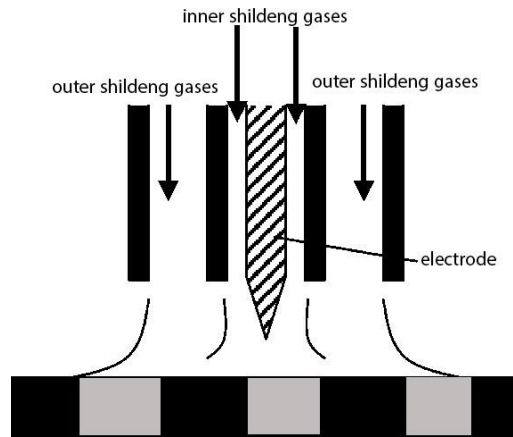


Figure 5. Mechanism of double torch of active flux TIG welding method. Adapted from [12]

By examining of this new TIG welding method on stainless steel plates, there was a noticeable change in welded parts shape, which are from wide and thin shape to a deep and slim shape depending on the changing of Marangoni convection direction. Also, a significant reduction in tungsten electrode consumption was clearly observed even if there was an oxidation gas. By V notch Charpy impact test and bending test, very good mechanical properties were found in joints welded by using active flux TIG welding method. For a comparison of joints welded by using normal TIG method, tensile strength of the welded joints increased to 510 MPa. Results indicate that very good joints can be made between stainless steel sheets for aerospace industries under any sever condition with a high mass production rate by using active flux TIG welding method.

CONCLUSION

Due to the considerable interest in welding of aerospace materials, many developments have done to increase the weld quality of aerospace materials such as laser welding assisted by energetic layers (RMFs) which led to produce very high strength joints for aerospace field. Also, improving the laser speed and power output leads to a very good width to depth ratio. On the other hand, the new welding process is known as active flux TIG welding that improved the welding process by controlling the Marangoni convection direction and thus this make welded joints with high welding quality for aerospace industry.

REFERENCES

- [1] Hong, H. A. T. J. M., Riga, A. T., Gahoon, J. M., & Scott, C. G. (1993). Machinability of steels and titanium alloys under lubrication. *Wear*, 162, 34-39. [https://doi.org/10.1016/0043-1648\(93\)90481-Z](https://doi.org/10.1016/0043-1648(93)90481-Z)
- [2] Auwal, S. T., Ramesh, S., Yusof, F., & Manladan, S. M. (2018). A review on laser beam welding of titanium alloys. *The International Journal of Advanced Manufacturing Technology*, 97(1-4), 1071-1098. <https://doi.org/10.1007/s00170-018-2030-x>
- [3] Karlsson, L. (2012). Welding duplex stainless steels-A review of current recommendations. *Weld. World*, 56(5), 65-76. <https://doi.org/10.1007/BF03321351>
- [4] Li, L., Tan, C., Chen, Y., Guo, W., & Song, F. (2013). Comparative study on microstructure and mechanical properties of laser welded– brazed Mg/mild steel and Mg/stainless steel joints. *Materials & Design*, 43, 59-65 <https://doi.org/10.1016/j.matdes.2012.06.057>
- [5] Akman, E., Demir, A., Canel, T., & Sınmazçelik, T. (2009). Laser welding of Ti6Al4V titanium alloys. *Journal of materials processing technology*, 209(8), 3705-3713. <https://doi.org/10.1016/j.jmatprotec.2008.08.026>
- [6] Li, H., Ma, Y., Xu, B., Bridges, D., Zhang, L., Feng, Z., & Hu, A. (2019). Laser welding of Ti6Al4V assisted with nanostructured Ni/Al reactive multilayer films. *Materials & Design*, 181, 108097. <https://doi.org/10.1016/j.matdes.2019.108097>
- [7] Yang, J., Zhang, H., & Li, Y. L. (2015). Optimization of Nd: YAG laser Welding of aluminum alloy to stainless steel thin sheets via taguchi method and response surface methodology (RSM). *Lasers in Engineering*, 31(3–4), 141-159. *Lasers in Eng.*, Vol. 0, pp. 1–19
- [8] Ma, E., Thompson, C. V., Clevenger, L. A., & Tu, K. N. (1990). Self-propagating explosive reactions in Al/Ni multilayer thin films. *Applied physics letters*, 57(12), 1262-1264. <https://doi.org/10.1063/1.103504>

- [9] Kabir, A. S. H., Cao, X., Medraj, M., Wanjara, P., Cuddy, J., & Birur, A. (2010, October). Effect of welding speed and defocusing distance on the quality of laser welded Ti-6Al-4V. In *Proceedings of the Materials Science and Technology (MS&T) 2010 Conference*, Houston, TX (pp. 2787-2797).
- [10] AWS. (2001). *Specification for Fusion Welding for Aerospace Applications*.
- [11] Pastor, M., Zhao, H., Martukanitz, R. P., & Debroy, T. (1999). Porosity, underfill and magnesium loss during continuous wave Nd: YAG laser welding of thin plates of aluminum alloys 5182 and 5754. *Welding Journal-New York-*, 78, 207-s.
- [12] Fujii, H., Sato, T., Lu, S., & Nogi, K. (2008). Development of an advanced A-TIG (AA-TIG) welding method by control of Marangoni convection. *Materials Science and Engineering: A*, 495(1-2), 296-303. <https://doi.org/10.1016/j.msea.2007.10.116>

BÖLÜM 6
ENVIRONMENTAL IMPACT ASSESSMENT REGULATIONS
IN TURKEY: EVALUATION OF METAL RECYCLING
PROJECT DECISIONS

Assoc. Prof. Dr. Ayla BILGIN*

* Artvin Coruh University, Department of Environmental Engineering, 08100, Artvin/Turkey, E-mail: ayla.bilgin@gmail.com <https://orcid.org/0000-0002-1873-6038>

INTRODUCTION

Environmental Impact Assessment (EIA) is a process that investigates and analyzes the environmental impacts of human activities. EIA is to guarantee a sustainable development suitable for the protection of ecosystems. The EIA has proven to be an effective environmental management tool (Jay et al., 2007; Toro et al., 2013). The EIA includes environmental impact assessment of the project, plan environmental impact assessment and strategic environmental assessment. With the regionalization and globalization of environmental problems, transboundary environmental impact assessment is also increasing (Zhuang et al., 2011).

The European vision of 2050 is mainly focused on preserving natural capital and producing resource-efficient products. Although the main objective of the EU (European Union) is to improve air and water quality, the main concerns regarding the loss of soil functions, land degradation and climate change require more protection. EU is planned to reduce greenhouse gas emissions, fossil fuel use, resource use, waste generation and improve recycling rates (Piattoni & Polverari, 2016).

In Europe, it is seen that the most waste is formed in France, considering the hazardous and non-hazardous waste recycling data (Figure 1). In some countries, the amount of waste decreased from 2010 to 2016. These countries are Bulgaria, Denmark, Belgium, Switzerland, Netherlands, Ireland, Sweden, Finland and Italy. In

some countries, the amount of waste has increased from 2010 to 2016. These countries are Germany, France and Turkey etc.

General regulations on waste management in Turkey; The regulations on waste diversity and EU Directives have been published and put into practice (MEU, 2012). The amount of waste can be recycled in Turkey has increased between the years 2010-2016 when evaluated. It is seen that the amount of metal waste increased on a yearly basis. This situation is considered as the result of industrialization (Figure 2). The wastes are recovered in order to reuse them or to remove the hazardous properties they contain. Wastes containing precious metals such as aluminum, zinc and copper are recovered by appropriate processes and thus contribute to the economy. Statistics show that the main metal industry wastes are in the first place, followed by manufacturing of food products, manufacturing of other non-metallic mineral products and production of chemicals and chemical products, respectively (BSTB, 2017).

Environmental Impact Assessment with the EIA Directive entered into force on February 7, 1993 in Turkey was defined as a legal process (OG, 1993). The EIA Regulation was revised on 23 June 1997 (OG, 1997), 6 June 2002 (OG, 2002), 16 December 2003(OG, 2003), 17 July 2008(OG, 2008), 3 October 2013 (OG, 2013)and lastly 25 November 2014(OG, 2014). From 1993 to 2018, the EIA Regulation has been amended 7 times (Bilgin, 2015). Turkey in the process of Environmental Impact Assessment projects is examined Annex 1 (Environmental Impact Assessment to Implementation Projects List)

and Annex 2 (Screening Selection Criteria will be implemented Projects List). For projects listed in Annex 1, "EIA Positive" or "EIA Negative" decision is given. For projects listed in Annex-2 list, "EIA Required" or "EIA Not Required" decision is given. It is determined according to the capacities of the project.

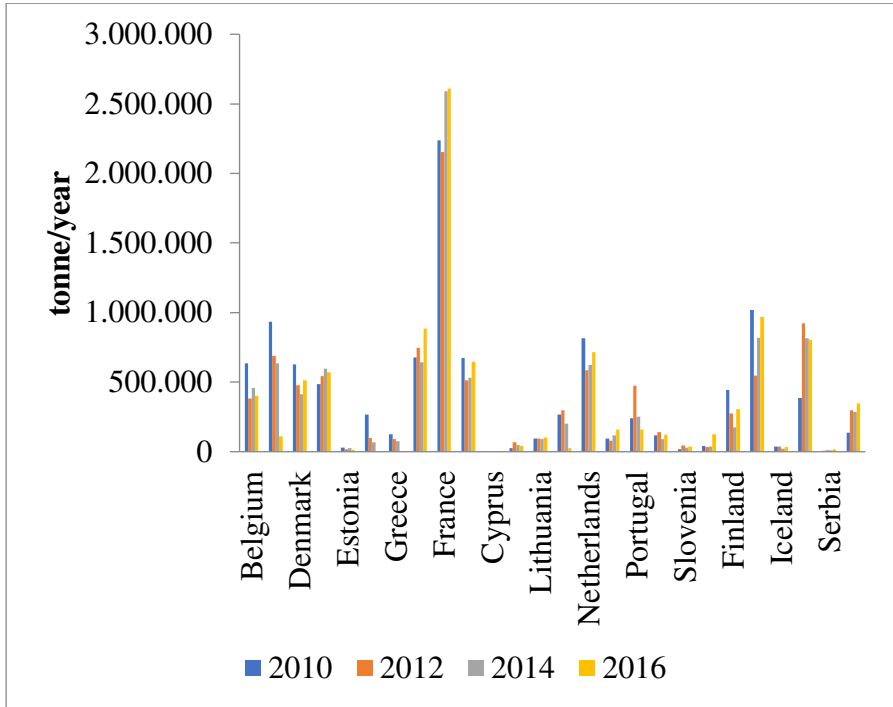


Figure 1. Hazardous -Non-Hazardous Metal Waste Quantities In European Union Countries [8].

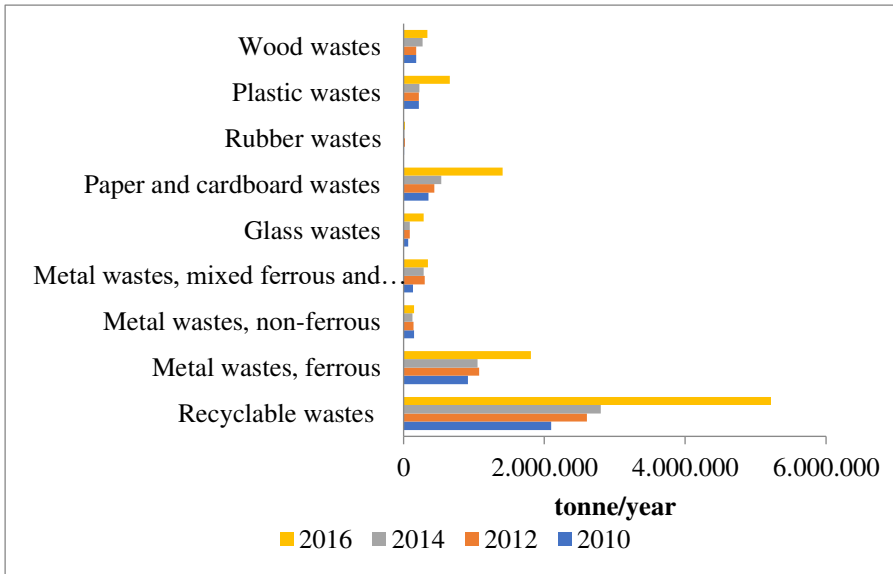


Figure 2. Recycling Waste Amount In Turkey (URL, 2019).

EIA Annex-1 recycling project list in Turkey are;

- 1) Waste disposal installations for the recovery and / or final disposal of hazardous and specially processed wastes,
- 2) Facilities designed for waste oil recovery with a capacity equal to and above 2.000 tonne per year,
- 3) Facilities where waste of more than 10 hectares, and / or target year, including 100 tonne and more per day, excluding construction ruins and excavation wastes, within the scope of the EIA (OG, 2014).

In this study, the EIA decisions of recycling between 1993 and 2018 were examined. This study results show that the scope of recycling practices at EIA in Turkey.

1. METHODOLOGY/METHODS

The data were taken from the Ministry of Environment and Urbanization web site (URL, 2018). EIA projects in Turkey are evaluated under seven headings. In this study, recycling processes under waste-chemical EIA projects were evaluated. The EIA decisions between 1993-2018 were evaluated. SPSS-19 program was used to evaluate the data. Frequency and crosstab analyzes were used in the program. In the study, Annex-1 (big capacity projects) recycling projects was evaluated within the scope of EIA.

2. RESULTS

Recycling EIA decisions within the scope of Turkey EIA Regulation are evaluated from 1993 to 2018. Accordingly, the EIA project decision was carried out for the highest number of tire recycling projects. Secondly, the EIA project was carried out for metal recycling projects in Turkey (Figure 3).

Recycling projects EIA decisions were made on the basis of a yearly evaluation and in 2013 the highest recycling project was carried out (Figure 4). On the basis of the province, it is seen that the recycling facilities are established in the places where the industry is the most (Figure 5). According to the results, it indicates that recycling projects are carried out because there is more waste in areas close to industrial areas.

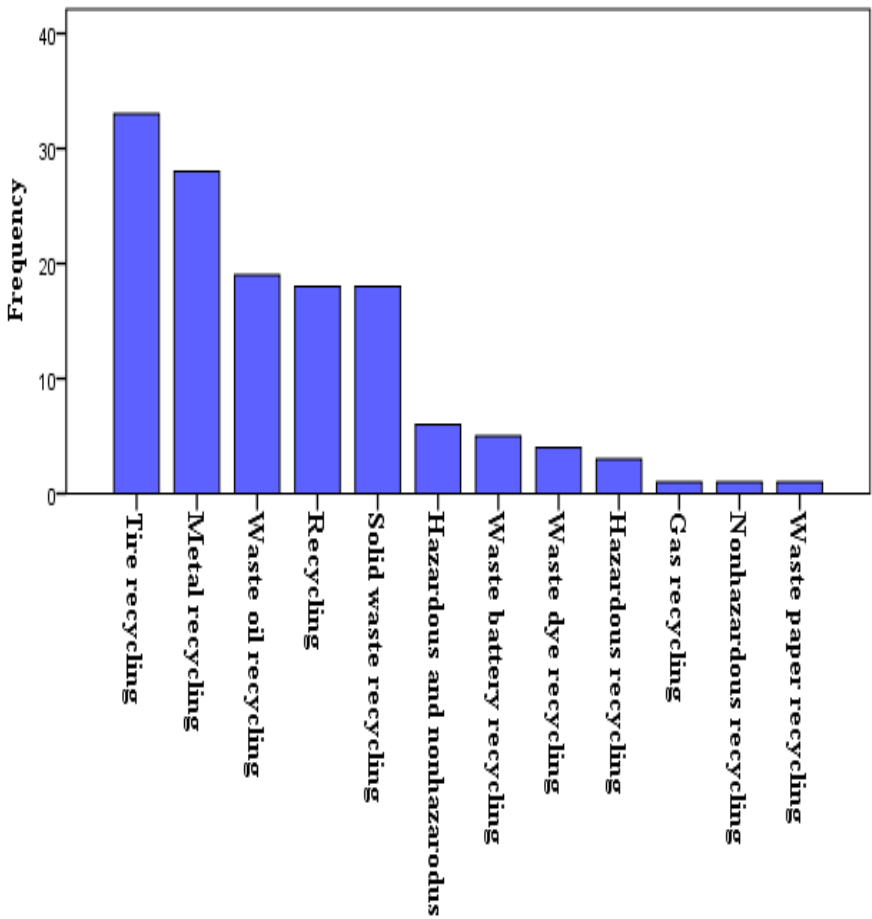


Figure 3. Annex-1 EIA Recycling Projects In Turkey, (EIA-Annex-1;1993-2018)

Metal recycling projects EIA decisions were evaluated on the basis of region, province and year. When these projects are evaluated regionally; the Marmara Region (9), the Central Anatolian Region (7), the Aegean Region (6), the Mediterranean Region (5) and the Black Sea Region (1), respectively (Figure 6). When the evaluation is made on the basis of year, it shows that the maximum number of projects increased in 2018 (Figure 7). On the basis of the province; most metal recycling projects in Turkey's largest city Istanbul and Izmir, are made (Figure 8). This result shows that metal recycling companies are established in the area where industry is very high.

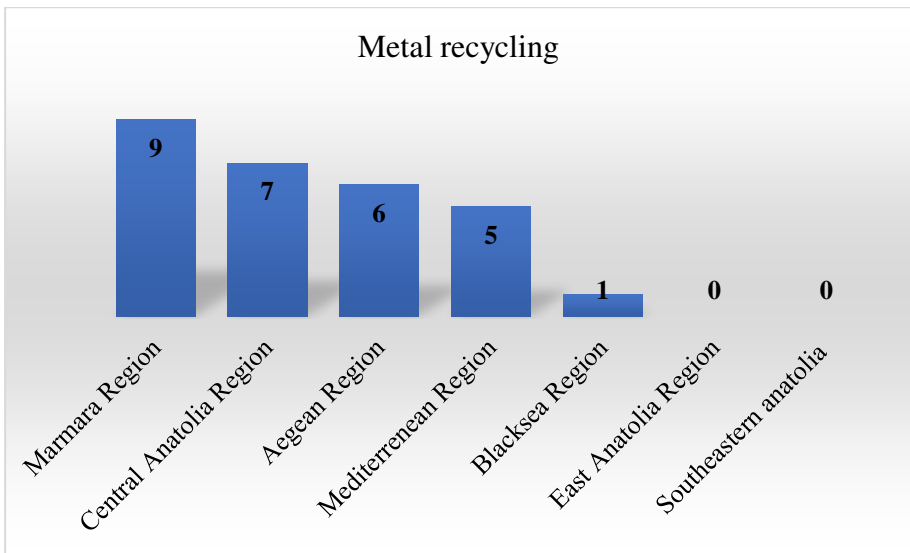


Figure 6. Metal Recycling Projects in Turkey According to Regions (EIA-Annex-1;1993-2018)

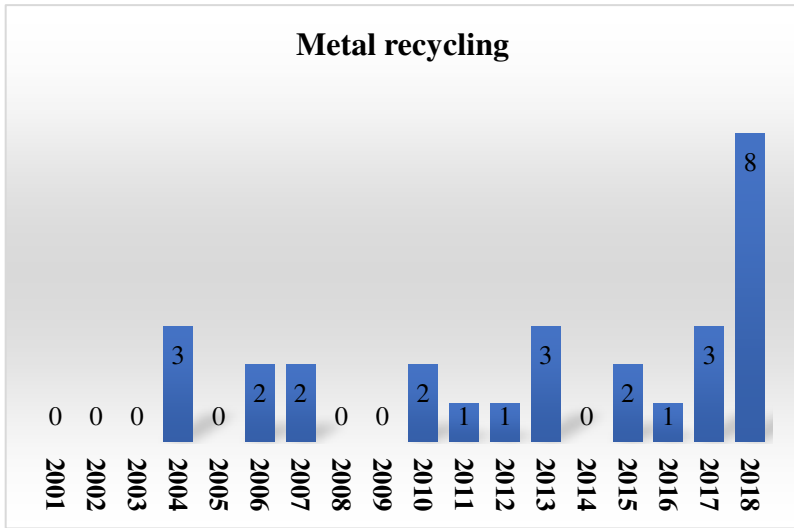


Figure 7. Metal Recycling Projects in Turkey According to years (EIA-Annex-1;1993-2018)

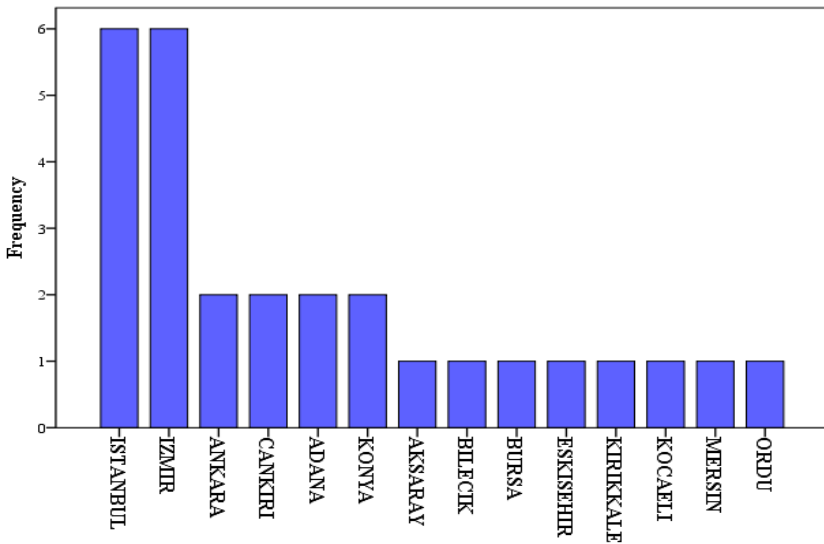


Figure 8. Metal Recycling Projects in Turkey According to Provinces (EIA-Annex-1;1993-2018)

CONCLUSION

In this study was evaluated according to the EIA recycling projects in Turkey. Social, environmental and economic impacts of recycling are considered to be important, since natural resources are limited with sustainable development. The most important phase of waste management is recycling; It is defined as the inclusion of recyclable wastes in the production process by converting them into secondary raw materials with various physical and / or chemical methods. With increasing technology, the environment is getting more and more polluted. The EIA regulation is an important tool for the planned management of the environment around the world. When the EIA applications are evaluated, it is seen that the implementation of the legislation from country to country has changed. Environmental pollution is important on a global scale. Different evaluations of countries are insufficient to solve common problems. It is seen that the number of metal recycling projects has increased in recent years. It shows that the recycling projects have increased in places where the industry is close.

REFERENCES

- Bilgin, A. (2015). Analysis of the Environmental Impact Assessment (EIA) Directive and the EIA decision in Turkey. *Environmental Impact Assessment Review*. <https://doi.org/10.1016/j.eiar.2015.04.001>
- BSTB. (2017). No Title. *Bilim, Sanayi Ve Teknoloji Bakanlığı, Ulusal Geri Dönüşüm Strateji Belgesi Ve Eylem Planı 2014-2017*.
- Jay, S., Jones, C., Slinn, P., & Wood, C. (2007). Environmental impact assessment: Retrospect and prospect. *Environmental Impact Assessment Review*. <https://doi.org/10.1016/j.eiar.2006.12.001>
- MEU. (2012). *Ministry of Environment and Urbanization, Turkey*.
- OG. (1993). *Official Gazette, Environmental Impact Assessment Regulation. Turkish Official Gazette 21489, 7 February*.
- OG. (1997). *Official Gazette, Environmental Impact Assessment Regulation. Turkish Official Gazette, 23028, 23 June*.
- OG. (2002). *Official Gazette, Environmental Impact Assessment Regulation. Turkish Official Gazette 24777, 6 June*.
- OG. (2003). *Official Gazette, Environmental Impact Assessment Regulation. Turkish Official Gazette, 25318, 16 December*.
- OG. (2008). *Official Gazette, "Environmental Impact Assessment Regulation", Turkish Official Gazette, 26939, 17 July*.
- OG. (2013). *Official Gazette, Environmental Impact Assessment Regulation. Turkish Official Gazette, 28784, 16 October*.
- OG. (2014). *Official Gazette, Environmental Impact Assessment Regulation, 29186, Turkish Official Gazette (2014) (25 November)*.
- Piattoni, S., & Polverari, L. (2016). Handbook on Cohesion Policy in the EU. In *Handbook on Cohesion Policy in the EU*. <https://doi.org/10.4337/9781784715670>
- Toro, J., Requena, I., Duarte, O., & Zamorano, M. (2013). A qualitative method proposal to improve environmental impact assessment. *Environmental Impact Assessment Review*. <https://doi.org/10.1016/j.eiar.2013.04.004>

URL. (2019). [Http://Ced.Csb.Gov.Tr/Ced-Kararlari-i-82321](http://Ced.Csb.Gov.Tr/Ced-Kararlari-i-82321).

Zhuang, Y., Hong, S., Lin, H., & Niu, B. (2011). Global environmental impact assessment research trends (1973-2009). *Procedia Environmental Sciences*. <https://doi.org/10.1016/j.proenv.2011.12.226>

CHAPTER 7

DETERMINATION OF BIOGAS POTENTIAL OF WASTES FROM DIFFERENT ANIMAL SPECIES IN TUNCELI PROVINCE

Dr. Erdal ILĐIN¹

¹ Dicle University Technical Sciences Vocational School, Department of Motor Vehicles and Transportation Technologies. DIYARBAKIR TURKEY
cilgin_erdal@hotmail.com.tr.

INTRODUCTION

In 1804, the world population hit 1 billion; in 1927, 2 billion; in 1961, 3 billion; and in 1971, 4 billion. The rapid population growth started at 5 billion in 1987 and the world population was 6 billion in 1999 and 7 billion in 2011, respectively. Especially with the impact of the rapid increase observed after 1950, every 12 years the world population has increased by 1 billion. In addition to this rapid growth of the world 's population, there is a rise in manufacturing and the resulting demand for oil. Rising energy demand is typically met by conventional reserves of fossil fuels. Fossil fuels are created as a result of thermochemical reactions to plant animal waste buried under the ground in a certain area millions of years ago. It is possible to identify fossil fuels as coal, oil and natural gas. The world's fossil fuel reserves consist of 70% of coal, 14% of oil, 14% of natural gas and 2% of other fossil resources. That is, in some regions, fossil fuels have small amounts (reserves). Because the production of these limited fuel reserves takes far longer than their consumption, it is known that in the near future, these fuels will not respond to growing energy demand. Furthermore, during the mining, refining and use of these conventional sources of fossil fuels, emissions have a detrimental influence on living conditions and the climate. These limitations of conventional sources have targeted researchers towards modern and sustainable sources of energy.

Solar energy, geothermal energy, hydroelectric energy, hydrogen, wave / ocean, wind and biomass energy are new and alternative energy sources. Biogas is one of the sources of biomass oil. Biogas is

characterized as a flammable gas with a high methane content produced by the digestive activities of anaerobic bacteria in the absence of oxygen, which allows organic wastes that cause environmental and health problems to be made harmless and converted into energy. It contains mainly of methane gas. In general, it contains 55-75% methane, 44-24% carbon dioxide and at least 1% separate gases. Since biogas is manufactured from organic materials, it. With oxygen, these gases can be burned or oxidized. It is possible to burn and convert the chemical energy found in the gases to heat energy, and this heat can be used in many places. By burning it in a gas engine, it can also be used in electricity generation. Due to its biogas composition, it has a compression property and can be used as fuel in motor vehicles like CNG (compressed natural gas).

1. MATERIALS USED IN PROCESSING BIOGAS

The products used for the production of biogas, such as animal fertilizers, organic waste and industrial waste, can be analyzed under three headings.

In this sense, materials used,
Waste of Livestock
Wastes obtained by horses,
Fertilizers from plants,
From vegetable waste
Waste in the garden,
The excess of food,
Industrial garbage

Waste from agriculture,
Forest Business Wastes,
Wastes from the leather and textile business,
The paper industry wastes,
Waste from the food industry,
The Wastes
Waste water purification plant waste.

The processing of biogas can be accomplished using agricultural waste or industrial waste. By processing municipal waste separately and sewage waste in treatment plants, there is a major biogas production potential. Turkey-İzmir Metropolitan Municipality In this sense, some studies have been carried out within the framework of the Grand Canal Project(Wu, L. 1999).

2. BIOGAS PRODUCTION

As a consequence of a biological operation, biogas exists. Leaving the organic mass without oxygen and then producing a gas mixture called biogas is the fundamental feature of the process. In living spaces, this mechanism takes place naturally. For example, it occurs on ruminant animals' seabed, manure pits, marshes and rumen. The conversion from biomass to biogas is achieved by a number of microorganisms in this process. While low levels of hydrogen, hydrogen sulfide, ammonia and ammonia are contained in biogas(Adebayo,2013).

2.1. Hydrolysis stage

In the first step, the compounds that are not soluble in the sludge become soluble with the cellular enzymes secreted by the microorganisms. In short-chain structures, they transform long-chain complex carbohydrates, proteins, fats and lipids. The first step of hydrolysis is completed as a consequence of the conversion to these basic organics (ilkiliç,2011).

2.2. Acid forming phase

At this stage, acetogenic (acid-forming) bacterial groups that are released as a result of the first stage and transform into acetic acid volatile fatty acids come into action, and some acetogenic bacteria transform into acetic acid and hydrogen volatile fatty acids(Borjesson,2005).



By using the released carbon dioxide and hydrogen, another element of the acetogenic bacterial group forms acetic acid. The quantity of acetic acid provided by this second route is, however, lower than the first.

2.3. Methane formation

The method is the process of transforming bacteria into biogas by breaking down acetic acid or synthesizing hydrogen and carbon dioxide. Producing methane is a process that is slower than other processes. Effective bacteria are highly influenced by environmental conditions when methane is produced(Kalia VC, 2000).

3. FACTORS AFFECTING BIOGAS PRODUCTION

Generally speaking, any factor that is influenced by microbiological bacteria affecting the formation of biogas also affects the development of biogas. To continue its vital activities, a bacterium requires certain temperature and pH values. At the same time, toxicity affects the behaviors of bacteria directly. The C / N ratio (carbon / nitrogen) is significant because it affects a bacterium's rate of decomposition. The narrow C / N ratio means that the waste can be broken down quicker by bacteria. Finally, Organic Lo, Organic Lo, (Vindis, 2009).

3.1. Effects of Temperature on Biogas Production

At very high and very low temperatures, methanogenic bacteria are non-active. Therefore, the temperature of the reactor where the production of biogas would take place directly affects the production or speed of biogas. These bacteria are very sensitive to differences in temperature. Inside the reactor, the temperature also determines the waiting period and the volume of the reactor. Temperature classification according to its degree can be achieved in three ways.

Psychophilic temperature range = 12-20 Degrees

Mesophilic temperature range = 20-40 Degrees

Thermophilic temperature range = 40-65 Degrees

3.2. Ph's Effects on Biogas Production

Neutral or slightly alkaline values are the best pH values for methane-forming bacteria. As the fermentation process continues, it varies between 7-7.5 under anaerobic conditions. It has a toxic effect on

bacteria in cases where the pH value decreases to 6.7 levels. There could be an rise in the number of acid-forming bacteria, causing the pH to drop and methane to stop. The loading of organic matter is disrupted in such situations and the acid ratio is decreased. It is also possible to use chemistry to make the pH stable.

3.3. Effects of toxicity on biogas production

Negative effects on bacterial growth are caused by contaminants such as mineral ions, heavy metals and detergents. Production can slow down or stop with these substances leaking into bioreactors. In systems where chicken manure is used in gas processing, the addition of antibiotics to the feed in poultry farming has toxic effects. In the fertilizers of chickens fed with this type of feed, antibiotics are also present, and these antibiotics have a negative effect on methane-forming bacteria(Sun and Qi, 1993).

3.4. Effects of C / N Ratio on Biogas Production

To get energy, anaerobic bacteria use biomass. Another material essential for bacteria to expand and propagate is nitrogen. For waste to be generated from biogas, the C / N ratio should be at an acceptable value. Not more than 23/1 and less than 10/1 should be the ratio. Because of the formation of ammonia, the high nitrogen rate negatively impacts the production of biogas.

3.5. Effects of Organic Loading Speed on Biogas Production

One of the most significant features that should be recognized in anaerobic fermentation is the loading rate. A factor dependent on the

quality of dry matter and waiting time is the loading rate. Usually, the loading rate is kg-UK / m³-reactor. It is given in the form of a day. Volatile solid removal in general decreases as the loading rate increases. The quantity of volatile solids does not provide conclusive results concerning the production of biogas. The ideal organic loading rate during the anaerobic fermentation should be preserved wherever possible. The explanation for this is that acid bacteria become dominant as H₂ is not eliminated by the methane bacteria at a sufficient rate and volatile organic acid production increases and acid accumulation occurs. The organic loading rate is the amount of organic material fed to the bioreactors per unit volume (m³) per day. It decreases or even stops the production rate of gas. Keeping the organic loading rate as optimal as possible is important. The pH level could otherwise decrease and stop the formation of gas compound

Table 1: Optimum organic loading rate for reactors operating in mesophilic conditions(Öztürk,2017).

Waste Material	Loading Amount / Day
Beef Manure	2.5. – 3.5. kg-UK/ m ³ Day
Additional Nutrient Cattle Fertilizer	5 – 7 kg-UK/ m ³ Day
Pig Fertilizer	3.0 – 3.5. kg-UK/ m ³ Day

4. OBTAINING BIOGAS FROM ANIMAL WASTES

Depending on the increasing population in the world and Turkey, both major rises in animal waste and environmental emissions are highly significant. The use of animal waste in non-processed agricultural areas both decreases the consistency of the commodity and distorts the composition of the soil used for agricultural purposes. In addition, unwanted odor, insect, fly formation and especially clean water sources pollute if these waste is not routinely stored (Mutlu. 2003). Today, using all existing livestock manure, biogas can be generated. Animal waste used in biogas processing is also poultry, sheep, cattle, pigs and goats, single-nailed animal fertilizers (Eryaşar. 2009). In contrast to sheep and goat fertilizers, anaerobic decay times are shorter and more biogas is thus collected. Maybe it is. Therefore, a condition that improves productivity is the combining of sheep and goat fertilizers with cattle manure (Cestonaro.2015). Poultry manure with the highest fertilizer value is the most fertilized value of organic matter. However, in the biogas production process, elevated nitrogen content in poultry manure may cause ammonia to accumulate (Görmiş.2018).

Advantages Of Biogas

Biogas is a renewable energy source.

The raw materials (animal, vegetable, industrial wastes) used in biogas production are idle substances.

It can be produced using a cheap technology.

It can also be used for electricity generation and for heating purposes.

Biogas is easy to install, so it does not require large-scale investments.

It also reduces the greenhouse effect by using the gases produced in the storage areas as energy form.

Disadvantages of Biogas;

Biogas contains a number of impurities even after refining processes are carried out.

The process of using biogas on a large scale is not economically viable, and it is very difficult to increase the effectiveness of biogas systems.

It is unstable, if methane comes into contact with oxygen and is flammable in nature, it can cause explosions (Chinese,1985).

5. MATERIAL AND METHOD

In Turkey, the installed capacity of power plants is 81,356 MW. The province with the highest capacity is izmir, as the installed electricity, and Ağrı, which has no production plant, is the province with the lowest capacity. Wind power plants Fırat-Dicle Basin and Çoruh Basin hydroelectric power plants, coal mine domestic coal power plants, imported coal power plants in coastal towns, natural gas power plants in high-electricity regions In the regions of the Aegean coast and east of the Mediterranean,

Table 2: Cities' Power Plant Installed Powers and Production and Consumption Information (Enerji atlası,2020).

	City	Installed Power	Annual Approximate Production	Production / Consumption Rate
1	Kahramanmaraş	4.328 MW	6.568 GWh	121 %
2	İzmir	4.281 MW	18.320 GWh	85 %
3	Çanakkale	3.979 MW	21.085 GWh	438 %
4	Adana	3.751 MW	15.365 GWh	201 %
5	Şanlıurfa	3.431 MW	9.971 GWh	132 %
65	Tunceli	107 MW	282 GWh	238 %

Tunceli's power plant, which is situated entirely in the Euphrates Basin in the area of Eastern Anatolia, is 107 MW. Tunceli's power plants, which have a total of 6 power plants, generate 282 GW of electricity per year. Profile of power plants of the province in Table.3 Table.4. PBX data is entered in.

Table 3: Profile of Tunceli Power Plants (Enerji atlası,2020).

Number of Active Plants	6
Installed Power	107 MW
Installed Power Ratio	% 0,13
Annual Electricity Production	~ 282 GWh
Consumption Rate to Turkey	% 0,11
License Status	4 licensed, 2 unlicensed

Table 4: Tunceli Power Plant information (Enerji atlası,2020).

Switchboard Name	Facility Type	Installed Power
Uzunçayır Dam and HES	Hydroelectric	82 MW
Mercan HES	Hydroelectric	20 MW
Dinar HES	Hydroelectric	4.4 MW
Çemişgezek HES	Hydroelectric	0.12 MW
Tunceli Solar Power Plant	Sun	0.10 MW
Aydın Sarıtaş Solar Power Plant	Sun	0.015 MW

The power plant of Tunceli, which is situated entirely in the Euphrates Basin in the Eastern Anatolia region, is 107 MW. The power plants of Tunceli, which have 6 power plants in total, produce 282 GW of electricity per year. The profile of the province's power plants in Table.3 Table.4. PBX information is entered in.

Assumptions:

3.6 tons / year fertilizer from cattle,

0.7 tons / year fertilizer from sheep and goats,

It is accepted that 0.022 ton / year fertilizer is obtained from poultry on average (Deniz 1987).

Biogas assumptions:

33 m3 of biogas from 1 ton of bovine manure,

58 m3 of biogas from 1 ton of ovine manure,

A research result of 78 m3 of biogas from 1 ton poultry manure was found

The value of 1m3 biogas in terms of electrical energy; 1 m3 of biogas is 4.70 kWh energy (Knows. 1983).

The number of cattle, sheep and poultry and total fertilizer amount of Tunceli provinces and districts are given in Table 5. However, the fertilizer formation amounts given here are potential fertilizer production and in practice only a certain part of this fertilizer can be collected. The collectability of animal fertilizers is related to the duration of the animals in the closed area and the possibilities of collecting and accumulating the wastes generated in closed areas (Bulut.2019). Considering the 2020 Animal numbers obtained from the

Tunceli Provincial Directorate of Agriculture and Forestry, Table.5 is the district with the highest number of cattle. The district with the lowest number of cattle is Hozat.

Table 5: The equivalent of biogas potential that can be obtained from cattle of Tunceli provinces and districts as electrical energy

District	Cattle	Tons / year of fertilizer	Biogas m3	kWh
City Center	5714	20.570.4	678.823	3.190.468
Ovacık	6.153	22.150.8	730.963	3.435.526
Çemişgezek	4737	17.053.2	562.755	2.644.948
Mazgirt	7906	28.461.6	939.232	4.414.390
Pertek	6562	23.623.2	779.565	3.663.955
Hozat	2418	08.704.8	287.258	1.350.112
Pülümür	4619	16.628.4	548.737	2.579.063
Nazimiye	3593	12.934.8	426.848	2.006.185
Genel Toplam	41702	150.127.2	4.954.197	23.284.725

In this table, where the number of animals and the related fertilizer production is calculated, the total amount of bovine manure in the province was calculated as 150.127 m3. In the same table, the number of cattle belonging to the province of Tunceli and the amount of biogas that can be obtained were calculated as 4.954.197 m3. Since 1 m3 of biogas is considered to be the equivalent of 4.70 kWh, the energy value that can be obtained from bovine manure in the province was calculated as 23.284.725 kWh. When the table.6 where the number of ovine animals and the fertilizer, biogas and energy values of Tunceli province are given is analyzed, it was seen that the number of ovine animals increased by 932,81% compared to the number of bovine animals. The amount of fertilizer that can be obtained with the number of ovine

animals throughout the province has been calculated as 301.490 Ton / year. Table 6, below. The amount of biogas that can be obtained with ovine livestock manure was 17.486.460m³, while the energy that can be obtained was calculated as 82.186.365kWh.

Table 6: The equivalent of biogas potential that can be obtained from small ruminants of Tunceli provinces and districts as electrical energy

District	Small cattle	Tons / year of fertilizer	Biogas m ³	kWh
City Center	20423	014.296	829.173	3.897.113
Ovacık	25.340	017.738	1.028.804	4.835.379
Çemişgezek	144068	100.847	5.849.160	27.491.052
Mazgirt	40226	028.158	1.663.175	7.816.922
Pertek	161.750	113.225	6.567.050	30.865.135
Hozat	26379	018.465	1.070.987	5.033.638
Pülümür	7848	005.493	318.628	1.497.551
Nazimiye	4667	003.266	189.480	890.556
The overall total	430701	301.490	17.486.460	82.186.365

When Table.5, where the number of poultry and the related fertilizer, biogas and energy values are given in Tunceli province, it is seen that the poultry is inadequate in the province. The amount of poultry that can be obtained with the number of poultry in the province was calculated as 754.84 Ton / year. Tablo.7. While the amount of biogas that can be obtained with poultry manure is 58718 m³, the energy that can be obtained has been calculated as 275.974 kWh.

Table 7: The equivalent of biogas potential that can be obtained from poultry of Tunceli provinces and districts as electrical energy

District	Poultry	Tons / year of fertilizer	Biogas m3	kWh
City Center	*	*	*	*
Ovacık	*	*	*	*
Çemişgezek	*	*	*	*
Mazgirt	31000	682	53.196	250.021
Pertek	*	*	*	*
Hozat	3220	70.84	5.522	25.953
Pülümür	*	*	*	*
Nazimiye	*	*	*	*
Genel Toplam	34.220	754.84	58718	275.974

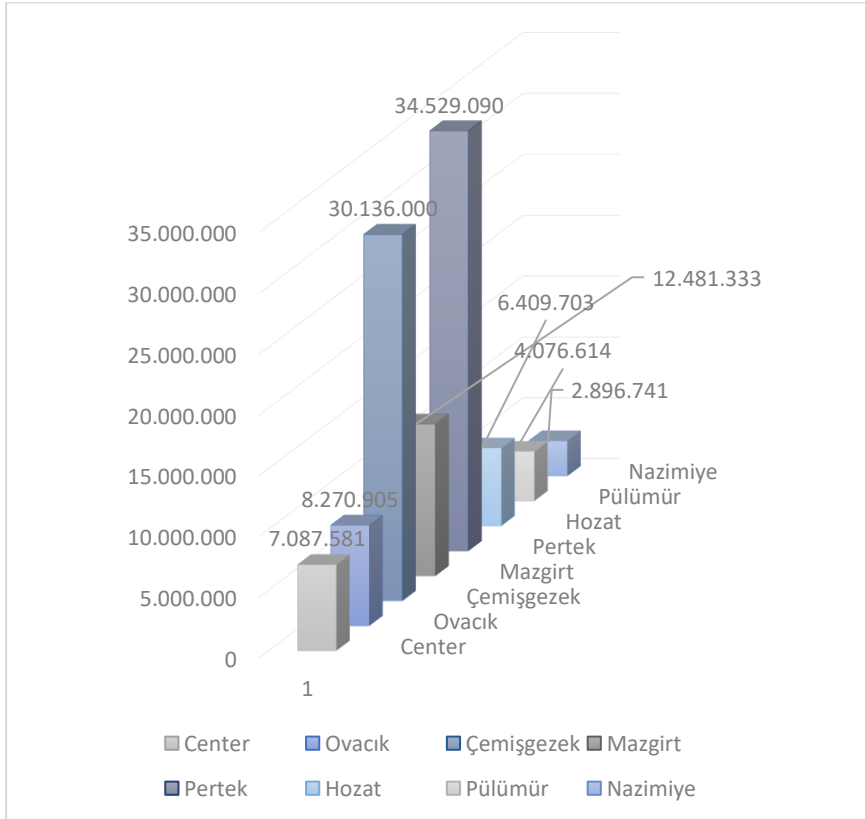


Figure 1: Kwh potential that can be obtained from Tunceli provinces and districts

In the light of the obtained data, 22.449.375 m³ biogas can be produced in the province of Tunceli in 2020 with the number of cattle, sheep and poultry, and 77.89% of this value is obtained from sheep and 22.06% from cattle and only 0.26% from poultry. The biogas energy equivalent that can be produced with the number of animals available in the city is 105.747.064kWh. The percentage contribution of the number of ovine to 77.7% of the number of bovine animals was 22.01% and the contribution of poultry to 0.26% of the electricity potential that can be produced. The distribution of this total energy value to the districts is given in Figure.1.

CONCLUSSION

Total number of cattle: 41702, number of ovine: 430701 and number of poultry: 34.220 belonging to Tunceli province. Annual fertilizer amount that can be obtained with the number of cattle: 150.127 tons, annual fertilizer amount that can be obtained with the number of ovine animals: 301.490 tons and annual fertilizer amount that can be obtained with the number of poultry: 754.84 tons. The annual amount of biogas that can be obtained with the number of cattle in the city is 4.954.197m³, the annual amount of biogas that can be obtained with the number of ovine animals: 17.486.4606 m³ and the annual amount of biogas that can be obtained with the number of poultry: 58718 m³. Annual electricity energy that can be obtained with the number of cattle: 23,284,725 kwh, the annual amount of electricity that can be obtained with the number of sheep and goats: 82,186,365 kWh and the annual amount of electricity that can be obtained with the number of poultry:

275,974 kWh. While the total amount of biogas that can be obtained with the total number of animals in the province is determined as 22.449.375m³, the total energy that can be obtained has been calculated as 105.747.064 kwh.

REFERENCES

- Adebayo AO, Jekayinfa SO, Linke B. Effect of co-digestion on anaerobic digestion of cattle slurry with maize cob at mesophilic temperature. *Journal of Energy Technologies and Policy*. 2013;3(7):47-54
- Bilir, M. Deniz, Y. Karabay, E. (1983). Biyogaz Üretimine Yönelik Değerlerin Saptanması. Toprak Su Araştırma Ana Projesi, Proje No: 872. Ankara.
- Borjesson R, Berglund M. Manuscript: Environmental system analysis of biogas systems-part II. Environmental Impacts of Replacing Various Reference system. *Biomass and Bioenergy* Submitted for Publication; 2005.
- Braun, R. (1982). *Biogas – Methangärung organischer Abfallstoffe*; Springer Verlag Wien, New York.
- Bulut, A.P. Canbaz G.T. (2019). Investigation of Sivas Province's Biogas Potential of Animal Wastes. *Karaelmas Fen ve Müh. Derg.* 9(1):1-10.
- Cestonaro, T. de Mendonça Costa, M.S.S., de Mendonça Costa, L.A., Rozatti, M.A.T., Pereira, D.C., Lorin, H.E.F., Carneiro, L.J., (2015). The Anaerobic Co-digestion of Sheep Bedding and $\geq 50\%$ Cattle Manure Increases Biogas Production and Improves Biofertilizer Quality. *Waste Management*, 46, 612-618.
- Chinese Biogas Construction Leader Group (CBCLG), Chengdu Biogas Science Institute (CBSI), 1985. *An Illustrated Handbook on the Standard Construction of Chinese Rural Household Biogas Digesters (GB4750-84)*. China Agriculture Press, Beijing, pp. 30–45.
- Deniz, Y. (1987). *Türkiye’de Biyogaz Potansiyeli ve Biyogazın Sağlayacağı Yararlar*, Ankara.
- Enerji atlası ebülten (2020)
- Eryaşar, A. Koçar, G. (2009). Biyogaz Üretiminde Basıncın Etkisi. *Pamukkale Üniversitesi Mühendislik Bilimleri Dergisi*, 15(2), 181-186.
- Görmüş, C. (2018). *Türkiye’deki Hayvan Gübrelerinin Biyogaz Enerji Potansiyelinin Belirlenmesi*, Namık Kemal Üniversitesi, Fen Bilimleri Enstitüsü, Yüksek Lisans Tezi, 78. Tekirdağ.

- İlkiliç, C. Deviren. H (2011). Biyogazın Oluşumunu Etkileyen Fiziksel Ve Kimyasal Parametreler. 6th International Advanced Technologies Symposium (IATS'11), 16-18 May 2011, Elazığ, Turkey.
- Kalia VC, Sonakya V, Raizada N. Anaerobic digestion of banana stem waste. *Bioresource Technology*. 2000;73: 191-193.
- Kaltschmitt, M. Hartmann, H. (2001). *Energie aus Biomasse – Grundlagen, Techniken und Verfahren*; Springer Verlag Berlin, Heidelberg, New York,
- Kloss, R. (1986). *Planung von Biogasanlagen*; Oldenbourg Verlag München, Wien.
- Öztürk, M.(2017). *Hayvan Gübresinden Biogaz Üretimi Çevre ve Şehircilik Bakanlığı. ANKARA-2017*
- Marañón, E., Castrillón, L., Quiroga, G., Fernández-Nava, Y., Gómez, L., García, M.M.(2012). Co-digestion of Cattle Manure with Food Waste and Sludge to Increase Biogas Production. *Waste Management*, 32(10), 1821-1825.
- Mutlu, S.F. (2003). Biyogazın Kırsal Kesimde Kullanımı ve Tasarım Temelleri. *Türk Tesisat Mühendisleri Derneği Dergisi*, 27, 39-41.
- Schattner, S. Gronauer, A.(2015). *Methangärung verschiedener Substrate – Kenntnisstand und offene Fragen*, Gülzower Fachgespräche, Band 15:
- Sun and Qi, 1993 G. Sun, X. Qi A study on the fine circle of eco-agriculture system and its mechanism of high yield and high benefit in Xishan village Shandong Environ., 1993 (1) (1993), pp. 31-33
- Vindis, P. Mursec, B Janzekovic, M and G. Cus, “The impact of mesophilic and thermophilic anaerobic digestion on biogas production,” *Journal of Achievements in Materials and Manufacturing Engineering*, vol. 36, no. 2, pp. 192–198, 2009, http://www.journalamme.org/papers_vol36_2/36210.pdf.
- Zhang, Z., Deng, K., Ralph, O., 1998. *Design for Market-oriented Development Strategy of Bioenergy Technologies in China*. China Environmental Science Press, Beijing, pp. 74–104
- Wu, B., Fei, L., 1999. *Modern Technologies for Monitoring Environment*. China Environmental Science Press, Beijing, pp. 263–274.

BÖLÜM 8

EVALUATION OF SOME INDUSTRIAL WASTES AND VOLCANIC PUMICE AS BUILDING MATERIALS IN THE CEMENT SECTOR

Assist. Prof. Dr. Abdulvahap KORKMAZ¹

¹ Afyon Kocatepe University, School of Applied Sciences, Dinar / Afyonkarahisar, TURKEY. *avkorkmaz@aku.edu.tr

INTRODUCTION

Marble and natural stone exports from Turkey to 179 countries have been realized until today. Large scale wastes and natural stone dusts produced during the cutting and polishing of marble and travertine blocks and slabs in natural stone enterprises can be used as building elements in the construction sector. Production should be developed in an environmentally sensitive manner and should be made the sector turn towards the products with high added value. This study is clarified the processing of marble in marble factories and prevented environmental pollution from solid marble residues causing environmental and visual pollution. [1].

Marble, travertine dust and sludge produced during the cutting, polishing and final product stages of natural stones (marble and travertine) are quite high. If pollutants are not managed and recycled in an environmentally compatible way, most waste and cause environmental pollution. Marble production should be done in harmony with the environment. The recovery and use of these wastes that are not classified as hazardous wastes pollution will be contribute to the enviromental pollution reduction. [2].

Despite the increasing attempt to use natural stone (NSW) waste Various studies are carried out on the method of utilizing marble wastes in different areas in the construction sector and it is known that there are some applications in the industry. In recent years, studies are being carried out in the technology laboratories of the universities especially on the evaluation of marble powders, which are wastes of

the marble industry, in concrete and soil improvement technology. Based on these studies, the systematic investigation was carried out to bring the wastes of marble plants in Afyon region to the economy. In this context, this study was carried out on the evaluation of natural stone cutting wastes as filler material in concrete mixtures as its use in cement [3].

Cement production is an energy intensive process. Therefore, in recent years, various alternative additives are added to the cement clinker during the grinding stage. Thus, technically better quality cement can be produced and energy saving is achieved and economic profit is provided. At the same time, the amount of fuel required for heat energy is saved, thus reducing CO₂ emissions and contributing to environmental protection. For this purpose, pozzolans can be used in the cement production.[4].

In the developing industry, pumice is a raw material that finds a new area of use the other each day. Volcanic ash, sometimes referred to as pumice and sometimes called volcanic dust, was made as cementitious material. For pumice, this property is characterized by its high pozzolonic activity. Therefore, in this study, the use of volcanic pumices in cement in various proportions and usability as additives in the cement sector was investigated.

1. EXPERIMENTAL STUDIES

The cementitious materials used in this study were Portland cement clinker (PC), gypsum (G), natural stone wastes (NSW), and volcanic pumice (VP). The PC, and gypsum were obtained from Adocim

cement Plant (Tokat, Turkey). The NSW was taken from deposits of marble factories. Volcanic pumice was obtained from Cappadocia Region. Chemical properties of natural stone wastes and volcanic pumice samples were determined by XRF and mineralogical properties by XRD and SEM analyzes. Thin sections of natural stone wastes and pumice samples were made and mineralogical petrographic investigations were performed. Based on the experimental data obtained, the usability of pumice and natural stone wastes as additive in cement industry was investigated. For this purpose, cements with different amounts of pumice and natural stone wastes were produced.

Grinding operations were carried out with laboratory type jaw crusher and ball mill in Tokat Cement Plant Laboratory. Specific surface areas of natural stone wastes, pumice and cement samples used in the experiments were determined by Blaine brand ASBL-01 model. Thinness values were determined by using Alpine brand 45, 90 and 200 μm sieves. Specific weights of the samples were determined by picnometer. The setting times of the cement samples were determined according to TS EN 196-3 (2010). The preparation of the cement paste by mixing the cement, water and sand was carried out with the Atom Teknik brand mixer and the vibration of the cement paste was carried out using the Atom Teknik Brand shaking device. The setting time of cement paste by using Atom Teknik brand Vicat tool, was ensured that the cements remain at constant humidity and temperature for 24 hours. WK 600 brand humidity cabinet and the compressive strength of the concrete were determined with Atom Teknik brand pressure

resistance device. Expansion determination test was performed according to TS EN 196-3 (2010) standard.

Table 1 . Chemical composition of raw materials (by XRF, wt%)

Oxides	Chemical analysis (wt.%)			
	Clinker	Gypsum	Volcanic Pumice	Natural Stone Waste
SiO ₂	21,24	0,7	70,11	1,15
Al ₂ O ₃	5,07	0,32	13,16	0,31
Fe ₂ O ₃	3,64	0,13	1,37	0,64
CaO	66,07	33,71	1,38	51,43
MgO	1,42	0,78	0,25	0,46
Na ₂ O	0,14	0	3,23	0,1
K ₂ O	0,59	0,03	4,54	0,14
SO ₃	0,53	41,58	0,25	0,03
LoI	0,28	22,39	5,71	45,24

Table 2. Mix Proportion of Cement Pastes.

Codes	Material Types	%PC	%G	%VP	%NSW
NSW1	PC+G+NSW	55	5	0	10
NSW2	PC+G+NSW	55	5	0	20
NSW3	PC+G+NSW	55	5	0	30
NSW4	PC+G+NSW	55	5	0	40
VP1	PC+G+VP	55	5	10	0
VP2	PC+G+VP	55	5	20	0
VP3	PC+G+VP	55	5	30	0
VP4	PC+G+VP	55	5	40	0

2. RESULTS AND DISCUSSION

Considering the chemical structure of the pumice, it was determined that the main structure consists of SiO_2 , Al_2O_3 and Fe_2O_3 . It was observed that SiO_2 and Al_2O_3 amounts increased in proportion with the increase of pumice contribution rate in the chemical structure of cements. The same increase is valid for K_2O and Na_2O amounts. Fe_2O_3 , SO_3 , MgO and CaO amounts decreased. It was determined that the chemical change observed in blended cements using pumice was totally related to the chemical structure of pumice (Table 3).

Table 3.Chemical Composition of Cements (by XRF, wt%)

Codes	SiO_2	Al_2O_3	Fe_2O_3	CaO	MgO	SO_3	K_2O	Na_2O	LoI
NSW1	17,66	4,49	3,12	59,66	2,32	1,73	0,49	0,18	10,35
NSW2	16,24	4,26	3,15	61,58	2,26	1,88	0,54	0,5	8,95
NSW3	14,33	3,85	2,82	62,77	1,65	1,76	0,4	0,41	10,48
NSW4	15,44	4,11	2,79	61,14	1,29	0,51	0,64	0,51	3,64
VP1	26,06	6,12	4,22	55,01	2,11	1,79	1,11	0,93	2,25
VP2	31,05	6,73	4,4	49,16	2,04	1,71	1,4	0,93	1,85
VP3	34,78	7,31	4,7	43,19	1,39	1,79	0,9	0,21	4,48
VP4	40,85	8,25	4,75	31,31	1,60	2,30	0,80	0,23	3,64

For blended cements, the amount of SO_3 is very important in TS EN 197-1 (2012) standard and the upper limit value is expressed as 4% and 4.5% in pozzolanic cements of CEM IV class and Portland calcareous cements of CEM II class. When the blended cements

obtained in this study were examined, it was found that the SO_3 content of the cements produced for all pumice contribution ratios was lower than the specified limit values. According to this result, it is concluded that pumices evaluated within the scope of the study can be used as additive material.

Previously, the limestone contribution rate for producing limestone admixture was limited to 5%, but this value was increased to 40% with the enactment of TS EN 197-1 (2012) standard. For this reason, the upper limit of the NSW contribution rate in the preparation of NSW admixtures was taken as 40%.

When the tables are examined, it is observed that SiO_2 , Al_2O_3 , Fe_2O_3 , MgO amounts decrease due to increase of NSW addition (Table 3). The amount of CaO increased in direct proportion with the addition of NSW. The highest amount of SO_3 in NSW blended cements is 1.88% and 1.76% and is below the limit value (4%) stated in TS EN 197-1 (2012).

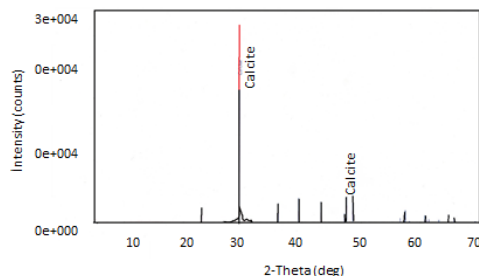


Fig. 1. XRD pattern of natural stone wastes.

The XRD patterns of the VP and NSW are shown in Figures 1 and 2, respectively. XRD patterns of all natural stone wastes showed that they were composed of pure calcite. The identified crystalline phases of NSW was calcite. It contains CaO, SiO₂, and small amount of MgO, Al₂O₃ and Fe₂O₃ (Figure 1).

The XRD patterns are compatible with the chemical structure and show that the main composition of the natural stone wastes used is CaCO₃.

SEM images of NSW are presented in Figure 2. When SEM photographs are evaluated considering XRD graphs, it is observed that NSW sample is composed of irregular calcite crystals.

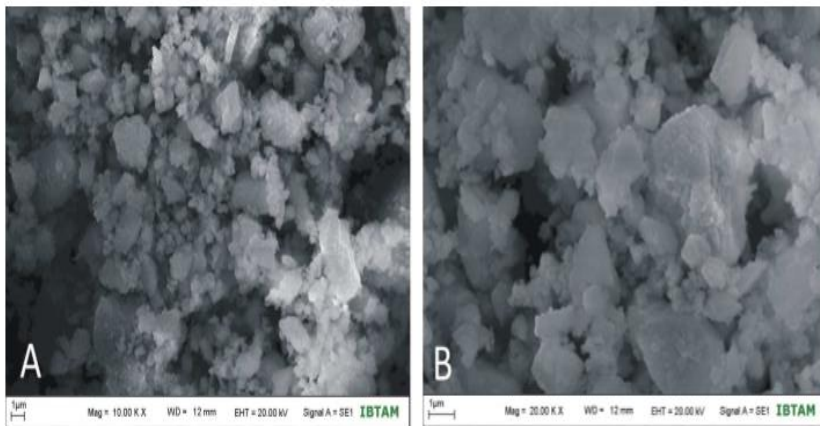


Fig. 3. SEM micrographs of NSW

When evaluating the petrographical studies together with X-ray Diffractometer result; the petrographical studies were supported by the XRD results and all the pumice samples show amorphous texture together with a negligible amount of crystals. In the observations

made in volcanic pumice thin section studies, crystal fragments were found in pumice. Although the main structures are amorphous quartz, XRD pattern where the crystalline structures of the pumice are captured is presented in Figure 3. When XRD patterns are examined, it is observed that there are quartz and sanidine crystals in the structure. But in pumice, the main structure is amorphous silica.

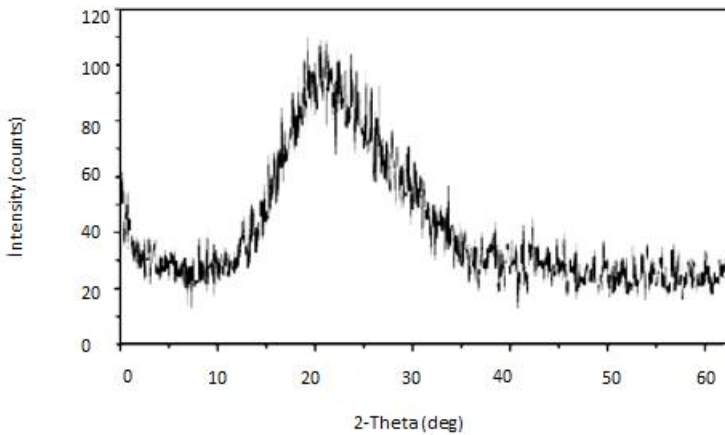


Fig. 4. XRD pattern of volcanic pumice

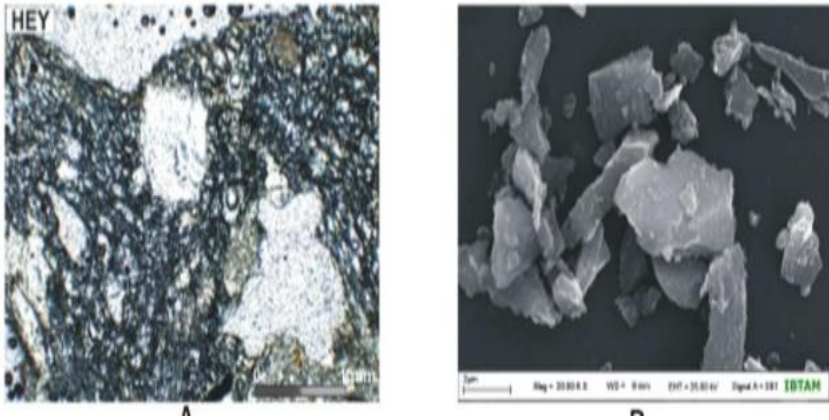


Fig. 5. SEM micrographs of volkanik pumice

Amorphous pumice is an important element in the cement sector. Further, the amount of energy required to grind a crystallized material is greater than the energy required to grind an amorphous material. This is an important issue in terms of energy saving. Amorphous materials are more easily grinded between the pores and strengthen the skeletal structure increases the compressive strength [5,6,7]. At the same time by reacting with amorphous silica lime increases the binding property of cement [8,9].

As mentioned in the XRD section, crystalline structures were found in the pumice sample. When the thin section view of the pumice sample is observed, it is seen that the dough ratio with phenocrystals is almost half (Figure 4). However, the dominant structure in pumice is amorphous silica. Thin section and SEM photographs support the XRD result.

In all pumice blended cements, it was determined that the fineness and blaine specific surface area increased in general due to the increase in the amount of pumice. The results of the examples of pumice blended cement is given Table 4. Due to the increase in the pumice additive ratio, the increase in fineness and blaine specific surface area values is due to the mass increase in the pumice ratio, which is an easier meal than the clinker in cement. As is known, pumice is easy to grind materials.

Table 4. Physical Characteristics of Cementitious Mixes

Codes	45	90	200	Blaine (cm ² /g)	Specific gravity (g/cm ³)
NSW1	10,6	1,8	0,8	3955	3,07
NSW2	9,8	1,2	0,5	4395	3,03
NSW3	7,2	2,3	0,7	4300	2,99
NSW4	6	1,7	0,8	4057	2,96
VP1	28,7	9,3	2,5	4195	3,01
VP2	31,3	11,4	2,9	4181	3,03
VP3	35	13,1	2,6	4972	2,99
VP4	32,6	15,5	3,3	5429	2,98

Since NSW are difficult to grind materials compared to pumice (except basic pumice), sieve analysis of NSW blended cements was higher than pumice blended cements. The amount of NSW remaining on the sieve decreased as the sieve opening decreased. Therefore, specific surface areas (blaine) increased.

Regarding the setting times and volume expansion, TS EN 197-1 (2012) states that the initial value of the setting time should be at least

60 minutes and above the volume expansion should be less than or equal to 10 mm. When the starting and finishing times of all pumice blended cement samples were examined, it was found that the cements obtained in all additive ratios provided the standard values (Table 5).

Table 5. Water Content, Setting Time of Cementitious Mixes

Codes	Water ratio	Setting Time(min)		Soundness (mm)
	%	Initial	Final	
NSW1	27,6	140	190	1
NSW2	26,7	120	170	0
NSW3	26,9	120	150	1
NSW4	33,7	110	140	1
VP1	25,1	120	165	1
VP2	25,4	115	155	1
VP3	25,3	115	155	1
VP4	25,1	115	160	0

The setting times and volume expansion values of pumice added cement samples are given in Table 5. Generally, the start and finishing times of the setting time were increased due to the amount of pumice. This result is consistent with the literature data, and it has been found in the literature that cements obtained with more than 35% pumice additive cause great increases in setting times [10,11,12]. In pumice blended cements, low specific surface area and clinker amount decrease the hydration process speed and this may cause an increase in setting time [13].

When the cement / water ratio of Portland cement and Pumice added cement is compared with each other, it is observed that the water content increases due to the increase of the pumice ratio especially after the 20% additive ratio. This is due to finely ground pozzolans increase the specific surface area of cement and increase the water requirement of the cement. The low water content makes the workability of the concrete more difficult and increases the compressive strength [14]. The amount of water required for cement is half of the amount of cement, ie the water / cement ratio is determined as 0.50 (TS EN, 196-3, 2010).

In TS EN 197-1 (2012), it is stated that the 2 day compressive strength of cements should be greater than 10 MPa (101.971 kgf / cm²) and the 28 day compressive strength should be greater than 32.5 MPa (433.379 kgf / cm²). Table 6 shows the compressive strength results of pumice added cement samples according to the amount of additives. As it can be seen from the tables and figures, it has been determined that the maximum additive ratio of 30% in pumice blended cements provides the value given in the standard (TS EN 197-1, 2012).

It has been found that compressive strength decreases due to pumice contribution rate increase and this result is consistent with the literature. The literature studies accept that the compressive strength of blended cement decreases as a result of increasing pumice amount and decreasing clinker amount. [15,16,17].

Early strength of pozzolanic cements is relatively low and long term strength is high [18]. The high amount of active silica in pozzolans increases pozzolanic activity and increases the compressive strength in later years [19,20]. The reactive silica content of all pumices studied has exceeded the standard value of 25%. Therefore, compressive strength results of pozzolan blended cements increased gradually. As a result of the experimental studies, it has been seen that blended cements obtained by adding 35% pumice meet the standards and it is thought that it will provide energy saving and economic gain due to clinker decrease.

Table 6. Compressive Strength of the Mortar Containing NSW and VP

Compressive Strength (MPa)	Age (days)		
	2 day	7 day	28 day
Codes			
NSW1	18,8	40	51,3
NSW2	20,3	42	47,3
NSW3	11,8	39,8	43,6
NSW4	15,6	25	39,2
VP1	19,2	37,6	45,7
VP2	18,6	32,5	43,7
VP3	15	28	34
VP4	14,1	25,3	31,9

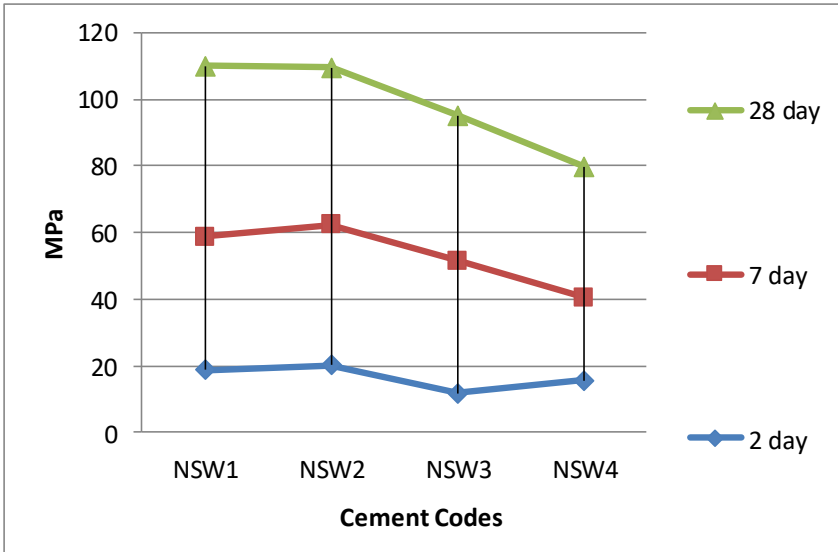


Fig.7. Compressive strength of the mortar containing NSW

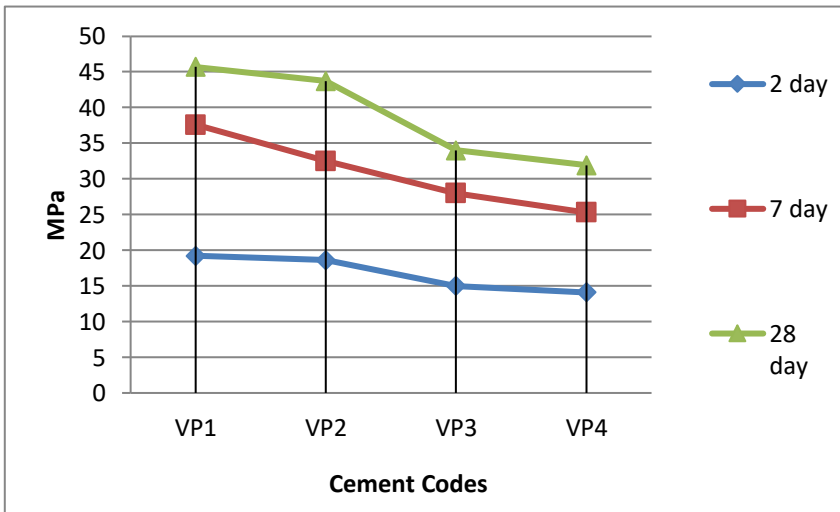


Fig. 8. Compressive strength of the mortar containing NSW

The 28-day compressive strength values of NSW blended cements provide 32.5 MPa (433.37 kgf / cm²) which is the limit value at 5%, 10% and 20% additive rates. Other contribution rates were below the limit value. Decreases in standard strengths have been observed due to increase in contribution rate. It was observed that the most effective result in NSW blended cements was 20% (table 6).

Limestone does not have any effect on compressive strength, it is known to have only filling properties [21]. However, 5% limestone additive increases the early compressive strength indirectly as it accelerates the hydration reactions of cement. In addition, if it is used in high rates, it causes an effect that reduces the compressive strength [22]. In one of the studies on limestone blended cements, cement samples with 5%, 10%, 20% and 40% lime additive ratios were prepared and physical and mechanical properties of the cements were investigated. Although there is not much change in the compressive strength of 5% limestone admixture, early strength has been observed to increase slightly. However, they stated that there is a decrease in compressive strength at all ages at higher additive rates. They obtained the most appropriate strength results at 5% and 20% contribution rates [23].

CONCLUSIONS

The main conclusion derived from this study may be summarized as follows:

1. Chemical analysis of pumice samples showed that the chemical structure of pumice consisted of more than 70% SiO₂. XRD, SEM and mineralogy-petrography studies show that pumice are mostly glassy and consist of amorphous SiO₂.
2. In this study, SiO₂, Al₂O₃ and Fe₂O₃ in pumice are more than 70%, MgO amounts are less than 5%, reactive silica content is more than 25% and pozzolanic activity values are higher than the limit values specified in TS EN 25. Therefore, pumice used in the study can be used as pozzolanic additive in cement production.
3. As a result of the chemical analyzes performed on natural stone waste samples, it was shown that the natural stone wastes were similar to the limestone chemical structure and that the main structure consisted of CaCO₃. These results show that natural stone wastes can be used as a CaO source for both additives and clinker raw materials in cement industry.
4. When the chemical structure of the blended cements obtained within the scope of the study was examined, it was determined that the changes in the chemical content were completely related to the chemical structure of the admixtures. One of the most important parameters in the chemical structure is the amount of SO₃. As stated in TS EN 197-1 (2012) standard, SO₃ amount is very important for

admixture cements and the limit value is 4% and 4.5%. When the blended cements obtained in this study were examined, it was found that the S_{O_3} content of the cements produced for all pumice contribution ratios was lower than the specified limit values.

5. When the blended cements obtained were examined according to the fineness and blaine values, it was found that the pumice blended cements increased the fineness and blaine specific surface area due to the increase in the amount of pumice. This is because the pumice are more easily ground materials than clinker. Sieve made from the other side

As a result of the analysis, it was found that the fineness values of NSW blended cements and pumice blended cements at the same grinding time and additive ratios were higher than the fineness values of pumice blended cements. This is because NSW are more difficult to grind than pumice.

6. When the blended cements obtained were evaluated in terms of setting time and volume expansion, it was observed that all blended cements provided the values specified in TS EN 197-1 (2012). Especially in pumice blended cements, it has been determined that the start and end times of setting time increase due to the increase of pumice ratio. When the pumice blended cements are compared with each other, it is found that there is a good relationship between the porosity of pumice and the setting times of pumice blended cement mortars. The high porosity of the pumice causes the setting times to decrease.

7. The compressive strength of the blended cements obtained in the scope of the study was determined depending on the curing age. A decrease in compressive strength was observed when compared with Portland cement. According to the data obtained, maximum 30% additives in pumice-added cements rate and maximum 20% additive ratio of natural stone waste blended cements (TS EN 197-1, 2012) 28-day compressive strength value (> 32.5 MPa) was found to provide.

8. It was determined that there was a significant relationship between cement fineness and compressive strength and compressive strength increased due to the decrease in fineness (cement particle size). The decrease in the size of the particles constituting the cement shows that the cement will absorb much more water in a much shorter time. Thus, chemical reactions (hydration reactions) occurring in the cement will be accelerated and thus the formation of C_3A will be increased.

Buddha

will increase early strength.

9. Within the scope of this thesis, it is determined that there is a relationship between Na_2O ratios of pumice used as additive material and compressive strength of pumice blended cements and poured concrete. Additive with compressive strength of concrete. There is an inverse ratio between the Na_2O ratios of the pumice used as the material. Even if the compressive strengths are relatively low, the Na_2O content decreases. This shows that alkali contents negatively affect the compressive strength of cement.

REFERENCES

- 1 Shirule, P. A., Ataur Rahman, and Rakesh D. Gupta. "Partial replacement of cement with marble dust powder." *International Journal of Advanced Engineering Research and Studies* 1.3 (2012): 175-177.
- 2 Shehata, Medhat H., and Michael DA Thomas. "The effect of fly ash composition on the expansion of concrete due to alkali-silica reaction." *Cement and Concrete Research* 30.7 (2000): 1063-1072.
- 3 Topcu, Ilker Bekir, Turhan Bilir, and Tayfun Uygunoğlu. "Effect of waste marble dust content as filler on properties of self-compacting concrete." *Construction and building Materials* 23.5 (2009): 1947-1953.
- 4 Kavas, Taner, and Asim Olgun. "Properties of cement and mortar incorporating marble dust and crushed brick." *CERAMICS SILIKATY* 52.1 (2008): 24.
- 5 Mirza, J., et al. "Pakistani bentonite in mortars and concrete as low cost construction material." *Applied Clay Science* 45.4 (2009): 220-226.
- 6 Uysal, Mucteba, et al. "Optimization of durability properties of concrete containing fly ash using Taguchi's approach and Anova analysis." *Revista de la Construcción. Journal of Construction* 17.3 (2018): 364-382.
- 7 Pawar, Savita Gangadharrao. Design, development and performance evaluation of grader for Kagzi-Lime. Diss. Vasantrao Naik Marathwada Krishi Vidyapeeth, Parbhani, 2011.
- 8 Aruntaş, Hüseyin Yılmaz, et al. "Utilization of waste marble dust as an additive in cement production." *Materials & Design* 31.8 (2010): 4039-4042.
- 9 Shirule, P. A., Ataur Rahman, and Rakesh D. Gupta. "Partial replacement of cement with marble dust powder." *International Journal of Advanced Engineering Research and Studies* 1.3 (2012): 175-177.
- 10 Yetgin, Şükrü, and Ahmet Çavdar. "Study of effects of natural pozzolan on properties of cement mortars." *Journal of materials in civil engineering* 18.6 (2006): 813-816.
11. Alp, I., Deveci, H., Süngün, Y. H., Yılmaz, A. O., Kesimal, A., & Yılmaz, E. (2009). Pozzolanic characteristics of a natural raw material for use in blended cements. *Iranian Journal of Science and Technology*, 33(B4), 291.

12. Khan, M. I., and A. M. Alhozaimy. "Properties of natural pozzolan and its potential utilization in environmental friendly concrete." *Canadian Journal of Civil Engineering* 38.1 (2010): 71-78.
13. Al-Swaidani, A. M., et al. "Prediction of corrosion resistance of concrete containing natural pozzolan from compressive strength." *IOP Conference Series: Materials Science and Engineering*. Vol. 96. No. 1. IOP Publishing, 2015.
14. Aliabdo, Ali A., Abd Elmoaty M. Abd Elmoaty, and Esraa M. Auda. "Re-use of waste marble dust in the production of cement and concrete." *Construction and building materials* 50 (2014): 28-41.
15. Bibi, Sadia, et al. "Evaluation of industrial based adsorbents for simultaneous removal of arsenic and fluoride from drinking water." *Journal of Cleaner Production* 87 (2015): 882-896.
16. Anwar, Abdullah, et al. "Replacement of cement by marble dust and ceramic waste in concrete for sustainable development." *International Journal of Innovative Science, Engineering & Technology* 2.6 (2015): 496-503.
17. Gandhi, Khushbu S. "Stabilization of expansive soil of Surat region using rice husk ash and marble dust." *International Journal of Current Engineering and Technology* 3.4 (2013): 1516-1521.
18. Kabay, Nihat, et al. "Properties of concrete with pumice powder and fly ash as cement replacement materials." *Construction and Building Materials* 85 (2015): 1-8.
19. Hossain, Khandaker M. Anwar. "Blended cement using volcanic ash and pumice." *Cement and Concrete Research* 33.10 (2003): 1601-1605.
20. Ardalan, Reza Bani, Alireza Joshaghani, and R. Douglas Hooton. "Workability retention and compressive strength of self-compacting concrete incorporating pumice powder and silica fume." *Construction and Building Materials* 134 (2017): 116-122.
21. Hossain, Khandaker M. Anwar. "Potential use of volcanic pumice as a construction material." *Journal of materials in civil engineering* 16.6 (2004): 573-577.

22. Granata, Michele Fabio. "Pumice powder as filler of self-compacting concrete." *Construction and Building Materials* 96 (2015): 581-590.
23. Sahin, Sirri, et al. "Properties of prefabricated building materials produced from ground pumice aggregate and binders." *Construction and Building Materials* 22.5 (2008): 989-992.



ISBN: 978-625-7279-67-3